NTNU
Norwegian University of
Science and Technology

Master's thesis

2019

Ragil Destriawan Prasetyo

Master's thesis

NTNU
Norwegian University of
Science and Technology
Faculty of Engineering
Department of Geoscience and Petroleum

Ragil Destriawan Prasetyo

Seismic Signature in Fractured Reservoir

June 2019

NTNU
Norwegian University of
Science and Technology

NTNU
Norwegian University of
Science and Technology

Seismic Signature in Fractured Reservoir

Ragil Destriawan Prasetyo

Petroleum Geosciences
Submission date: June 2019
Supervisor: Alexey Stovas

Norwegian University of Science and Technology
Department of Geoscience and Petroleum

To my parents, brother, sister and all of my friends in Trondheim.

Acknowledgement

First, I wish to express my sincere gratitude to my supervisor, Professor Alexey Stovas, for introducing me to this topic, sharing his knowledge, and giving me excellent guidance. It is such an honor being supervised and working with him.

I want to thank all my friends and colleagues; Gungde, Hieu, Ofeliya, Patience, Xingyu, and Wasif who are also mostly doing their thesis in Schlumberger lab for providing a friendly atmosphere throughout the year. Special thanks to Iffan for willingly to be disturbed whenever I have questions in coding.

Formidable thanks to my sponsor, LPDP Indonesia, for giving me a financial scholarship for two years of continuing my study abroad. It was such a fantastic experience, and I have learned a lot from studying here.

Last but not least, I express my sincerest thanks and gratitude to my lovely family, my dad, mom, sister, and brother. I do not know how to thank my parent for constant support and care during my whole life. I am really thankful for all their love toward me.

Trondheim, June 2018
Ragil Destriawan Prasetyo

Summary

Anisotropy in large parts of the earth's crust, particularly in sedimentary basins is well modeled by orthorhombic (ORT) symmetry. Schoenberg and Helbig (1997) introduced the orthorhombic medium as a combination of vertical fractures and horizontal fine layering, which resembles quite much of a petroleum reservoir. Hence understanding the behavior of the seismic response for this particular medium has become quite popular for this past years.

A well data is provided in this study for observing the seismic signature of a fractured reservoir, which known as ORT medium. The kinematic parameters derived by Stovas (2016) are utilized in this study. Polar plot of azimuthal dependence of these kinematic parameters is conducted in order to observe the difference signature of a fractured and non-fractured medium. Furthermore, the effect of considering overburden above the fractured reservoir is also discussed.

Since well data and seismic wavelength work in a slightly different frequency domain, a process that helps to transfer a series of a thin layered model that match with seismic wavelength is required. Upscaling is commonly known to handle this issue. Two methods of upscaling, which are classic or famously known as Backus average and least square, are conducted, and the results are compared. In addition to that, in a fractured reservoir observation, two approaches to introducing fractures are also discussed and compared. These approaches are to introduce the fractures before and after the upscaling process.

This study aims to observe the seismic signature in the form of kinematic parameters that are azimuthally dependent for a fractured reservoir with the condition, as stated before.

Table of Contents

List of Tables

List of Figures

Chapter 1

Introduction

1.1 Background

Anisotropy is a real life scenario that contribute in petroleum exploration activities. It is there in most parts of the earth's crust, particularly in sedimentary basins. Anisotropy can be defined into several medium which depend on the condition of the earth's layer itself. For example, if the layers are homogeneous in one of the symmetry axis, then the medium is called Transversely Isotropic. This case mainly can be found in shale lithology where it's properties appear to be homogeneous along the axis that perpendicular to the vertical axis. This type of lithology is classified as Vertical Transverse Isotropic (VTI) medium. Another common condition is in a fractured reservoir where the lithologies are consist of several stacks of thin layers of sandstone and shale with vertical fractures embedded in it. Such condition is classified as Orthorhombic medium which become an interest of study for the past years.

Schoenberg and Helbig (1997) introduced the orthorhombic medium as a combination of vertical fractures and horizontal fine layering that is equivalent to a long wavelength. Such condition is relevant to a fractured reservoir that is commonly found in petroleum exploration. The approach for analyzing this medium requires knowledge from anisotropy in VTI medium, fracture weaknesses and a method to transform a stack of several thin layers into one effective medium that fit with seismic wavelength.

Along with understanding the anisotropy parameters, kinematic properties help us to understand how the seismic signature behaves in anisotropic media. Stovas (2016) derived the kinematic properties for P-wave and S-wave velocity in orthorhombic media for both pure-mode and converted waves. This study however, will only be focused to pure-mode waves only. Additionally, the responds of azimuth dependent of this kinematic properties will also be conducted.

In a matter of observing seismic signature in a fractured reservoir, one needs to consider how it will be observed from the surface. It brings to a condition where the overburden layers above the fractured reservoir need to be included in the calculation of the kinematic parameters. This will come to a series of reflections being recorded in the function of time and recorded on a seismogram. Then, these travel time can be computed and converted into layer parameters, famously known as Dix (1955) inversion.

1.2 Objectives

The objectives of this study are listed as:

1. To work with anisotropy concept that focuses on Schoenberg-Helbig Orthorhombic model.
2. Comparing Backus Average and Least Square as an upscaling method to acquire effective medium properties.
3. Comparing two different approaches of introducing fractures to the medium. They will be introduced before and after upscaling methods.
4. To observe kinematic properties on pure-mode waves based on the designated approaches.
5. To perform a dix-type equation in order to simulate how the kinematic parameters of a medium at certain depth are observed from the surface.

1.3 Outline

In this study, nine chapters will be presented, including this introduction. Each chapter is presented, and there will be a brief explanation about it at the beginning of each chapter. A summary of the chapters is given below.

Chapter one gives background information, objectives, and the outline of this study. This content is provided for giving a brief explanation of what this study is all about.

Chapter two explains the anisotropy models that are mainly discussed for this study. Two anisotropy models will be highlighted, Vertical Transverse Isotropic or VTI medium and Orthorhombic or ORT medium. A brief discussion about symmetry class is also discussed beforehand.

Chapter three discusses the averaging or upscaling methods, which is used to obtain an effective parameter that is gathered from well log data. Two upscaling methods will be compared, the first one is classic upscaling or commonly known as Backus Averaging, and the second one is least square upscaling. These methods are conducted in both VTI and ORT media.

Chapter four explains about Dix-type equations. A discussion about these equations that is intended to calculate the effective parameters with several layers to be accounted for is provided. This approach illustrates how a specific layer's parameters at a certain depth are observed from the surface.

Chapter five contains the observation of well log data that is used in this study. General interpretation regarding this data is also provided. Furthermore, how the methods are going to be performed are also defined in this chapter.

Chapter six discusses the fracturing effect in a medium. Preliminary consideration that state any necessary assumption and notation are discussed at the beginning. The condition of the medium before fracturing will be calculated and observed beforehand, along with that, upscaling methods will also be performed in this chapter. The effect of the fractures when they are introduced to a medium will be the main observation in the form of kinematic parameters.

Chapter seven mainly focused on a comparison of the methods and approaches that are conducted in this study. These will relate to upscaling comparison and fracturing approach comparison. Whether these methods give significant different to the kinematic parameters or not will be explained at the end of this chapter.

Chapter eight is involving an overburden effect on the study. The kinematic parameters of a layer at a certain depth will be observed when the overburden layers are included. Chapter nine summarizes the work of what has been done in this project. There will be a conclusion based on analyzing the results.

Chapter 2

Anisotropy Models

Anisotropy is commonly defined as the variation of a physical property depending on the direction in which it is measured (Sheriff, 2002). Therefore, in term of seismic anisotropy, it refers to the directional variation of a layer's response to the path of seismic waves. Specifically, it can be referred to as the dependence of seismic velocity upon angle. In here, velocity is commonly described as the speed of a seismic wave. It is the physical property that affects traveltime, amplitude, frequency, attenuation, and many other properties which are measured from seismic data. The angle is commonly described as directions including polar or incident angle (offset) and source-receiver azimuth (Liu and Martinez, 2012).

In some occasions, the term anisotropy and heterogeneity may lead to confusion. A similar case such as isotropic and homogeneous may also lead to some misunderstanding. Figure 2.1 can give clarity about these terms. The figure illustrates how each medium is affecting the seismic velocity. Note that the arrow represents the velocity value and direction.

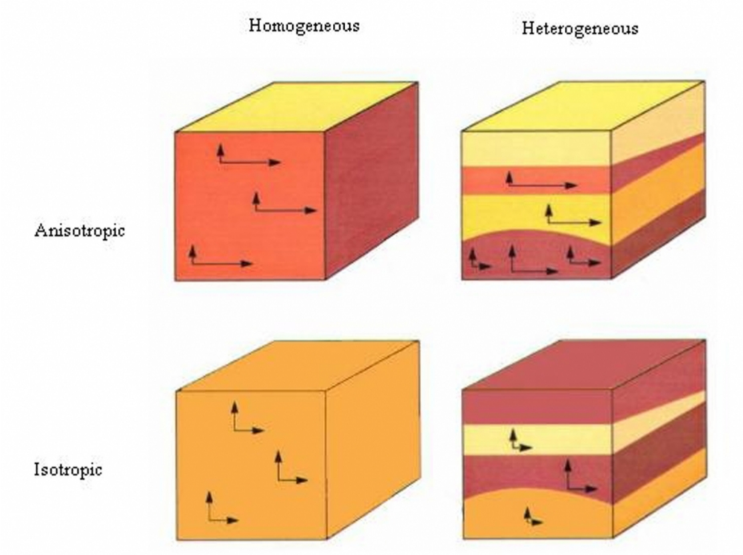

Figure 2.1: Illustration of how velocity behave given different model of medium. The value of the velocity is represented by the length of the arrow.

2.1 Symmetry Class

The symmetry of a medium is reflected in the structure of the elastic stiffness tensor C_{ijkl}. In anisotropic media, stiffness tensor is related to stress σ_{ij} and strain ε_{ij} through Hooke's law.

Hooke's law states that for sufficiently small stresses, the strain is proportional to the stress. For an anisotropic medium, Hooke's law can be written as:

$$\varepsilon_{ij} = S_{ijkl}\sigma_{kl} \tag{2.1}$$

where ε_{ij} and σ_{ij} denote components of the second-rank strain tensor and the stress tensor respectively. S_{ijkl} denotes the component of the fourth-rank elastic compliance tensor.

Equation 2.1 can be inverted to express the components of the stress tensor in terms of the components of the strain tensor, hence:

$$\sigma_{ij} = C_{ijkl}\varepsilon_{kl} \tag{2.2}$$

Where C_{ijkl} denotes a component of the fourth-rank elastic stiffness tensor, C. The second rank tensor ε and σ possess the following symmetries:

$$\varepsilon_{ij} = \varepsilon_{ji},\ \sigma_{ij} = \sigma_{ji} \tag{2.3}$$

The fourth-rank tensors S and C possess the following symmetries:

$$S_{ijkl} = S_{ijlk},\ S_{ijkl} = S_{jikl},\ C_{ijkl} = C_{ijlk},\ C_{ijkl} = C_{jikl} \tag{2.4}$$

The relationship shown in Equation 2.3 and Equation 2.4 reduce the number of independent elements of S_{ijkl} and C_{ijkl} and therefore make it possible to introduce the Voight notation in which pairs of subscript ij and kl are abbreviated by single subscripts.

$$11 \to 1,\ 22 \to 2,\ 33 \to 3,\ 44 \to 4,\ 31\&13 \to 5,\ 12\&21 \to 6 \tag{2.5}$$

Combining the Hooke's law in Equation 2.2 with equation of motion below:

$$\rho \frac{\partial^2 u_i}{\partial t^2} = \frac{\partial \sigma_{ij}}{\partial x_j} \tag{2.6}$$

will give result in wave equation such that:

$$\rho \frac{\partial^2 u_i}{\partial t^2} = C_{ijkl} \frac{\partial u_k^2}{\partial x_l \partial x_j} \tag{2.7}$$

Using Equation 2.5, the stiffness tensor C$_{ijkl}$ can be written as a matrix C$_{ab}$ which can be shown below:

$$\mathrm{C}_{ab} = \begin{bmatrix} \mathrm{C}_{11} & \mathrm{C}_{12} & \mathrm{C}_{13} & \mathrm{C}_{14} & \mathrm{C}_{15} & \mathrm{C}_{16} \\ \mathrm{C}_{12} & \mathrm{C}_{22} & \mathrm{C}_{23} & \mathrm{C}_{24} & \mathrm{C}_{25} & \mathrm{C}_{26} \\ \mathrm{C}_{13} & \mathrm{C}_{23} & \mathrm{C}_{33} & \mathrm{C}_{34} & \mathrm{C}_{35} & \mathrm{C}_{36} \\ \mathrm{C}_{14} & \mathrm{C}_{24} & \mathrm{C}_{34} & \mathrm{C}_{44} & \mathrm{C}_{45} & \mathrm{C}_{46} \\ \mathrm{C}_{15} & \mathrm{C}_{25} & \mathrm{C}_{35} & \mathrm{C}_{45} & \mathrm{C}_{55} & \mathrm{C}_{56} \\ \mathrm{C}_{16} & \mathrm{C}_{26} & \mathrm{C}_{36} & \mathrm{C}_{46} & \mathrm{C}_{56} & \mathrm{C}_{66} \end{bmatrix} \tag{2.8}$$

From the symmetry in matrix C$_{ab}$, it follows that the maximum number of independent stiffness coefficients is 21 in an anisotropic medium. These independent stiffness coefficients range in term of complexity from Isotropic medium with two independent stiffness coefficient to the most complex Triclinic medium with 21 independent stiffness coefficient. In this study, VTI and ORT medium that have five and nine independent stiffness coefficient will be mainly discussed.

2.2 Vertical Transverse Isotropic Medium

Vertical Transverse Isotropic (VTI) medium is one of the class which belonged to transversely isotropic medium that has one single rotational symmetry axis, so that, in directions perpendicular to this, the material's properties appear to be directionally invariant. As in VTI case, it has the vertical rotational symmetry axis.

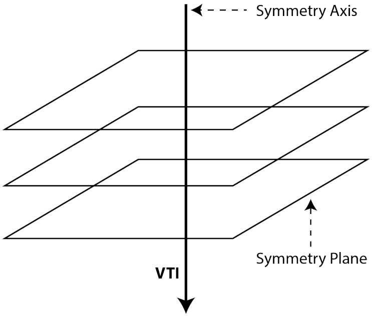

Figure 2.2: Illustration of VTI medium.

The common cause for VTI anisotropy in the subsurface are thin horizontal bedding or the preferential alignment of minerals and grains during deposition. An example of a VTI medium is a fine layering of shale.

2.2.1 Stiffness Coefficients

VTI is described by five independent stiffness coefficients (C_{11}, C_{33}, C_{44}, C_{66}, and C_{13}) which have the following matrix form:

$$\mathrm{C}_{ij} = \begin{bmatrix} \mathrm{C}_{11} & \mathrm{C}_{11}-2\mathrm{C}_{66} & \mathrm{C}_{13} & 0 & 0 & 0 \\ \mathrm{C}_{11}-2\mathrm{C}_{66} & \mathrm{C}_{11} & \mathrm{C}_{13} & 0 & 0 & 0 \\ \mathrm{C}_{13} & \mathrm{C}_{13} & \mathrm{C}_{33} & 0 & 0 & 0 \\ 0 & 0 & 0 & \mathrm{C}_{44} & 0 & 0 \\ 0 & 0 & 0 & 0 & \mathrm{C}_{44} & 0 \\ 0 & 0 & 0 & 0 & 0 & \mathrm{C}_{66} \end{bmatrix} \tag{2.9}$$

Individual components of the stiffness matrix which representing individual layers are shown below, following (Thomsen, 1986).

$$\begin{aligned} \mathrm{C}_{33} &= \mathrm{V}_{p_0}^2\,\rho, \\ \mathrm{C}_{55} &= \mathrm{C}_{44} = \mathrm{V}_{s_0}^2\,\rho, \\ \mathrm{C}_{11} &= (1+2\varepsilon)\,\mathrm{C}_{33}, \\ \mathrm{C}_{66} &= (1+2\gamma)\,\mathrm{C}_{44},\ \text{and} \\ \mathrm{C}_{13} &= \sqrt{2\delta\mathrm{C}_{33}(\mathrm{C}_{33}-\mathrm{C}_{55})+(\mathrm{C}_{33}-\mathrm{C}_{55})^2}-\mathrm{C}_{55} \end{aligned} \tag{2.10}$$

where ρ is density, V_{p0} and V_{s0} are vertical velocity of P-wave and S-wave respectively. ε, γ, and δ are the anisotropy parameters which will be discussed later on.

2.2.2 Anisotropy Parameters

For seismic applications, it is not convenient to use parameterization in terms of stiffness coefficients. It is best to split the parameters relevant to velocities and anisotropy itself which concisely characterize a wide range of seismic signatures.

In VTI effective medium where there are several isotropic layers stacked together, parameterization is referred to (Thomsen, 1986), in which there are two vertical velocities explained as,

$$\begin{aligned} \mathrm{V}_{\mathrm{p}_0} &= \sqrt{\frac{\mathrm{C}_{33}}{\rho}} \\ \mathrm{V}_{\mathrm{s}_0} &= \sqrt{\frac{\mathrm{C}_{44}}{\rho}} \end{aligned} \tag{2.11}$$

and three anisotropy parameters described as,

$$\begin{aligned} \varepsilon &= \frac{\mathrm{C}_{11}-\mathrm{C}_{33}}{2\mathrm{C}_{33}}, \\ \gamma &= \frac{\mathrm{C}_{66}-\mathrm{C}_{44}}{2\mathrm{C}_{44}}, \\ \delta &= \frac{(\mathrm{C}_{13}+\mathrm{C}_{44})^2-(\mathrm{C}_{33}-\mathrm{C}_{44})^2}{2\mathrm{C}_{33}(\mathrm{C}_{33}-\mathrm{C}_{44})} \end{aligned} \tag{2.12}$$

Here, ε and γ are controlling the horizontal propagation of P-wave and SH-wave, respectively. Note that, S-wave has two different polarization, vertical and horizontal to its propagation, and they are equal while propagating vertically in VTI medium. For horizontal velocities, the equations are provided below and note that the horizontal velocity for SV-wave is equal to vertical S-wave velocity.

$$\begin{aligned} \mathrm{V}_{\mathrm{p}}^2\left(\frac{\pi}{2}\right) &= \mathrm{V}_{\mathrm{p}0}^2(1+2\varepsilon) \\ \mathrm{V}_{\mathrm{SH}}^2\left(\frac{\pi}{2}\right) &= \mathrm{V}_{\mathrm{s}0}^2(1+2\gamma) \end{aligned} \tag{2.13}$$

For parameter δ, it is responsible for NMO velocity of P-wave,

$$\mathrm{V}_{\mathrm{p(nmo)}}^2 = \mathrm{V}_{\mathrm{p}0}^2(1+2\delta) \tag{2.14}$$

Parameter σ is introduced when dealing with SV-waves,

$$\sigma = \frac{V_{p0}^2}{V_{s0}^2}(\varepsilon - \delta) \tag{2.15}$$

σ is responsible for SV-wave NMO velocity,

$$V_{SV(nmo)}^2 = V_{s0}^2(1 + 2\sigma) \tag{2.16}$$

2.3 Schoenberg & Helbig: Orthorhombic Medium

Vertical fractures and horizontal fine layering combine to form a long-wavelength equivalent orthorhombic medium (Schoenberg and Helbig, 1997). Such media can also be described as vertical fractures which are embedded into a transversely isotropic background medium with a vertical axis of symmetry (VTI) as illustrated in Figure 2.3. Note that symmetry planes are defined in such a way according to the axis, which is defined in the figure.

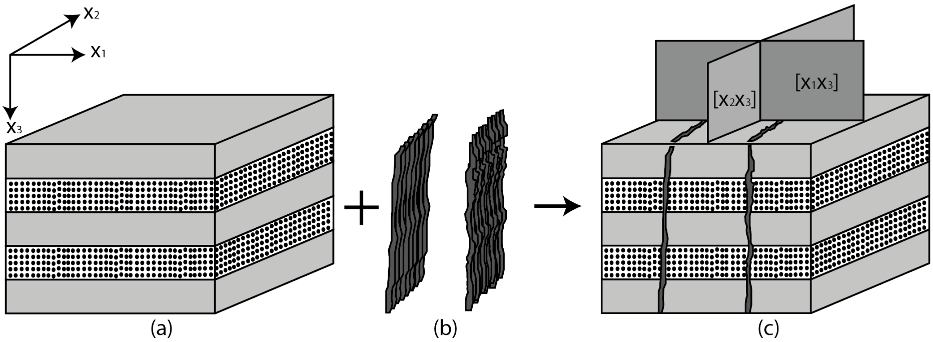

Figure 2.3: Schematic diagram of vertical fractures embedded in VTI medium adopted from (Schoenberg and Helbig, 1997). (a) VTI medium, (b) Vertical fractures set, and (c) ORT medium.

Here, an agreement to the symmetry planes are set, where [x_1,x_2] and [x_2,x_3] are the vertical symmetry planes that perpendicular to the fractures and parallel to the fractures respectively. As for the [x_1,x_2], it is the horizontal symmetry plane.

2.3.1 Stiffness Coefficients

There are nine independent stiffness coefficients in ORT medium: six diagonal elements that relate specifically to velocities along the coordinate axes and three independent off-diagonal elements.

The stiffness matrix C of such medium can be described as follow:

$$\mathrm{C} = \begin{bmatrix} \mathrm{C}_{11} & \mathrm{C}_{12} & \mathrm{C}_{13} & 0 & 0 & 0 \\ \mathrm{C}_{12} & \mathrm{C}_{22} & \mathrm{C}_{23} & 0 & 0 & 0 \\ \mathrm{C}_{13} & \mathrm{C}_{23} & \mathrm{C}_{33} & 0 & 0 & 0 \\ 0 & 0 & 0 & \mathrm{C}_{44} & 0 & 0 \\ 0 & 0 & 0 & 0 & \mathrm{C}_{55} & 0 \\ 0 & 0 & 0 & 0 & 0 & \mathrm{C}_{66} \end{bmatrix} = \begin{bmatrix} \tilde{c_1} & 0 \\ 0 & \tilde{c_2} \end{bmatrix}, \tag{2.17}$$

Here, the velocities along the coordinate axes are illustrated in the Table 2.1 based on how the propagation and polarization are from. The P-waves in the x_1, x_2, and x_3 directions are given by $\sqrt{\mathrm{C}_{11}}$, $\sqrt{\mathrm{C}_{22}}$, and $\sqrt{\mathrm{C}_{33}}$ respectively. The S-waves are expressed on the off-diagonal elements.

	Propagation		
Polarization	x_1	x_2	x_3
x_1	$\sqrt{\mathrm{C}_{11}}$	$\sqrt{\mathrm{C}_{66}}$	$\sqrt{\mathrm{C}_{55}}$
x_2	$\sqrt{\mathrm{C}_{66}}$	$\sqrt{\mathrm{C}_{22}}$	$\sqrt{\mathrm{C}_{44}}$
x_3	$\sqrt{\mathrm{C}_{55}}$	$\sqrt{\mathrm{C}_{44}}$	$\sqrt{\mathrm{C}_{33}}$

Table 2.1: Axial Propagation

Now, returning to Equation 2.17, the 0 is the 3 x 3 zero matrix and $\tilde{c_1}$ and $\tilde{c_2}$ are given by:

$$\tilde{c_1} = \begin{bmatrix} \mathrm{C}_{11_b}(1-\Delta_N) & \mathrm{C}_{12_b}(1-\Delta_N) & \mathrm{C}_{13_b}(1-\Delta_N) \\ \mathrm{C}_{12_b}(1-\Delta_N) & \mathrm{C}_{11_b}\left(1-\Delta_N\dfrac{\mathrm{C}^2_{12_b}}{\mathrm{C}^2_{11_b}}\right) & \mathrm{C}_{13_b}\left(1-\Delta_N\dfrac{\mathrm{C}_{12_b}}{\mathrm{C}_{11_b}}\right) \\ \mathrm{C}_{13_b}(1-\Delta_N) & \mathrm{C}_{13_b}\left(1-\Delta_N\dfrac{\mathrm{C}_{12_b}}{\mathrm{C}_{11_b}}\right) & \mathrm{C}_{33_b}\left(1-\Delta_N\dfrac{\mathrm{C}^2_{13_b}}{\mathrm{C}_{11_b}\mathrm{C}_{33_b}}\right) \end{bmatrix} \tag{2.18}$$

and

$$\tilde{c_2} = \begin{bmatrix} \mathrm{C}_{44_b} & 0 & 0 \\ 0 & \mathrm{C}_{44_b}(1-\Delta_V) & 0 \\ 0 & 0 & \mathrm{C}_{66_b}(1-\Delta_H) \end{bmatrix} \tag{2.19}$$

Here, C_{ij_b} are the stiffness coefficients of the VTI background explained in Equation 2.10. Δ_N, Δ_V, and Δ_H are the dimensionless weakness of the fractures which change from zero (no fracture) to unity (extreme fracturing). Δ_V and Δ_H correspond to vertical and horizontal tangential fracture weaknesses respectively, and Δ_N corresponds to normal fracture weakness.

Fracture weaknesses also provide another definition term. The tangential weaknesses Δ_V and Δ_H provide a measure of crack density, whereas the normal weakness Δ_N provides information regarding fluid content of the fractures and possible fluid flow between the fractures and pore space, Δ_N = 0 indicates wet fractures and Δ_N = 0.5 indicates dry fractures (Bakulin et al., 2000).

Note again that matrix in (2.17) describes a particular type of orthorhombic medium with the stiffness satisfying the relation (Schoenberg and Helbig, 1997):

$$\mathrm{C}_{13}(\mathrm{C}_{22} + \mathrm{C}_{12}) = \mathrm{C}_{23}(\mathrm{C}_{11} + \mathrm{C}_{12}) \tag{2.20}$$

The existence of this additional constraint (2.20) come from the fact that while the general orthorhombic medium is described by nine independent values of C_{ij}, the vertical fracture induced mode considered in this model is defined by only eight quantities. Those are five stiffness coefficients of the VTI background medium (2.10) and three fracture weaknesses (Δ_N, Δ_V, and Δ_H).

Recollecting all the matrix shown in (2.18) and (2.19), individual components of the stiffness matrix can be written in the following form:

$$\begin{aligned}
\mathrm{C}_{11} &= \mathrm{C}_{11_b}(1 - \Delta_N), & \mathrm{C}_{44} &= \mathrm{C}_{44_b}, \\
\mathrm{C}_{22} &= \mathrm{C}_{11_b} - \Delta_N \frac{\mathrm{C}^2_{12_b}}{\mathrm{C}_{11_b}}, & \mathrm{C}_{33} &= \mathrm{C}_{33_b} - \Delta_N \frac{\mathrm{C}^2_{13_b}}{\mathrm{C}_{11_b}}, \\
\mathrm{C}_{23} &= \mathrm{C}_{13_b}\left(1 - \Delta_N \frac{\mathrm{C}_{12_b}}{\mathrm{C}_{11_b}}\right), & \mathrm{C}_{55} &= \mathrm{C}_{44_b}(1 - \Delta_V), \\
\mathrm{C}_{12} &= \mathrm{C}_{12_b}(1 - \Delta_N), & \mathrm{C}_{66} &= \mathrm{C}_{66_b}(1 - \Delta_H), \\
\mathrm{C}_{13} &= \mathrm{C}_{13_b}(1 - \Delta_N)
\end{aligned} \tag{2.21}$$

2.3.2 Anisotropy Parameters

In ORT effective medium, where there is a set of vertical fractures embedded in VTI medium as the background, anisotropy parameters are defined for each symmetrical plane accordingly. Those consist of two vertical symmetry planes and one horizontal symmetry plane (Tsvankin, 1997).

First of all, the vertical velocities of the P and S waves are still following the Thomsen's recipe in VTI medium. However, the preference of using S-wave polarized in x_1-direction is used for defining the S-wave vertical velocity (Tsvankin, 1997). The reason for that is due to C_{44} and C_{55} values are no longer the same as it is introduced in VTI medium. As the vertical fractures are embedded in VTI medium, the vertical S-wave velocity that polarized in [$\mathrm{x_1}$] direction ($\mathrm{C_{55}}$) will have different velocity compared to the one that polarized in [$\mathrm{x_2}$] direction ($\mathrm{C_{44}}$). Therefore the vertical velocities are expressed as:

$$\mathrm{V_{p_0}} = \sqrt{\frac{\mathrm{C_{33}}}{\rho}} \tag{2.22}$$

$$\mathrm{V_{s_0}} = \sqrt{\frac{\mathrm{C_{55}}}{\rho}} \tag{2.23}$$

For anisotropy parameters in the [$\mathrm{x_1}$,$\mathrm{x_3}$] vertical symmetry plane, they are defined as:

$$\varepsilon_1 = \frac{\mathrm{C_{11}} - \mathrm{C_{33}}}{2\mathrm{C_{33}}} \tag{2.24}$$

$$\gamma_1 = \frac{\mathrm{C_{66}} - \mathrm{C_{44}}}{2\mathrm{C_{44}}} \tag{2.25}$$

$$\delta_1 = \frac{(\mathrm{C_{13}} + \mathrm{C_{55}})^2 - (\mathrm{C_{33}} - \mathrm{C_{55}})^2}{2\mathrm{C_{33}}(\mathrm{C_{33}} - \mathrm{C_{55}})} \tag{2.26}$$

Note that in the definition of δ for VTI media in Equation 2.12, $\mathrm{C_{44}}$ is used rather than $\mathrm{C_{55}}$. The reason for that is since both values are the same in VTI medium as the vertical S-waves that polarized in [$\mathrm{x_1}$] and [$\mathrm{x_2}$] direction are identical. However, those two stiffness coefficients differ for orthorhombic media. Hence, $\mathrm{C_{55}}$ is always used in Equation 2.26 which correspond to vertical S-wave that polarized in [$\mathrm{x_1}$] direction. For anisotropy parameters in the [$\mathrm{x_2}$,$\mathrm{x_3}$] vertical symmetry plane, they are defined as:

$$\varepsilon_2 = \frac{\mathrm{C_{22}} - \mathrm{C_{33}}}{2\mathrm{C_{33}}} \tag{2.27}$$

$$\gamma_2 = \frac{\mathrm{C_{66}} - \mathrm{C_{55}}}{2\mathrm{C_{55}}} \tag{2.28}$$

$$\delta_2 = \frac{(\mathrm{C_{23}} + \mathrm{C_{44}})^2 - (\mathrm{C_{33}} - \mathrm{C_{44}})^2}{2\mathrm{C_{33}}(\mathrm{C_{33}} - \mathrm{C_{44}})} \tag{2.29}$$

As the two vertical velocities and six anisotropy parameters introduced above can be used instead of eight original stiffness coefficient: $\mathrm{C_{11}}$, $\mathrm{C_{22}}$, $\mathrm{C_{33}}$, $\mathrm{C_{44}}$, $\mathrm{C_{55}}$, $\mathrm{C_{66}}$, $\mathrm{C_{23}}$, and $\mathrm{C_{13}}$. The only remaining stiffness $\mathrm{C_{12}}$ can be replaced with a dimensionless anisotropic parameter analogous to the δ coefficients in the vertical planes of symmetry.

$$\delta_3 = \frac{(\mathrm{C_{12}} + \mathrm{C_{66}})^2 - (\mathrm{C_{11}} - \mathrm{C_{66}})^2}{2\mathrm{C_{11}}(\mathrm{C_{11}} - \mathrm{C_{66}})} \tag{2.30}$$

The coefficient δ_3 plays the role of Thomsen's δ for [$\mathrm{x_1}$,$\mathrm{x_2}$] horizontal symmetry plane. Note that the quantities for ε and γ in this horizontal symmetry plane would be redundant (Tsvankin, 1997).

2.3.3 Kinematic Parameters

In recent years, full azimuth seismic data processing and interpretation in ORT medium have earned popularity. ORT medium requires more attention on both parameterization and kinematic properties. Hence, experimenting on pure mode waves with azimuth dependent will be conducted in this study, and they will be defined in phase and group domain should they behave differently in the anisotropic medium.

Two kinematic parameters will be analyzed, and those are NMO velocity and anellipticity. These parameters are azimuthally dependent, and they can be expressed in phase and group domains. These parameters are related to the curvatures of the slowness surface computed at the point where both horizontal projections of the slowness vector are zero in the phase domain. In the group domain, these parameters are related to similar curvatures calculated from the travel time surface at zero offsets.

NMO velocity ellipses are known as the first order of curvatures in the group domain (Grechka and Tsvankin, 1998), while anellipticity is the second order of curvatures that responsible for the anelliptic behavior of either slowness or the traveltime surface in the phase domain (nonhyperbolic in the group domain). Here, they will be explained in systematic ways, and all the following formulas are referred to (Stovas, 2016) that has done the research in kinematic parameters of pure- and converted-mode waves for elastic orthorhombic medium.

First of all, P-wave kinematic parameters are calculated. Here, three properties are needed to obtain, those are V_0, V_1, and V_2 which correspond to vertical P-wave velocity and P-wave NMO velocity in the vertical symmetry plane of [x_1,x_3] and [x_2,x_3] respectively. Note that notation 1 and 2 in anisotropy parameters $\varepsilon, \gamma, \delta$ also represent those in [x_1,x_3] and [x_2,x_3] symmetry plane respectively.

$$\begin{aligned} \mathrm{V}_0 &= \mathrm{V}_{p_0}, \\ \mathrm{V}_1^2 &= \mathrm{V}_{p_0}^2(1+2\delta_1), \\ \mathrm{V}_2^2 &= \mathrm{V}_{p_0}^2(1+2\delta_2), \end{aligned} \tag{2.31}$$

Next is to define how to calculate the anellipticity for P-wave,

$$\begin{aligned} \eta_1 &= \frac{(\varepsilon_1-\delta_1)(1+2\delta_1-r_0^2)}{(1+2\delta_1)^2(1-r_0^2)}, \\ \eta_2 &= \frac{(\varepsilon_2-\delta_2)\left[(1+2\delta_2)(1+2\gamma_1)-r_0^2(1+2\gamma_2)\right]}{(1+2\delta_2)^2\left[1+2\gamma_1-r_0^2(1+2\gamma_2)\right]} \\ \eta_{xy} &= \frac{b_0+b_2r_0^2+b_4r_0^4+b_6r_0^6-2r_1r_2r_3}{2(1+2\delta_1)(1+2\delta_2)\left[1+2\gamma_1-r_0^2(1+2\gamma_2)\right]} \end{aligned} \tag{2.32}$$

where,

$$\begin{aligned}
b_0 &= 2(1+2\delta_1)(1+2\delta_2)(1+2\gamma_1),\\
b_2 &= -(1+2\delta_1)(1+2\gamma_2)-(1+2\delta_2)(1+2\gamma_1)\\
&\quad -2(1+2\delta_1)(1+2\delta_2)(1+\gamma_1+\gamma_2)\\
&\quad -2(1+2\gamma_1)(1+2\gamma_2)(1+\delta_1+\delta_2),\\
b_4 &= (1+2\gamma_2)\big[4+2\delta_1+2\delta_2+2\gamma_1+2\gamma_2\\
&\quad +(1+2\delta_1)(1+2\gamma_2)+(1+2\delta_2)(1+2\gamma_1)\big],\\
b_6 &= -2(1+2\gamma_2)^2
\end{aligned} \tag{2.33}$$

For S-wave kinematic properties, the term of S1 and S2 is used instead of saying faster or slower S-waves. They correlate with either C_{55} or C_{44}. The S1-wave is related to the vertical velocity of $\sqrt{C_{55}}$, and the kinematic properties are following the formula below. Note that the notations being used here are also the same as those in P-wave.

$$\begin{aligned}
V_0 &= V_{s_0},\\
V_1^2 &= V_{s_0}^2\Big(1+2\frac{\varepsilon_1-\delta_1}{r_0^2}\Big),\\
V_2^2 &= V_{s_0}^2(1+2\gamma_2),
\end{aligned} \tag{2.34}$$

Next is to define how to calculate anellipticity for S1-wave,

$$\begin{aligned}
\eta_1 &= -\frac{(\varepsilon_1-\delta_1)\,r_0^2\,(1+2\delta_1-r_0^2)}{\Big(1+2\frac{(\varepsilon_1-\delta_1)}{r_0^2}\Big)^2(1-r_0^2)},\\
\eta_2 &= 0,\\
\eta_{xy} &= -\frac{b_0+b_2r_0^2+b_4r_0^4+b_6r_0^6-2r_1r_2r_3}{4r_0^4(1-r_0^2)\Big(1+2\frac{(\varepsilon_1-\delta_1)}{r_0^2}\Big)(\gamma_2-\gamma_1)(1+2\gamma_2)}
\end{aligned} \tag{2.35}$$

where,

$$\begin{aligned}
b_0 &= (1+2\gamma_1)^2\big[(1+2\delta_1)(1+2\delta_2)+(1+2\delta_3)(1+2\varepsilon_1)^2\big],\\
b_2 &= -(1+2\gamma_1)\big[(1+2\delta_1)(1+2\gamma_2)+(1+2\delta_2)(1+2\gamma_1)\\
&\quad +(1+2\gamma_1)\big((1+2\delta_1)(1+\delta_2)(1+\varepsilon_1)(1+2\gamma_2)\big)\\
&\quad +2(1+2\varepsilon_1)(1+2\gamma_2)(1+\delta_3)(1+\varepsilon_1+\gamma_1)\big],\\
b_4 &= (1+2\gamma_1)(1+2\gamma_2)\big[3+2\delta_1+2\delta_2-2(1+2\delta_2)(\gamma_2-\gamma_1)\\
&\quad +2(1+2\gamma_2)(1+\varepsilon_1+\gamma_1)+(1+2\delta_3)(1+2\varepsilon_1)(1+2\gamma_2)\big],\\
b_6 &= -2(1+2\gamma_2)^2(1+2\gamma_1+2\gamma_1\gamma_2)
\end{aligned} \tag{2.36}$$

The last one that need to be calculated is S2-wave kinematic properties. The S2-wave is related to the vertical velocity of $\sqrt{\mathrm{C}_{44}}$, and the kinematic properties are defined below. And again the notation in here is also the same as the other two kinematic properties explained above.

$$\begin{aligned}
\mathrm{V}_0 &= \mathrm{V}_{s_0}\sqrt{\frac{1+2\gamma_2}{1+2\gamma_1}},\\
\mathrm{V}_1^2 &= \mathrm{V}_{s_0}^2(1+2\gamma_2),\\
\mathrm{V}_2^2 &= \mathrm{V}_{s_0}^2\left(\frac{1+2\gamma_2}{1+2\gamma_1}+2\frac{(\varepsilon_2-\delta_2)}{r_0^2}\right),
\end{aligned} \tag{2.37}$$

And finally to define the anellipticity of S2 wave,

$$\begin{aligned}
\eta_1 &= 0,\\
\eta_2 &= -\frac{(\varepsilon_2-\delta_2)\,r_0^2\left[(1+2\delta_2)-\frac{(1+2\gamma_2)}{(1+2\gamma_1)}r_0^2\right]}{(1+2\gamma_1)^2\left[\frac{(1+2\gamma_2)}{(1+2\gamma_1)}+2\frac{(\varepsilon_2-\delta_2)}{r_0^2}\right]^2\left[1-\frac{(1+2\gamma_2)}{(1+2\gamma_1)}r_0^2\right]},\\
\eta_{xy} &= -\frac{b_0+b_2r_0^2+b_4r_0^4+b_6r_0^6-2r_1r_2r_3}{4r_0^4(1+2\gamma_1)\big[1+2\gamma_1-(1+2\gamma_2)r_0^2\big]\left[\frac{(1+2\gamma_2)}{(1+2\gamma_1)}+2\frac{\varepsilon_2-\delta_2)}{r_0^2}\right](\gamma_2-\gamma_1)}
\end{aligned} \tag{2.38}$$

where,

$$\begin{aligned}
b_0 &= (1+2\gamma_1)\big[(1+2\delta_1)(1+2\delta_2)+(1+2\delta_3)(1+2\varepsilon_1)^2\big],\\
b_2 &= -(1+2\delta_1)(1+2\gamma_2)-(1+2\delta_2)(1+2\gamma_1)\\
&\quad -(1+2\gamma_2)\big[(1+2\delta_1)(1+2\delta_2)+(1+2\varepsilon_1)(1+2\gamma_1)\big]\\
&\quad -2(1+2\varepsilon_1)(1+2\gamma_1)(1+2\delta_3)(1+\varepsilon_1+\gamma_2),\\
b_4 &= (1+2\gamma_2)\big[3+2\delta_1+2\delta_2+2(1+2\delta_1)(\gamma_2-\gamma_1)\\
&\quad +2(1+2\gamma_1)(1+\varepsilon_1+\gamma_2)\\
&\quad +(1+2\delta_3)(1+2\varepsilon_1)(1+2\gamma_1)\big],\\
b_6 &= -2(1+2\gamma_2)(1+2\gamma_2+2\gamma_1\gamma_2)
\end{aligned} \tag{2.39}$$

And for all the equations for the kinematic parameters above, r_1, r_2, r_3, and r_0 are defined as:

$$\begin{aligned}
r_1 &= \sqrt{(1-r_0^2)(1+2\delta_1-r_0^2)},\\
r_2 &= \sqrt{\big[1+2\gamma_1-r_0^2(1+2\gamma_2)\big]\big[(1+2\delta_2)(1+2\gamma_1)-r_0^2(1+2\gamma_2)\big]},\\
r_3 &= \sqrt{\big[1+2\varepsilon_1-r_0^2(1+2\gamma_2)\big]\big[(1+2\delta_3)(1+2\varepsilon_1)-r_0^2(1+2\gamma_2)\big]},\\
r_0^2 &= \frac{\mathrm{V}_{s_0}^2}{\mathrm{V}_{p_0}^2}=\frac{\mathrm{C}_{55}}{\mathrm{C}_{33}}
\end{aligned} \tag{2.40}$$

When all the kinematic parameters are obtained, they can be observed in term of azimuthal dependent, and since the study is in anisotropic media, they need to be distinguished between phase and group domain. The difference for these domains can be seen in Figure 2.4. The wavefront has become ellipse and no longer circle comparing with the isotropic medium. The ray path that comes directly from the source is called group velocity, and normal to the wavefront point is called phase velocity.

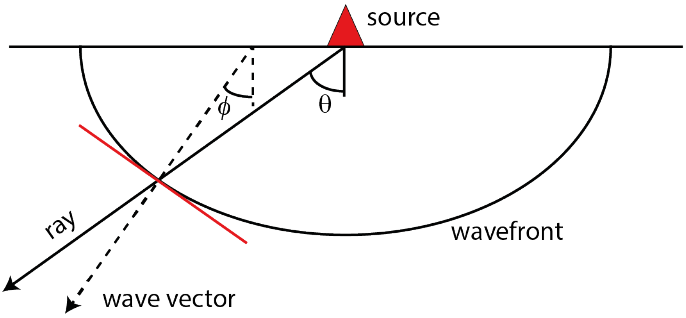

Figure 2.4: Illustration of group and phase velocity in anisotropic media.

The azimuthal kinematic properties in phase domain can be calculated as:

$$\begin{aligned} v_n^2(\phi) &= \mathrm{V}_1^2\cos^2\phi + \mathrm{V}_2^2\sin^2\phi \\ \eta(\phi) &= \frac{\eta_1 \mathrm{V}_1^4\cos^4\phi + \eta_2 \mathrm{V}_2^4\sin^4\phi + \eta_{xy}\mathrm{V}_1^2\mathrm{V}_2^2\sin^2\phi\cos^2\phi}{(\mathrm{V}_1^2\cos^2\phi + \mathrm{V}_2^2\sin^2\phi)^2}, \\ &= \frac{\eta_1 \mathrm{V}_1^4\cos^4\phi + \eta_2 \mathrm{V}_2^4\sin^4\phi + \eta_{xy}\mathrm{V}_1^2\mathrm{V}_2^2\sin^2\phi\cos^2\phi}{v_n^4(\phi)} \end{aligned} \tag{2.41}$$

While the azimuthal kinematic properties in group domain can be calculated as:

$$\begin{aligned} \frac{1}{\mathrm{V}_n^2(\theta)} &= \frac{\cos^2\theta}{\mathrm{V}_1^2} + \frac{\sin^2\theta}{\mathrm{V}_2^2} \\ \eta(\theta) &= \frac{\frac{\eta_1\cos^4\theta}{\mathrm{V}_1^4} + \frac{\eta_2\sin^4\theta}{\mathrm{V}_2^4} + \frac{\eta_{xy}\sin^2\theta\cos^2\theta}{\mathrm{V}_1^2\mathrm{V}_2^2}}{\left(\frac{\cos^2\theta}{\mathrm{V}_1^2} + \frac{\sin^2\theta}{\mathrm{V}_2^2}\right)^2}, \\ &= \mathrm{V}_n^4(\theta)\left(\frac{\eta_1\cos^4\theta}{\mathrm{V}_1^4} + \frac{\eta_2\sin^4\theta}{\mathrm{V}_2^4} + \frac{\eta_{xy}\sin^2\theta\cos^2\theta}{\mathrm{V}_1^2\mathrm{V}_2^2}\right) \end{aligned} \tag{2.42}$$

Chapter 3

Upscaling

Consider a series of thin layered model properties correspond to isotropic velocity model that is much smaller than the seismic wavelength. Such a circumstance will make the seismic wavelength to be unable to detect all those layers individually. However, all those thin layers can be estimated as an effectively homogeneous medium, hence translating it into anisotropy. This procedure to compute the parameters of an effective medium is what is called as an upscaling.

In this study, two ways of performing an upscaling will be tested. Both are used to calculate the effective stiffness coefficient 'C' for each medium, VTI, and ORT. The first one is called classic upscaling that operate by taking the mean value of the data by averaging them. It is often known as Backus Average for calculating effective medium in VTI which can also be applied in ORT. The second one is Least Square, which finds a line that best fits the data trend.

3.1 Classic

Classic upscaling is often known as Backus Average for calculating in VTI medium. It mathematically explained that a stack of homogeneous isotropic layers is equivalent to a homogeneous VTI medium in a long wavelength limit.

From the figure above, H is the length of Backus averaging, which represents the thickness that should be less than one-third of the dominant seismic wavelength (Kumar, 2013). The small thickness of each layer is represented by h$_i$. λ illustrates how the seismic wavelength is unable to represent several thin layers individually.

In term of math, Backus averaging can be explained in the following way. Consider a stack

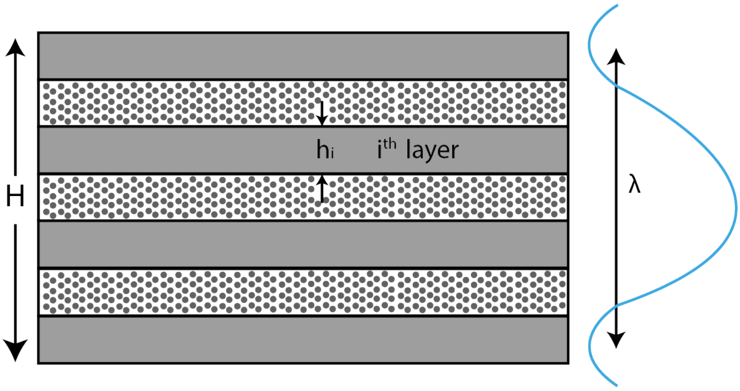

Figure 3.1: A stack of thin layers consisting of two rock types.

of thin layers of VTI symmetry. Then, define the equation of motion in 1D medium,

$$\frac{db}{dz} = i\omega A_i b \tag{3.1}$$

where b is the vector displacement and particle velocity projections, ω is the frequency and A_j is the 4x4 matrix of the medium parameters (for layer j) with the following symmetry,

$$A_i = \begin{bmatrix} 0 & M_j \\ N_j & 0 \end{bmatrix} \tag{3.2}$$

with matrices M_j and N_j expressed as 2x2 matrix. Upscaling results in arithmetic averaging of matrix A, assuming that each of the layers is weighted equally, it can be written as,

$$\tilde{A} = \langle A_i \rangle = \frac{1}{H} \sum_{i=1}^{N} h_i A_i \tag{3.3}$$

where H and h represent the stack of layers and individual layers respectively. The i represent the -th layer, which is being calculated.

3.1.1 Classic Upscaling for VTI

These equations are used to calculate the effective ’C’ for VTI medium (Kumar, 2013).

$$\begin{aligned}
\mathrm{C}^{e}_{33} &= \left\langle \frac{1}{\mathrm{C}_{33}} \right\rangle^{-1}, \\
\mathrm{C}^{e}_{44} = \mathrm{C}^{e}_{55} &= \left\langle \frac{1}{\mathrm{C}_{44}} \right\rangle^{-1}, \\
\mathrm{C}^{e}_{13} = \mathrm{C}^{e}_{23} &= \left\langle \frac{\mathrm{C}_{13}}{\mathrm{C}_{33}} \right\rangle \left\langle \frac{1}{\mathrm{C}_{33}} \right\rangle^{-1}, \\
\mathrm{C}^{e}_{66} &= \langle \mathrm{C}_{66} \rangle, \\
\mathrm{C}^{e}_{11} = \mathrm{C}^{e}_{22} &= \langle \mathrm{C}_{11} \rangle + \left\langle \frac{\mathrm{C}_{13}}{\mathrm{C}_{33}} \right\rangle^{2} \left\langle \frac{1}{\mathrm{C}_{33}} \right\rangle^{-1} - \left\langle \frac{\mathrm{C}^{2}_{13}}{\mathrm{C}_{33}} \right\rangle, \text{ and} \\
\mathrm{C}^{e}_{12} &= \mathrm{C}^{e}_{11} - 2\,\mathrm{C}^{e}_{66}
\end{aligned} \tag{3.4}$$

3.1.2 Classic Upscaling for ORT

The following equations are used to calculate the effective ’C’ for ORT medium (Kumar, 2013).

$$\begin{aligned}
\mathrm{C}^{\mathrm{e}}_{33} &= \left\langle \frac{1}{\mathrm{C}_{33}} \right\rangle^{-1}, \\
\mathrm{C}^{\mathrm{e}}_{44} &= \left\langle \frac{1}{\mathrm{C}_{44}} \right\rangle^{-1}, \\
\mathrm{C}^{\mathrm{e}}_{55} &= \left\langle \frac{1}{\mathrm{C}_{55}} \right\rangle^{-1}, \\
\mathrm{C}^{\mathrm{e}}_{13} &= \left\langle \frac{\mathrm{C}_{13}}{\mathrm{C}_{33}} \right\rangle \left\langle \frac{1}{\mathrm{C}_{33}} \right\rangle^{-1}, \\
\mathrm{C}^{\mathrm{e}}_{23} &= \left\langle \frac{\mathrm{C}_{23}}{\mathrm{C}_{33}} \right\rangle \left\langle \frac{1}{\mathrm{C}_{33}} \right\rangle^{-1}, \\
\mathrm{C}^{\mathrm{e}}_{66} &= \langle \mathrm{C}_{66} \rangle, \\
\mathrm{C}^{\mathrm{e}}_{11} &= \langle \mathrm{C}_{11} \rangle + \left\langle \frac{\mathrm{C}_{13}}{\mathrm{C}_{33}} \right\rangle^{2} \left\langle \frac{1}{\mathrm{C}_{33}} \right\rangle^{-1} - \left\langle \frac{\mathrm{C}^{2}_{13}}{\mathrm{C}_{33}} \right\rangle, \\
\mathrm{C}^{\mathrm{e}}_{22} &= \langle \mathrm{C}_{22} \rangle + \left\langle \frac{\mathrm{C}_{23}}{\mathrm{C}_{33}} \right\rangle^{2} \left\langle \frac{1}{\mathrm{C}_{33}} \right\rangle^{-1} - \left\langle \frac{\mathrm{C}^{2}_{23}}{\mathrm{C}_{33}} \right\rangle, \text{ and} \\
\mathrm{C}^{\mathrm{e}}_{12} &= \langle \mathrm{C}_{12} \rangle + \left\langle \frac{\mathrm{C}_{13}}{\mathrm{C}_{33}} \right\rangle \left\langle \frac{\mathrm{C}_{23}}{\mathrm{C}_{33}} \right\rangle \left\langle \frac{1}{\mathrm{C}_{33}} \right\rangle^{-1} - \left\langle \frac{\mathrm{C}_{13}\mathrm{C}_{23}}{\mathrm{C}_{33}} \right\rangle
\end{aligned} \tag{3.5}$$

3.2 Least Square

The method of Least Square is a form of mathematical regression analysis which finds the line of best fit for a set of data. It provides the overall rationale for the placement of the line of best fit among the data points being studied.

Suppose there are ’n’ data points that can be modeled by first-degree polynomial,

$$y = ax + b, \tag{3.6}$$

Here, there are unknown coefficients of a and b that need to be solved. A ’F’ function can be written as a system of ’n’ simultaneous linear equations in two unknowns of ’a’ and ’b’,

$$F = \sum_{i=1}^{n} (y_i - ax_i - b)^2 \tag{3.7}$$

Since the Least Square fitting process minimize the summed square of the residuals, the coefficients are determined by differentiating ’F’ with respect to each parameter and setting the result equal to zero,

$$\frac{\partial F}{\partial a} = 2\sum_{i=1}^{n} -x_i(y_i - ax_i - b) = 0 \tag{3.8}$$

$$\frac{\partial F}{\partial b} = 2\sum_{i=1}^{n} -1 \ \ (y_i - ax_i - b) = 0 \tag{3.9}$$

Hence, equation (3.8) and (3.9) become:

$$\sum_{i=1}^{n} x_i(y_i - ax_i - b) = 0 \tag{3.10}$$

$$\sum_{i=1}^{n} (y_i - ax_i - b) = 0 \tag{3.11}$$

where the summation run from i = 1 to n. The normal equation are defined as:

$$\sum x_i y_i = a\sum x_i^2 + b\sum x_i \tag{3.12}$$

$$\sum y_i = a\sum x_i + bn \tag{3.13}$$

From here, elimination process can be done to solve 'a':

$$a = \frac{n \sum x_i y_i - \sum x_i \sum y_i}{n \sum x_i^2 - \left(\sum x_i\right)^2} \tag{3.14}$$

Finally, 'b' can be solved using the 'a' value, such that:

$$b = \frac{1}{n}\left(\sum y_i - a \sum x_i\right) \tag{3.15}$$

3.2.1 Least Square Upscaling for VTI

In this study, 'a' and 'b' will be solved for every data of stiffness coefficients. First, every calculation for stiffness coefficients is gathered as a new curve in log data. For example, $\frac{1}{\mathrm{C}_{33}}$ will be calculated first and stored as a new curve in log data. Then, 'a' and 'b' are calculated at a targeted interval for solving C^e_{33} using the data points from curve $\frac{1}{\mathrm{C}_{33}}$.

Since each C^e_{ij} have different requirements to be solved, new 'a' and 'b' needs to be calculated which depend on the new curve that is required to solve certain C^e_{ij}.

The following formulas are used to obtain the C^e_{ij} for VTI medium as a function of x (depth):

$$\begin{aligned}
\mathrm{C}^e_{33} &= \left\langle \frac{1}{\mathrm{C}_{33}} \right\rangle^{-1} = \frac{1}{\mathrm{a}_1\mathrm{x}+\mathrm{b}_1},\\
\mathrm{C}^e_{44} = \mathrm{C}^e_{55} &= \left\langle \frac{1}{\mathrm{C}_{44}} \right\rangle^{-1} = \frac{1}{\mathrm{a}_2\mathrm{x}+\mathrm{b}_2},\\
\mathrm{C}^e_{13} = \mathrm{C}^e_{23} &= \left\langle \frac{\mathrm{C}_{13}}{\mathrm{C}_{33}} \right\rangle \left\langle \frac{1}{\mathrm{C}_{33}} \right\rangle^{-1} = \frac{\mathrm{a}_3\mathrm{x}+\mathrm{b}_3}{\mathrm{a}_1\mathrm{x}+\mathrm{b}_1},\\
\mathrm{C}^e_{66} &= \langle \mathrm{C}_{66} \rangle = \mathrm{a}_4\mathrm{x}+\mathrm{b}_4,\\
\mathrm{C}^e_{11} = \mathrm{C}^e_{22} &= \langle \mathrm{C}_{11} \rangle + \left\langle \frac{\mathrm{C}_{13}}{\mathrm{C}_{33}} \right\rangle^2 \left\langle \frac{1}{\mathrm{C}_{33}} \right\rangle^{-1} - \left\langle \frac{\mathrm{C}^2_{13}}{\mathrm{C}_{33}} \right\rangle\\
&= (\mathrm{a}_5\mathrm{x}+\mathrm{b}_5) + \frac{(\mathrm{a}_3\mathrm{x}+\mathrm{b}_3)^2}{\mathrm{a}_1\mathrm{x}+\mathrm{b}_1} - (\mathrm{a}_6\mathrm{x}+\mathrm{b}_6),\\
\mathrm{C}^e_{12} &= \mathrm{C}^e_{11} - 2\mathrm{C}^e_{66}
\end{aligned} \tag{3.16}$$

3.2.2 Least Square Upscaling for ORT

For ORT medium, the concept of obtaining the 'a' and 'b' are the same as it explained in VTI medium. The following formula are used to obtain the C^e_{ij} for VTI medium as a function of x (depth):

$$
\begin{aligned}
\mathrm{C}^e_{33} &= \left\langle \frac{1}{\mathrm{C}_{33}} \right\rangle^{-1} = \frac{1}{\mathrm{a}_1\mathrm{x}+\mathrm{b}_1},\\
\mathrm{C}^e_{44} &= \left\langle \frac{1}{\mathrm{C}_{44}} \right\rangle^{-1} = \frac{1}{\mathrm{a}_2\mathrm{x}+\mathrm{b}_2},\\
\mathrm{C}^e_{55} &= \left\langle \frac{1}{\mathrm{C}_{55}} \right\rangle^{-1} = \frac{1}{\mathrm{a}_3\mathrm{x}+\mathrm{b}_3},\\
\mathrm{C}^e_{13} &= \left\langle \frac{\mathrm{C}_{13}}{\mathrm{C}_{33}} \right\rangle \left\langle \frac{1}{\mathrm{C}_{33}} \right\rangle^{-1} = \frac{\mathrm{a}_4\mathrm{x}+\mathrm{b}_4}{\mathrm{a}_1\mathrm{x}+\mathrm{b}_1},\\
\mathrm{C}^e_{23} &= \left\langle \frac{\mathrm{C}_{23}}{\mathrm{C}_{33}} \right\rangle \left\langle \frac{1}{\mathrm{C}_{33}} \right\rangle^{-1} = \frac{\mathrm{a}_5\mathrm{x}+\mathrm{b}_5}{\mathrm{a}_1\mathrm{x}+\mathrm{b}_1},\\
\mathrm{C}^e_{66} &= \langle \mathrm{C}_{66} \rangle = \mathrm{a}_6\mathrm{x}+\mathrm{b}_6, \qquad (3.17)\\
\mathrm{C}^e_{11} &= \langle \mathrm{C}_{11} \rangle + \left\langle \frac{\mathrm{C}_{13}}{\mathrm{C}_{33}} \right\rangle^2 \left\langle \frac{1}{\mathrm{C}_{33}} \right\rangle^{-1} - \left\langle \frac{\mathrm{C}^2_{13}}{\mathrm{C}_{33}} \right\rangle\\
&= (\mathrm{a}_7\mathrm{x}+\mathrm{b}_7) + \frac{\mathrm{a}_4\mathrm{x}+\mathrm{b}_4}{\mathrm{a}_1\mathrm{x}+\mathrm{b}_1} - (\mathrm{a}_8\mathrm{x}+\mathrm{b}_8),\\
\mathrm{C}^e_{22} &= \langle \mathrm{C}_{22} \rangle + \left\langle \frac{\mathrm{C}_{23}}{\mathrm{C}_{33}} \right\rangle^2 \left\langle \frac{1}{\mathrm{C}_{33}} \right\rangle^{-1} - \left\langle \frac{\mathrm{C}^2_{23}}{\mathrm{C}_{33}} \right\rangle\\
&= (\mathrm{a}_9\mathrm{x}+\mathrm{b}_9) + \frac{\mathrm{a}_5\mathrm{x}+\mathrm{b}_5}{\mathrm{a}_1\mathrm{x}+\mathrm{b}_1} - (\mathrm{a}_{10}\mathrm{x}+\mathrm{b}_{10}),\\
\mathrm{C}^e_{12} &= \langle \mathrm{C}_{12} \rangle + \left\langle \frac{\mathrm{C}_{13}}{\mathrm{C}_{33}} \right\rangle \left\langle \frac{\mathrm{C}_{23}}{\mathrm{C}_{33}} \right\rangle \left\langle \frac{1}{\mathrm{C}_{33}} \right\rangle^{-1} - \left\langle \frac{\mathrm{C}_{13}\mathrm{C}_{23}}{\mathrm{C}_{33}} \right\rangle,\\
&= (\mathrm{a}_{11}\mathrm{x}+\mathrm{b}_{11}) + \frac{(\mathrm{a}_4\mathrm{x}+\mathrm{b}_4)(\mathrm{a}_5\mathrm{x}+\mathrm{b}_5)}{\mathrm{a}_1\mathrm{x}+\mathrm{b}_1} - (\mathrm{a}_{12}\mathrm{x}+\mathrm{b}_{12})
\end{aligned}
$$

Chapter 4

Dix-Type Equations

In practice of seismic acquisition, several reflections are recorded on seismic seismogram in the function of time. If a horizontally layered mediums are considered, these travel time functions can be processed and converted into layer parameters. Such procedure is famously known as (Dix, 1955) inversion.

(Stovas, 2015) derived the effective properties formulas in ORT medium that can be computed by the Dix-type equations. In this study, the ORT medium that is about to introduced is assumed to have the same azimuthal orientation in each layers. The effective NMO velocity can be computed as,

$$\begin{aligned} \mathrm{V}_0^2\,\mathrm{T}_0 &= \sum \mathrm{v}_{0j}^2 \mathrm{t}_{0j}\;, \\ \mathrm{V}_1^2\,\mathrm{T}_0 &= \sum \mathrm{v}_{1j}^2 \mathrm{t}_{0j}\;, \\ \mathrm{V}_2^2\,\mathrm{T}_0 &= \sum \mathrm{v}_{2j}^2 \mathrm{t}_{0j}\;, \end{aligned} \tag{4.1}$$

where t_{0j} is the interval travel time in layer j that calculated along the zero-offset ray. T_0 is the total travel time for the accounted layers. v_0, v_1, and v_2 are the vertical and NMO velocities for each layer. V_1 and V_2 are the effective NMO velocities. Note that the subscript 1 and 2 on the NMO velocities are relevant to those discussed in subsection 2.3.3. The t_{0j} and T_0 can be defined as,

$$\begin{aligned} \mathrm{t}_{0j} &= \frac{2\mathrm{z}_j}{\mathrm{v}_{0j}}\;, \\ \mathrm{T}_0 &= \sum \mathrm{t}_{0j} \end{aligned} \tag{4.2}$$

For anelliptic parameters, they are defined as,

$$\begin{aligned} \mathrm{N}_1 &= \frac{1}{8}\left(\frac{1}{\mathrm{V}_1^4\mathrm{T}_0}\sum(1+8\eta_1)\mathrm{v}_{1j}^4\mathrm{t}_{0j}-1\right), \\ \mathrm{N}_2 &= \frac{1}{8}\left(\frac{1}{\mathrm{V}_2^4\mathrm{T}_0}\sum(1+8\eta_2)\mathrm{v}_{2j}^4\mathrm{t}_{0j}-1\right), \\ \mathrm{N}_{xy} &= \frac{1}{4}\left(\frac{1}{\mathrm{V}_1^2\mathrm{V}_2^2\mathrm{T}_0}\sum(1+4\eta_{xy})\mathrm{v}_{1j}^2\mathrm{v}_{2j}^2\mathrm{t}_{0j}-1\right), \end{aligned} \tag{4.3}$$

Further explanation is given through Figure 4.1 to illustrate the notation for performing Dix calculations.

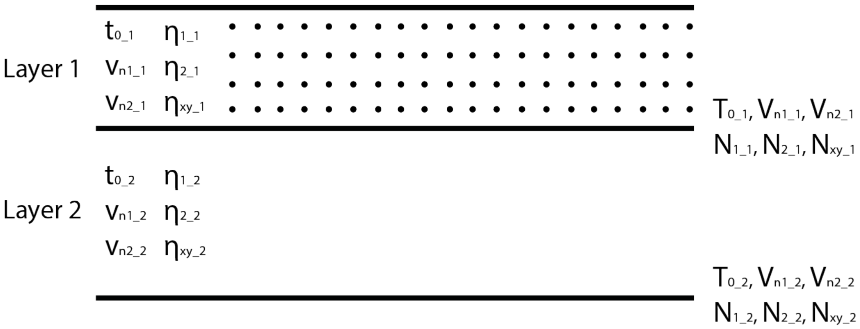

Figure 4.1: A horizontally layered model. The capital letters on the right side that are attached next to the reflector stand for kinematic parameters computed from corresponding reflector. Small letters inside the layers describe the kinematic parameters related to the individual layers.

Chapter 5

Data

In this chapter, the information about the data that is used in this study is provided. The first section is going to discuss the type of data that is available for this study, followed by the condition of the data itself, whether if it is a good data or should there be any necessary steps required to condition the data that seems to be logically impossible to exist.

Afterward, general observation and interpretation regarding the available data are discussed, followed by selecting the interval of the data that is going to be the main target of the study. Lastly, the methods that are conducted in this data will be defined.

5.1 Data Availability

In this study, log data is provided with a measurement that is reaching 2220 m deep. It can be seen in Figure 5.1 and consists of GR, density, Vp, Vs, and anisotropy parameters of epsilon, gamma, and delta. In total, the data sample for each curve reaches 12165 samples.

5.2 Log Conditioning

Log conditioning is done before some data that seems to be unrealistic. These unrealistic data are often observed as spike, which mostly caused as a miscalculation from the tool itself. However, the approach to removing this spike is limited to any number that contains -999 value and anisotropy parameters with value reach above one. This is due to the lack of information about lithology or well report.

Figure 5.2 are the log data after conditioning. Some of the data samples are removed, leaving to 11461 samples left.

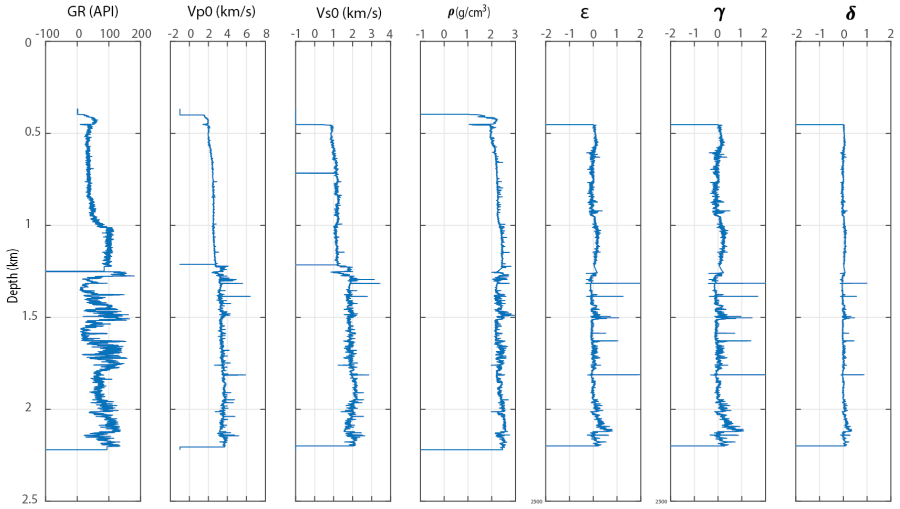

Figure 5.1: Original log data.

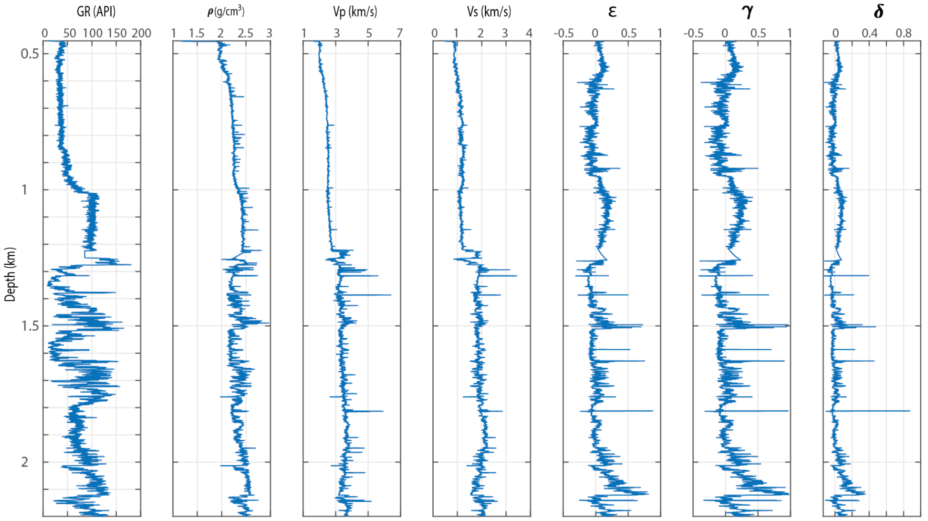

Figure 5.2: Log data after conditioning.

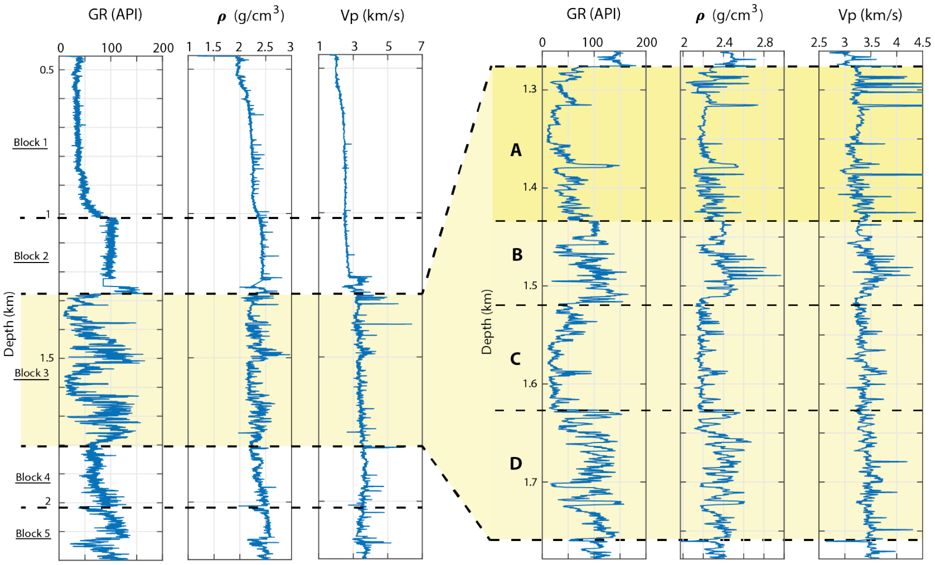

Figure 5.3: Zonation of the log data. The highlighted light yellow area is assume to be the reservoir which interpreted based on the GR and other log data. Dark yellow area represent the main target for this study.

5.3 Defining the Method

Here in this section, the methods that are performed on the log data set are explained. Two subsection are discussed, the first one is creating zonation that divide the log data set into several blocks is conducted. Following with that, a general observation regarding to the data availability in the targeted zone is also executed. The second one is to illustrate how classic and least square upscaling are performed in the log data set.

5.3.1 Zonation and Data Observation

Dividing the log into several blocks is done by observing the trend of log data, mainly focusing on GR. The target block for this study is the interval that resembles reservoir characteristic, which consists of sand and shale lithology, and it is highlighted in Figure 5.3 marked in the yellow area.

The thickness of the study interval reaches 495 m that start from the depth of 1275 m to 1770 m. Further zonation is done prior to changes in data trend. Here, block A with a depth interval of 1275 m to 1430 m is the main target of this study to be experimented with, and it is highlighted in the dark yellow area.

In data observation, anisotropy parameters obtained from the log are calculated for the highlighted area. By analyzing the anisotropy parameters obtained from the log in Fig-

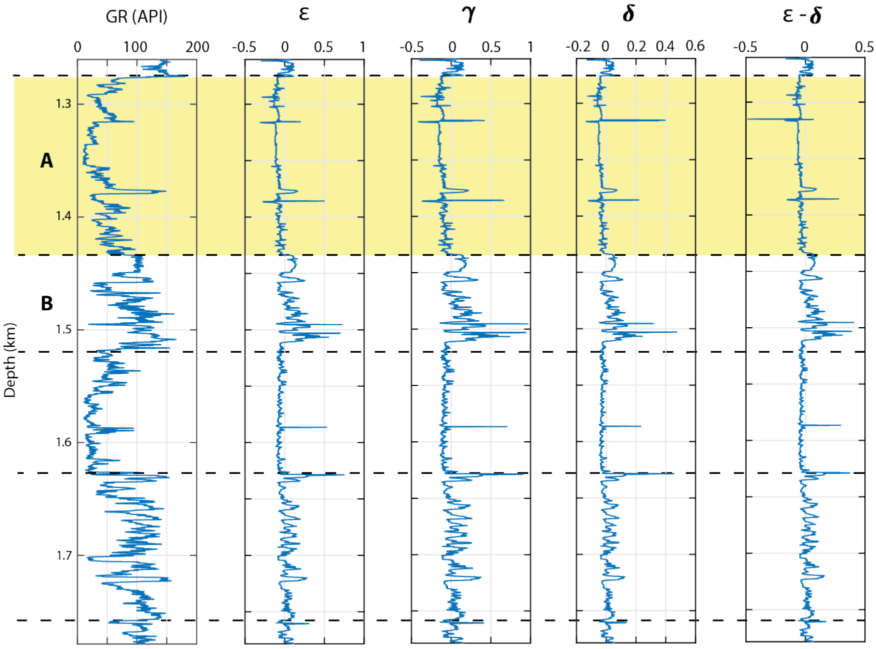

Figure 5.4: Data observation for anisotropy parameters in the area of study.

ure 5.4, one can notice that the value of $\varepsilon - \delta < 0$. This condition is actually not common for VTI condition that is dominated by shale, which corresponds to laboratory data experimented by (Wang, 2002). However, in this experiment, such condition is possible to appear in brine-saturated reservoir sand where essentially the reservoir is clay-free. Such condition indicates a very little intrinsic anisotropy exists in unfractured or clay free reservoir rocks such as sandstone.

Given the condition stated above and with the interval dominated by low GR value, block 3-A represents much of a sandstone reservoir with little clay-bearing. This situation leads to an interpretation of a sandstone reservoir, which is intrinsically isotropic, and it explains why the value of $\varepsilon - \delta$ is less than zero.

5.3.2 Classic and Least Square Upscaling

Two methods for upscaling are introduced, classic and least square upscaling. An illustration of those is provided in Figure 5.5. The log data are within the interval of block 3, and P-wave velocities are shown to illustrate how the upscaling work in the data. Starting from the left, (a) is the original Vp after log conditioning is performed, (b) is the classic upscaling of Backus average in VTI background for the entire block 3, (c) is the classic upscaling in ORT medium, and (d) is the least square upscaling in ORT medium. The log data in (a) represents the raw data measured from the log while (b), (c), and (d) represent

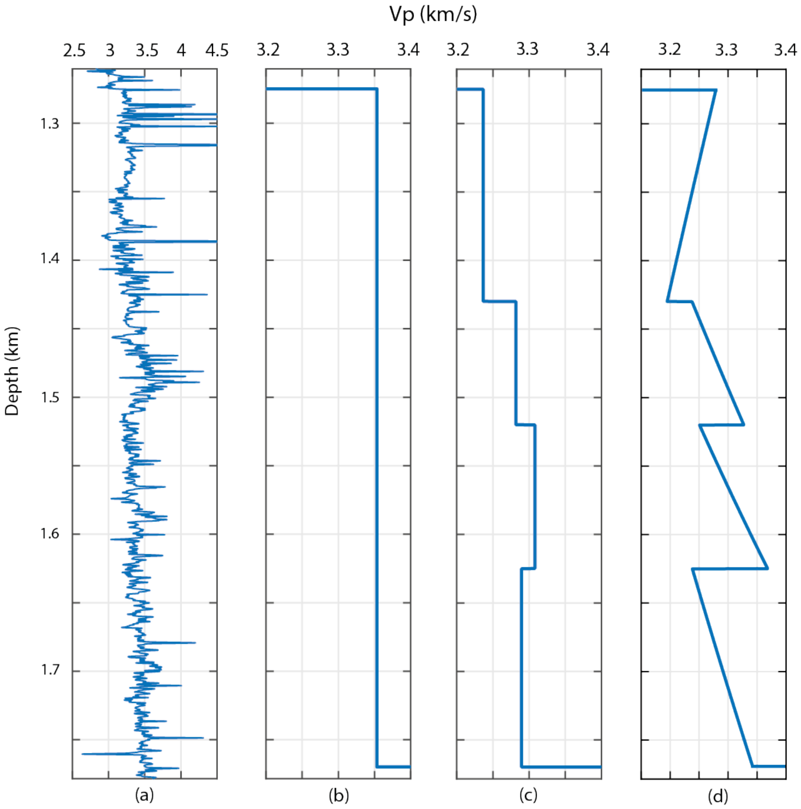

Figure 5.5: Upscaling illustration in log data. (a) Original Vp after conditioned, (b) Classic upscaling in VTI medium, (c) Classic upscaling in ORT medium, (d) Least square upscaling in ORT medium. Scale are adjusted to emphasize the differences.

the effective parameter measured after upscaling method is performed.

Note that there is a significant difference when upscaling is performed for the entire block 3 and when it is implemented in each divided interval that is based on the different data trendline. The latest approach suggests the better way of performing upscaling as the log data shows different trendline for each interval in block 3.

5.3.3 Fracturing After and Before Upscaling

Two approaches to introducing the fractures are suggested. The first one is to perform upscaling on VTI layers at the beginning in order to get the effective parameters of stiffness coefficients according to Equation 3.4 or Equation 3.16. Afterward, fracture parameters are introduced to the obtained effective stiffness matrix that makes the medium become ORT by using Equation 2.21.

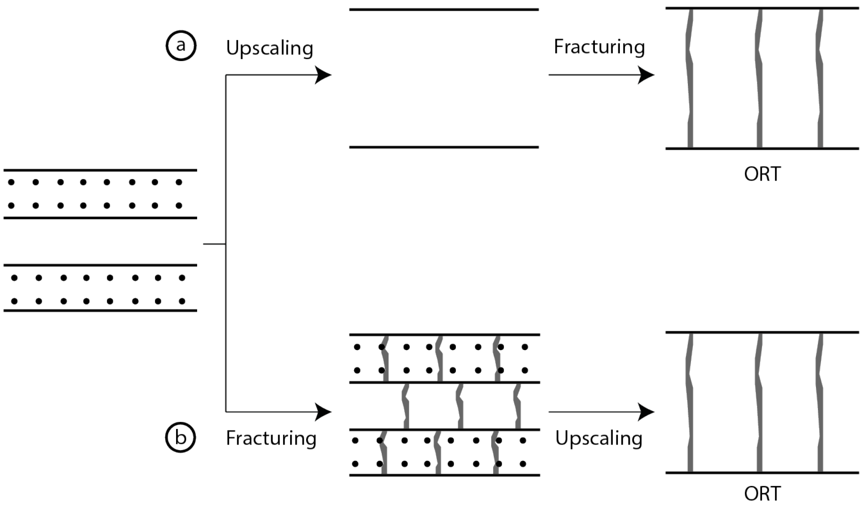

Figure 5.6: Illustration for fracturing approaches. a) Fractures are introduced later b) Fractures are introduced first.

The second one is to introduce fracture parameters at the beginning for every data sample of stiffness coefficients, which creates ORT layers by using Equation 2.21. After that, upscaling on ORT layers are computed in order to get the effective parameters of stiffness coefficients according to Equation 3.5 or Equation 3.17. Once each of the approaches is done, anisotropy parameters of the ORT medium can be obtained, and the kinematic parameters calculation for P- and S-waves will proceed.

Illustration for this approach is given in Figure 5.6. A similar approach has been conducted by (Ivanov and Stovas, 2016) for investigating the influence of fracturing on P-wave anellipticity parameters in full azimuth surveys.

Chapter 6

Fracturing

This chapter explains how fracturing in a targeted zone is done. In addition to that, the respond of a medium before fracturing is introduced is also observed beforehand. Fracturing is introduced based on Schoenberg-Helbig model that is explained in section 2.3. There are two approaches to be tested for introducing the fractures. The first one is to introduce the fractures after upscaling method is performed, and the second one is to introduce the fractures before upscaling method is performed. Furthermore, the calculation of two upscaling methods, classic and least square, are also provided in this chapter.

All of the calculations from upscaling and fracturing are shown here. The calculations include stiffness coefficients C$_{ij}$, anisotropy parameters in the effective medium, and kinematic parameters in group and phase domain.

6.1 Preliminary Consideration

First and foremost, in order to get not confused, preliminary consideration will be determined in defining the symmetry plane of the anisotropy medium. Such is required because some sources also have their own consideration that is different from others.

When fractures are introduced following Schoenberg-Helbig model, the fractures will be set as vertical fractures that aligned parallel to one of the vertical symmetry plane, as shown in Figure 6.1.

Here, [x$_1$,x$_3$], [x$_2$,x$_3$], represent vertical symmetry plane that is parallel to the fractures and perpendicular to the fractures respectively while [x$_1$,x$_2$] represent horizontal symmetry plane. [x$_1$,x$_3$], [x$_2$,x$_3$], and [x$_1$,x$_2$] are short noted as 1,2, and 3 respectively in any necessary equation.

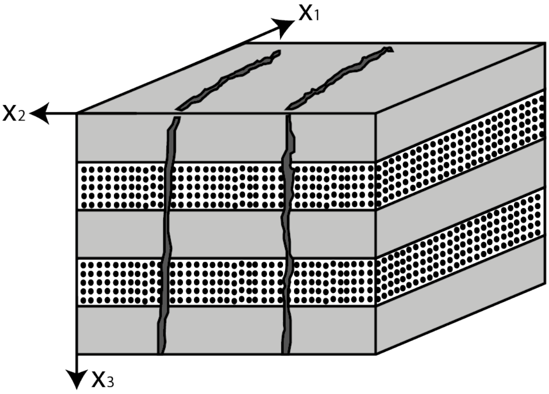

Figure 6.1: Notation agreement.

6.2 Upscaling for VTI Medium

It is known that the log data from chapter 5 are the VTI parameters. Hence, upscaling in a VTI medium is the first step that needs to be calculated. This step is needed to acquire the background medium that will be fractured later on and become ORT medium. The steps of this process can be listed as follow:

1. Calculate C$_{ij}$ for every sample in log data using the known vertical velocity of P-wave and S-wave, anisotropy parameters, and density. The formulas for calculating this are referred to Equation 2.9 and Equation 2.10.

2. Perform upscaling of C$_{ij}$ that have been obtained including density. The formulas for this calculation are referred to Equation 3.4 for classic upscaling and Equation 3.5 for least square upscaling.

3. Calculate the anisotropy parameters for effective medium following Thomsen's parameters, effective C$_{ij}$ that have been obtained previously is used. The formula is referred to Equation 2.11 and Equation 2.12.

4. Lastly, kinematic parameters are calculated to observe how pure mode waves behave when fractures are not introduced yet and compared later on with fractured medium.

The first step is done in order to obtain background parameters which represented as stiffness coefficient and the results of this calculation can be seen in Figure 6.2.

6.2.1 Classic Upscaling in VTI

Once all the required C$_{ij}$ are obtained, upscaling process is conducted and in this section, classic upscaling or also known as Backus averaging is used. The calculation for this step is done in block 3-A and the results can be seen in the matrix 6.1 below.

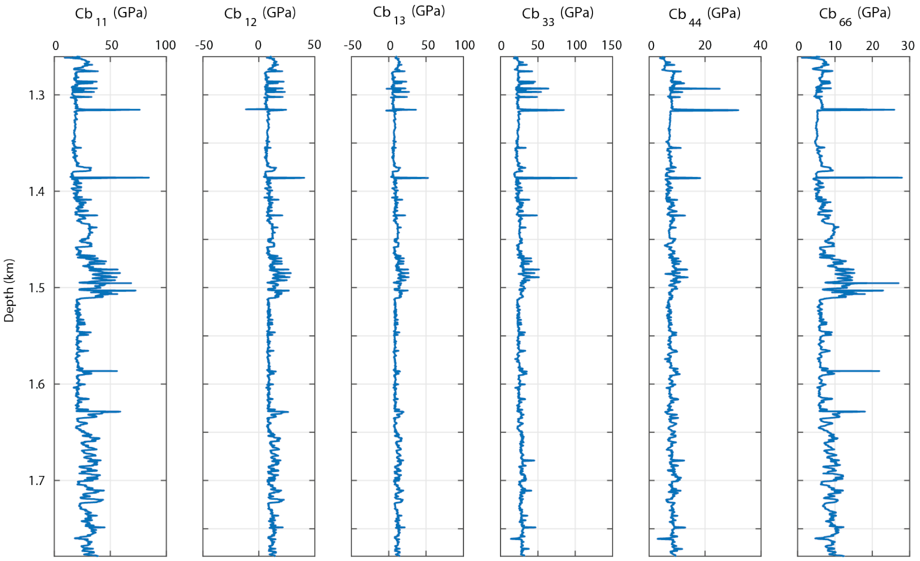

Figure 6.2: C_{ij} calculation for every sample in log data which highlighted the interval of block 3. The scale of C_{ij} are in Giga Pascal (GPa).

$$C_b^e = \begin{bmatrix} 20.32 & 8.140 & 7.762 & 0 & 0 & 0 \\ 8.140 & 20.320 & 7.762 & 0 & 0 & 0 \\ 7.762 & 7.762 & 24.008 & 0 & 0 & 0 \\ & 0 & 0 & 7.644 & 0 & 0 \\ & 0 & 0 & 0 & 7.644 & 0 \\ & 0 & 0 & 0 & 0 & 6.090 \end{bmatrix} \tag{6.1}$$

Notice that some of the C_{ij} have the same values. These results are an indication that the medium is homogeneous in one of the axis; for this case, it is homogeneous horizontally. For example, C_{11} and C_{22} are the stiffness coefficients that correspond to a P-wave velocity that is propagating in x_1 and x_2 direction respectively. The same value for these two C_{ij} indicate that the medium is invariant in the horizontal axis, causing the velocities of P-wave in these directions to become equal.

By utilizing the upscaled C_{ij} for calculating anisotropy parameters as referred to Equation 2.11 and Equation 2.12, it gives the effective parameters for this medium. Hence, the effective parameters for the background medium in this study are acquired and shown in Table 6.1.

After obtaining the effective medium parameters, kinematic parameters are calculated with formulas referred to those explained in subsection 2.3.3. However, as this calculations are now currently in VTI medium, the anisotropy parameters in both vertical symmetry plane

Block 3-A	ρ^e (g/cc)	V^e_{p0} (km/s)	V^e_{s0} (km/s)	ε^e	γ^e	δ^e
VTI effective	2.249	3.267	1.843	-0.0768	-0.1017	-0.0387

Table 6.1: Effective anisotropy parameters for VTI as background medium, block 3-A. The results are calculated using classic upscaling.

	VTI 3-A					
	V_0 (km/s)	V_1 (km/s)	V_2 (km/s)	η_1	η_2	η_{xy}
P wave	3.2670	3.1380	3.1380	-0.0397	-0.0397	-0.0794
S1 wave	1.8436	1.6079	1.6079	-0.1197	-0.1197	-0.2394
S2 wave	1.8436	1.6455	1.6455	0	0	0

Table 6.2: Kinematic parameters for VTI as background medium, block 3-A. The results are calculated using classic upscaling.

are equal. Hence, $\varepsilon_1 = \varepsilon_2 = \varepsilon^e$; $\gamma_1 = \gamma_2 = \gamma^e$; and $\delta_1 = \delta_2 = \delta^e$. Furthermore, as in VTI medium the layers are isotropic horizontally, δ_3 is then become 0 and it is proven by calculating it from C^e_b in matrix 6.1 by applying Equation 2.30. The results of this kinematic parameters are shown in Table 6.2.

Once the kinematic parameters are obtained, they are plotted in a polar plot which illustrates the azimuthal dependence for given quantity with the azimuth angle measured from the horizontal axis. These are all applied for any polar plot figures presented in this study.

Figure 6.3 shows the results of the azimuth-dependent of kinematic parameters which calculated using classic upscaling. The results are presented in phase and group domain. Note that there are no changes given in phase or group domain and the NMO velocities wavefront are appear to be circle rather than an ellipse. Such results correspond to homogeneity along the horizontal axis in the VTI medium.

6.2.2 Least Square Upscaling in VTI

A similar procedure is presented in this section with the difference in the upscaling method being used. Here, in matrix 6.2, the effective stiffness coefficients are very similar to those computed using classic upscaling. Similar results also appear in the effective anisotropy parameters and kinematic parameters when computed using classic upscaling. Such results suggest that least square upscaling provide similar results with an insignificant difference that can be negligible when compared with classic upscaling.

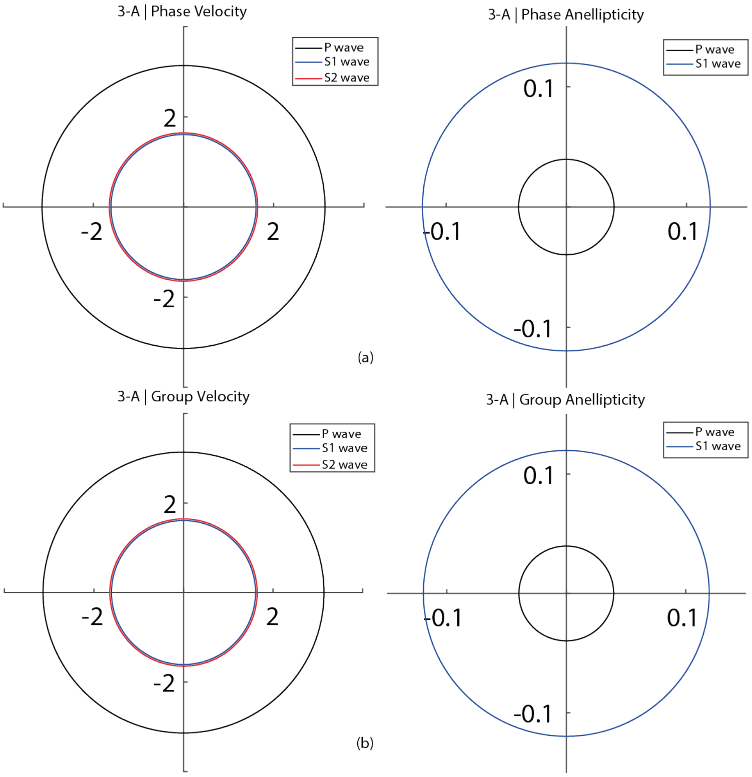

Figure 6.3: Azimuth dependent of kinematic parameters of pure mode waves using classic upscaling on VTI medium. Left images are V$_{nmo}$ and right images are anellipticity. (a) Parameters on phase domain (b) Parameters on group domain.

	ρ^e (g/cc)	V$^e_{p0}$ (km/s)	V$^e_{s0}$ (km/s)	ε^e	γ^e	δ^e
VTI effective	2.249	3.267	1.845	-0.0762	-0.1014	-0.0375

Table 6.3: Effective anisotropy parameters for VTI as background medium. The results are calculated using least square upscaling.

	VTI 3-A					
	V$_0$ (km/s)	V$_1$ (km/s)	V$_2$ (km/s)	η_1	η_2	η_{xy}
P wave	3.2670	3.1421	3.1421	-0.0402	-0.0402	-0.0804
S1 wave	1.8459	1.6065	1.6065	-0.1202	-0.1202	-0.2404
S2 wave	1.8459	1.6454	1.6454	0	0	0

Table 6.4: Kinematic parameters for VTI as background medium. The results are calculated using least square upscaling.

$$\mathrm{C^e_b} = \begin{bmatrix} 20.341 & 8.160 & 7.753 & 0 & 0 & 0 \\ 8.160 & 20.341 & 7.753 & 0 & 0 & 0 \\ 7.753 & 7.753 & 24.011 & 0 & 0 & 0 \\ & 0 & 0 & 7.663 & 0 & 0 \\ & 0 & 0 & 0 & 7.663 & 0 \\ & 0 & 0 & 0 & 0 & 6.090 \end{bmatrix} \tag{6.2}$$

Figure 6.4 shows further evidence and illustrations of kinematic parameters that is again similar to those calculated using classic upscaling in Figure 6.3. In Figure 6.5, a polar plot of both calculations from classic and least square upscaling in VTI medium are provided to be compared. The plot suggests that both methods are applicable for performing upscaling as they are overlapping with each other.

6.3 Introducing Fracture After Upscaling

Once the stiffness coefficients from VTI medium are obtained, they are used as background parameters for further calculation in ORT medium. Here, a set of vertical fractures are added after upscaling of stiffness coefficients in VTI medium are done.

For placing the fractures in the area of study, normal fracture weakness (Δ_N) is set to 0.15, and tangential (vertical, Δ_V and horizontal, Δ_H) weaknesses are set to 0.2 assuming the fractures are rotationally invariant. As it already discussed, once the VTI medium is introduced with fractures, it will become ORT medium, and matrix (6.3) and (6.4) shows the stiffness coefficient of the effective ORT medium that is obtained by using classic (U$_2$) and least square (U$_3$) upscaling.

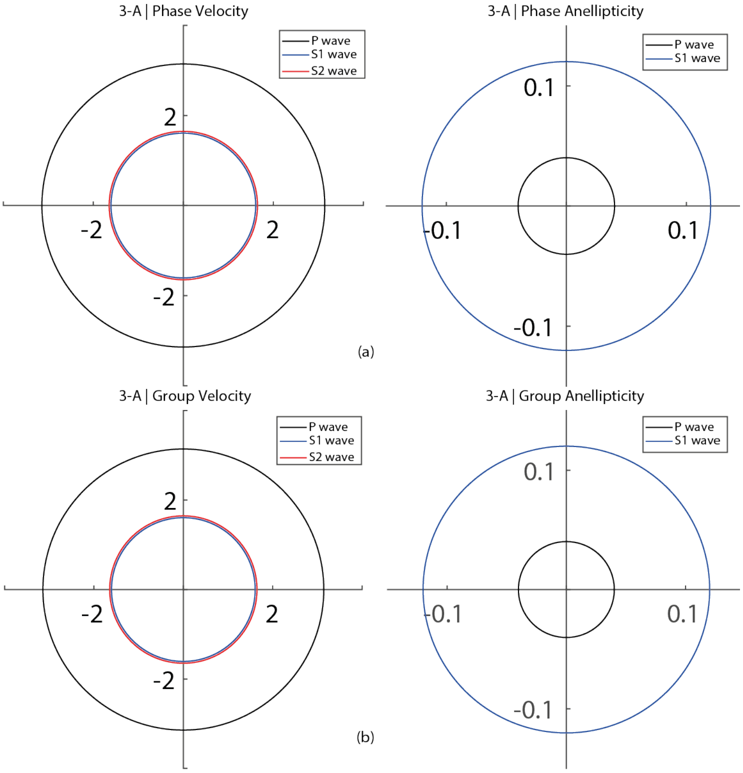

Figure 6.4: Azimuth dependent of kinematic parameters of pure mode waves using least square upscaling on VTI medium. Left images are V_{nmo} and right images are anellipticity. (a) Parameters on phase domain (b) Parameters on group domain.

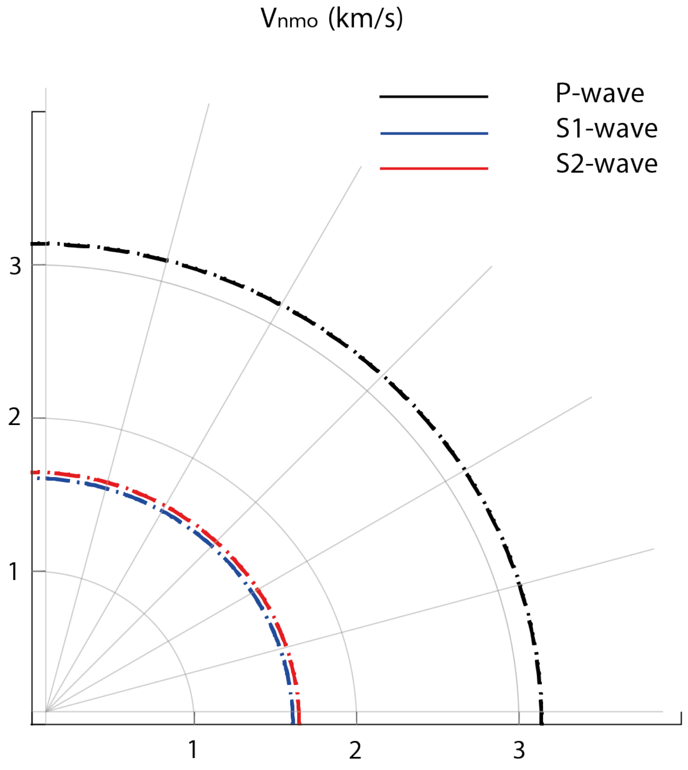

Figure 6.5: Polar plot of upscaling comparison in VTI medium block 3-A. Dash and dot line represent classic and least square upscaling respectively.

$$\mathbf{FU}_2 \;\; \mathrm{C}^{\mathrm{e}}_{\mathrm{ort}} = \begin{bmatrix} 17.272 & 6.919 & 6.598 & 0 & 0 & 0 \\ 6.919 & 19.831 & 7.295 & 0 & 0 & 0 \\ 6.598 & 7.295 & 23.563 & 0 & 0 & 0 \\ 0 & 0 & 7.644 & 0 & 0 \\ 0 & 0 & 0 & 6.116 & 0 \\ 0 & 0 & 0 & 0 & 4.872 \end{bmatrix} \tag{6.3}$$

$$\mathbf{FU}_3 \;\; \mathrm{C}^{\mathrm{e}}_{\mathrm{ort}} = \begin{bmatrix} 17.289 & 6.936 & 6.590 & 0 & 0 & 0 \\ 6.936 & 19.849 & 7.285 & 0 & 0 & 0 \\ 6.590 & 7.285 & 23.566 & 0 & 0 & 0 \\ 0 & 0 & 7.663 & 0 & 0 \\ 0 & 0 & 0 & 6.130 & 0 \\ 0 & 0 & 0 & 0 & 4.872 \end{bmatrix} \tag{6.4}$$

Once the stiffness coefficients are obtained, effective anisotropy parameters can be calculated and they are shown in Table 6.5:

ORT | 3-A	**FU$_2$**	**FU$_3$**
V$_{p0}$ (km/s)	3.2366	3.2367
V$_{s0}$ (km/s)	1.6489	1.6504
ε_1	-0.1335	-0.1329
γ_1	-0.1813	-0.1811
δ_1	-0.1737	-0.1727
ε_2	-0.0792	-0.0786
γ_2	-0.1017	-0.1014
δ_2	-0.0403	-0.0390
δ_3	-0.0344	-0.0344

Table 6.5: Effective anisotropy parameters for ORT medium when fractures are introduced after upscaling.

After all the anisotropy parameters are known, calculation of kinematic parameters for ORT medium is performed for both of the parameters obtained by classic and least square upscaling. The results are shown on the Table 6.6 for classic upscaling and Table 6.7 for least square upscaling.

Looking at Figure 6.6 and Figure 6.7, one can see that both upscaling methods give quite similar results for both NMO velocity and anellipticity. The noticeable difference is spotted between phase and group domain for both NMO velocity and anellipticity, indicating

	ORT FU$_2$ $\mid$ 3-A					
	V$_0$ (km/s)	V$_1$ (km/s)	V$_2$ (km/s)	η_1	η_2	η_{xy}
P wave	3.2366	2.6148	3.1036	0.0501	-0.0406	0.0535
S1 wave	1.6489	1.8869	1.4717	-0.0032	0	4.7219
S2 wave	1.8435	1.4717	1.6071	0	0.0243	-0.2175

Table 6.6: Kinematic parameters for ORT medium when fractures are introduced after classic upscaling.

	ORT FU$_3$ $\mid$ 3-A					
	V$_0$ (km/s)	V$_1$ (km/s)	V$_2$ (km/s)	η_1	η_2	η_{xy}
P wave	3.2367	2.6181	3.1075	0.0495	-0.0412	0.0540
S1 wave	1.6504	1.8861	1.4717	-0.0033	0	4.7072
S2 wave	1.8452	1.4717	1.6046	0	0.0281	-0.2324

Table 6.7: Kinematic parameters for ORT medium when fractures are introduced after least square upscaling.

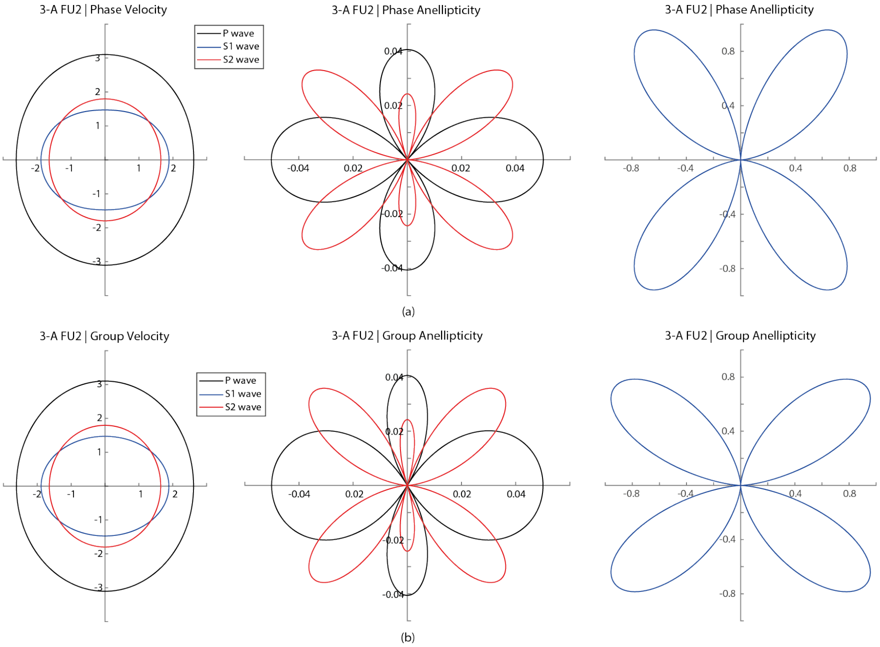

(a)

(b)

Figure 6.6: Azimuth dependent of kinematic parameters using classic upscaling on ORT medium when fractures are introduced after upscaling. (a) Parameters on phase domain (b) Parameters on group domain.

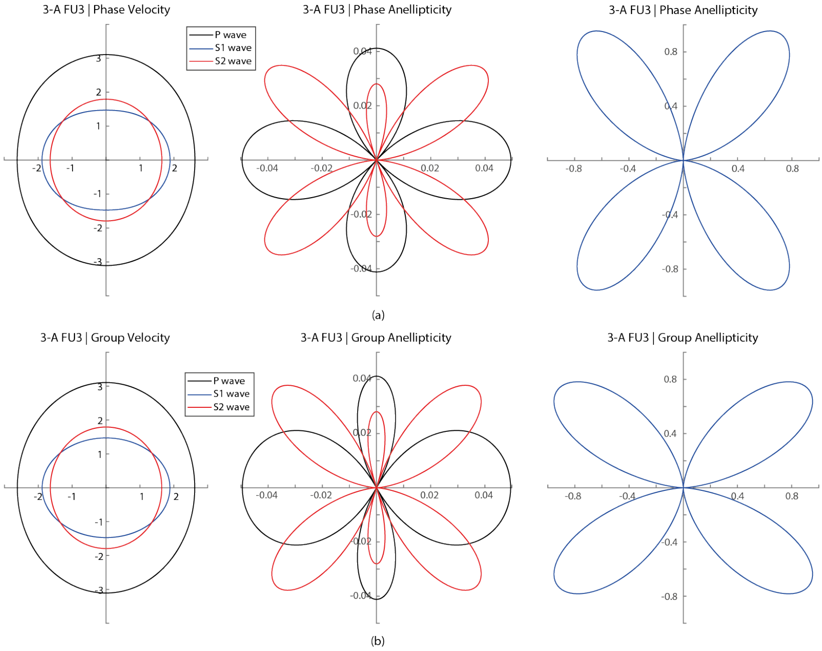

(a)

(b)

Figure 6.7: Azimuth dependent of kinematic parameters using least square upscaling on ORT medium when fractures are introduced after upscaling. (a) Parameters on phase domain (b) Parameters on group domain.

anisotropy effect that is affected by fracturing. The concentration of clay content has probability in contributing small effect to anisotropy due to low GR condition in this area, and reasons stated in chapter 5.

Concerning to fractures orientation, the observation from NMO velocity can explain it. Notice that the velocity for P-wave is slower in x-axis than in y-axis. Such condition indicates that P-wave is slower when it travels through the fractures as fractures can be considered as an empty space where the density is smaller compared to the surrounding. S2-wave travel slower in x-axis compared to S1-wave due to S2-wave polarization that goes through the fractures. The same explanation is relevant to what happened in y-axis when S1-wave and S2-wave behave in the opposite way than in x-axis.

6.4 Introducing Fracture Before Upscaling

In this approach, fracture parameters are introduced when the stiffness coefficients for every data sample in VTI layers are obtained. The fracture weaknesses are remain the same as before ($\Delta_N = 0.15$ and $\Delta_V = \Delta_H = 0.2$). Once the fractures are introduced, every data sample is no longer VTI medium anymore but ORT medium, hence the upscaling is performed under ORT condition. The stiffness matrix for this calculation is shown in matrix (6.5) for classic upscaling and matrix (6.6) for least square upscaling.

$$\mathbf{U_2F}\ \mathrm{C^e_{ort}} = \begin{bmatrix} 17.306 & 6.933 & 6.613 & 0 & 0 & 0 \\ 6.933 & 19.823 & 7.297 & 0 & 0 & 0 \\ 6.613 & 7.297 & 23.548 & 0 & 0 & 0 \\ 0 & 0 & 7.644 & 0 & 0 \\ 0 & 0 & 0 & 6.116 & 0 \\ 0 & 0 & 0 & 0 & 4.872 \end{bmatrix} \tag{6.5}$$

$$\mathbf{U_3F}\ \mathrm{C^e_{ort}} = \begin{bmatrix} 17.321 & 6.949 & 6.604 & 0 & 0 & 0 \\ 6.949 & 19.840 & 7.287 & 0 & 0 & 0 \\ 6.604 & 7.287 & 23.553 & 0 & 0 & 0 \\ 0 & 0 & 7.663 & 0 & 0 \\ 0 & 0 & 0 & 6.130 & 0 \\ 0 & 0 & 0 & 0 & 4.872 \end{bmatrix} \tag{6.6}$$

Once the stiffness coefficients for ORT effective medium are obtained, anisotropy parameters for the effective ORT medium can be calculated, and they are shown in Table 6.8.

ORT | 3-A	**U_2F**	**U_3F**
V_{p0} (km/s)	3.2356	3.2359
V_{s0} (km/s)	1.6489	1.6504
ε_1	-0.1325	-0.1320
γ_1	-0.1813	-0.1811
δ_1	-0.1728	-0.1720
ε_2	-0.0791	-0.0785
γ_2	-0.1017	-0.1014
δ_2	-0.0396	-0.0385
δ_3	-0.0355	-0.0354

Table 6.8: Effective anisotropy parameters for ORT medium when fractures are introduced before upscaling.

After anisotropy parameters are obtained, the calculation for kinematic parameters of NMO velocity and anellipticity are performed, and the results can be seen in Table 6.9 when using classic upscaling and Table 6.10 when using least square upscaling.

	ORT U_2F | 3-A					
	V_0 (km/s)	V_1 (km/s)	V_2 (km/s)	η_1	η_2	η_{xy}
P wave	3.2356	2.6175	3.1048	0.0501	-0.0411	0.0540
S1 wave	1.6489	1.8873	1.4717	-0.0032	0	4.7360
S2 wave	1.8435	1.4717	1.6036	0	0.0249	-0.2229

Table 6.9: Kinematic parameters for ORT medium when fractures are introduced before classic upscaling.

	ORT U_3F | 3-A					
	V_0 (km/s)	V_1 (km/s)	V_2 (km/s)	η_1	η_2	η_{xy}
P wave	3.2359	2.6205	3.1085	0.0496	-0.0415	0.0540
S1 wave	1.6504	1.8866	1.4717	-0.0033	0	4.7193
S2 wave	1.8452	1.4717	1.6013	0	0.0244	-0.2604

Table 6.10: Kinematic parameters for ORT medium when fractures are introduced before least square upscaling.

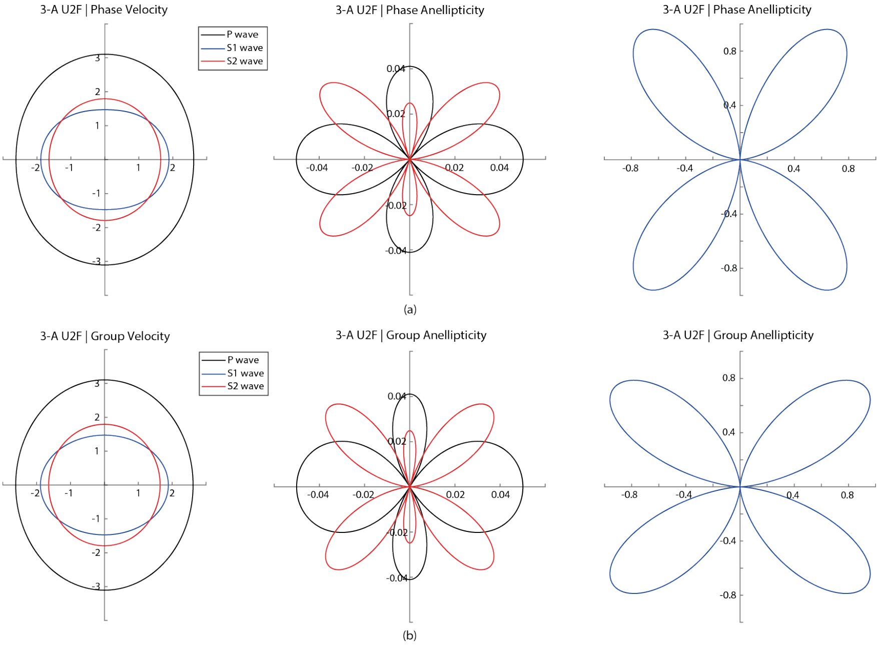

(a)

(b)

Figure 6.8: Azimuth dependent of kinematic parameters using classic upscaling on ORT medium when fractures are introduced before upscaling. (a) Parameters on phase domain (b) Parameters on group domain.

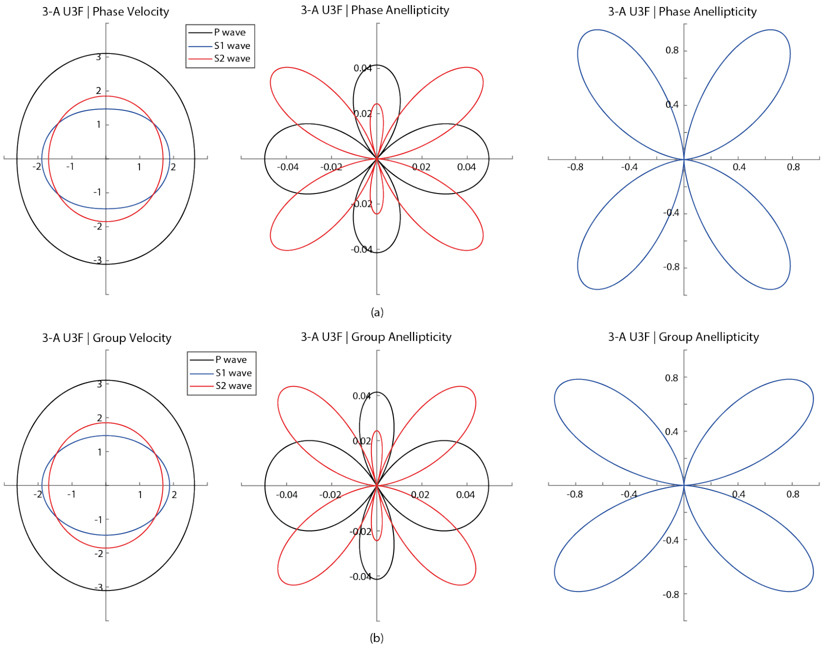

(a)

(b)

Figure 6.9: Azimuth dependent of kinematic parameters using least square upscaling on ORT medium when fractures are introduced before upscaling. (a) Parameters on phase domain (b) Parameters on group domain.

Looking at Figure 6.8 and Figure 6.9, one can see similar observation with those done in section 6.3. Both upscaling methods have no significant difference at the selected interval. Notice the difference of NMO velocity and anellipticity when plotted in group and phase domain, which indicating an anisotropic medium. Also notice that the difference can be seen more obvious for anelliptic parameters, meaning that anelliptic parameters are more sensitive in domain changes.

Same explanation regarding to fractures orientation is discussed in section 6.3. By observing the P-wave NMO velocity only, and noticing that the NMO velocity is slower in the x-axis, the fracture orientation is vertically parallel at [x1,x3] symmetry plane.

Chapter 7

Methods Comparison

In this chapter, the discussions are highlighted in comparing the results of the two upscaling methods and the two fracturing approaches that are performed in the interval of block 3-A of the given well log data.

7.1 Upscaling Comparison

In this section, the two methods of upscaling, as explained in subsection 5.3.2 for gaining the kinematic parameters will be further discussed with fractures being introduced before upscaling is performed.

Figure 7.1 shows the polar plot of the kinematic parameters that are going to be compared. The plots are only drawn in one quadrant since the kinematic parameters plot is symmetric with respect to origin in term of azimuth dependent in ORT medium. U_2 stands for classic upscaling and U_3 stands for least square upscaling. Both cases have fractures that are introduced before upscaling is conducted.

It is observed that both upscaling methods, classic and least square that are represented by a dash and dot lines respectively are overlapping with each other in NMO velocities and anellipticity of S1-wave. Small changes can be observed in anellipticity of P-wave and S2-wave.

These outcomes suggest that the impact of choosing different methods for upscaling only appeared at the second order of curvatures while they are less affecting the first order of curvatures.

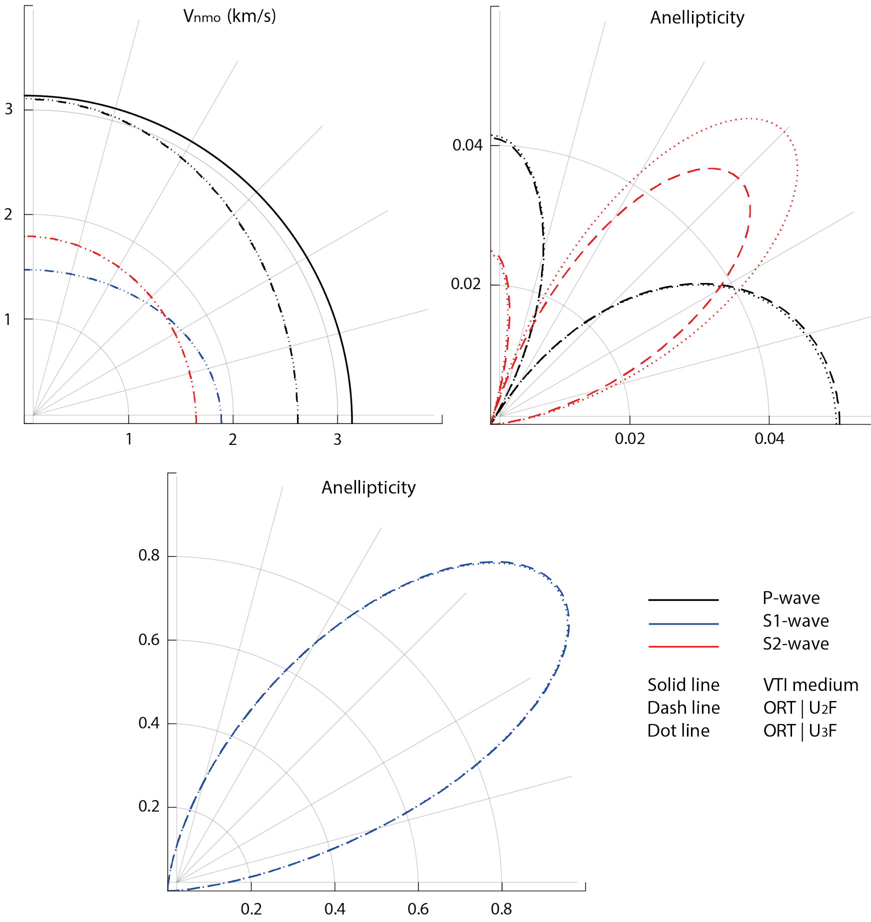

Figure 7.1: Polar plot of upscaling comparison of kinematic parameters when fractures are introduced before upscaling. Parameters are plotted in group domain.

7.2 Fracturing Approach Comparison

In this section, the two approaches of introducing the fractures, as explained in subsection 5.3.3 for obtaining the kinematic parameters will be observed further. Least square method is used for conducting the upscaling process in order to retrieve the effective parameters.

Figure 7.2 shows the polar plot that is about to be compared. FU_3 stands as fracturing after least square upscaling is done, and U_3F stands as fracturing before least square upscaling is performed. Similar results are observed as those in Figure 7.1, which suggest both approaches for introducing fractures are working either way. However, minor changes in S2-wave anellipticity can still be observed that affect the second order of curvatures.

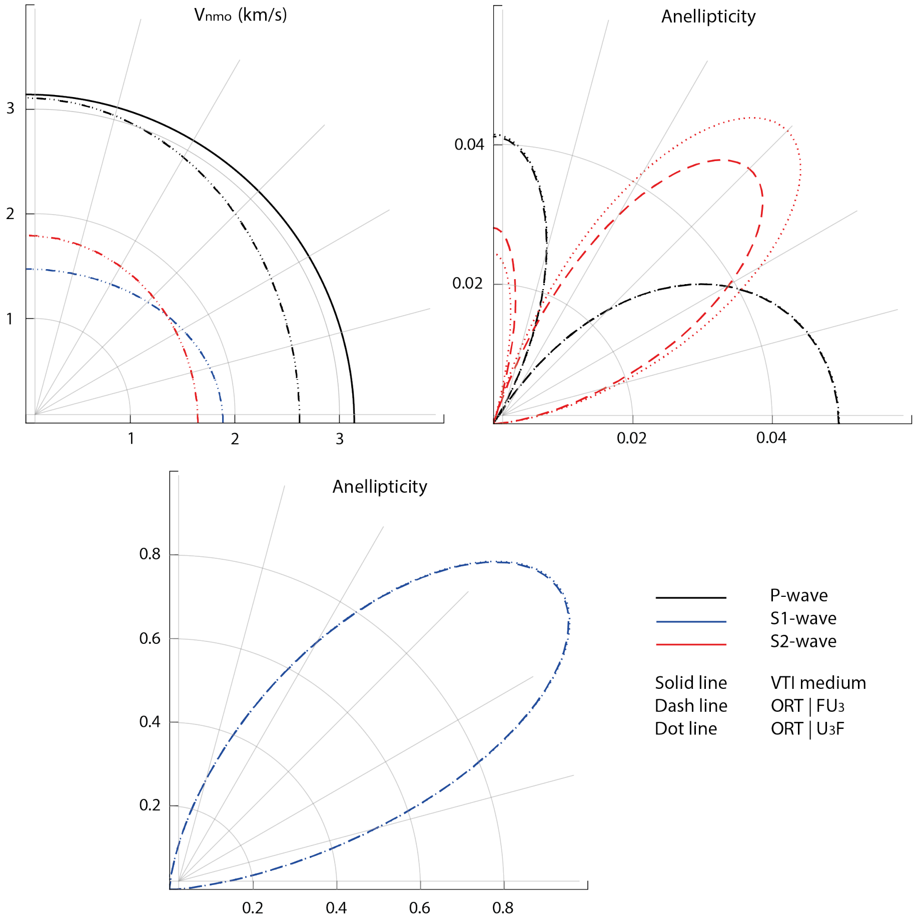

Figure 7.2: Polar plot of fracturing comparison of kinematic parameters with least square upscaling. Parameters are plotted in group domain.

Chapter 8

Overburden Effect

This chapter explains how the kinematic parameters of the ORT medium react when the overburden layers above it are included in the calculation. The NMO velocity and anellipticity for P-wave and S-wave are observed in order to see how these parameters actually behave given the seismic acquisition is performed from the surface.

The application of Dix-type equations is implemented for this case. Block 1 and block 2 are defined as the overburden layers, while block 3-A is the ORT medium. For calculating the effective parameters in each zone, both of upscaling methods can be used in this case as their results have no significant difference.

8.1 Effective Parameters of the Overburden

In order to see the seismic signature of the fractured reservoir with overburden being included in the scenario, the effective anisotropy parameters for the layers above the fractured reservoir need to be calculated. Looking back at Figure 5.3, two blocks; block 1 and block 2 are defined as the overburden and their effective parameter are calculated as VTI parameter. The upscaling process for these calculations is using least square upscaling.

VTI effective	ρ^e (g/cc)	V$^e_{p0}$ (km/s)	V$^e_{s0}$ (km/s)	ε^e	γ^e	δ^e
Block 1	2.1739	2.3619	1.0886	-0.0043	0.0035	-0.0063
Block 2	2.4200	2.7087	1.2086	0.1340	0.2002	0.0447
Block 3-A	2.2493	3.2672	1.8452	-0.0762	-0.1014	-0.0375

Table 8.1: Effective anisotropy parameters for VTI as background medium for block 1, 2, and 3-A. The results are calculated using least square upscaling.

Table 8.1 shows the calculation of the anisotropy parameters in VTI medium, including block 3-A that has not introduced with the fractures yet. Notice that on block 1, the anisotropy parameters are rather small compared to block 2. These results correspond to the GR log data in block 1, where they are relatively low that resembles more to a layer that is more sandstone dominated. Hence, indicating very little intrinsic anisotropy exist in this particular layer.

	VTI | 1					
	V_0 (km/s)	V_1 (km/s)	V_2 (km/s)	η_1	η_2	η_{xy}
P wave	2.3619	2.3478	2.3478	0.0025	0.0025	0.0049
S1 wave	1.0886	1.0514	1.0514	0.0266	0.0266	0.0532
S2 wave	1.0886	1.0793	1.0793	0	0	0

Table 8.2: Kinematic parameters for VTI of block 1. The results are calculated using least square upscaling.

	VTI | 2					
	V_0 (km/s)	V_1 (km/s)	V_2 (km/s)	η_1	η_2	η_{xy}
P wave	2.7087	2.8212	2.8212	0.0840	0.0840	0.1681
S1 wave	1.2086	1.6655	1.6655	0.4494	0.4494	0.8988
S2 wave	1.2086	1.4300	1.4300	0	0	0

Table 8.3: Kinematic parameters for VTI of block 2. The results are calculated using least square upscaling.

Table 8.2 and Table 8.3 shows the calculation for kinematic parameters of NMO velocity and anellipticity parameters for block 1 and block 2 respectively. Notice that those parameters are represented as a circle if they are plotted with azimuth dependent, which corresponds to VTI medium characteristic.

	ORT FU$_3$ | 3-A					
	V_0 (km/s)	V_1 (km/s)	V_2 (km/s)	η_1	η_2	η_{xy}
P wave	3.2367	2.6181	3.1075	0.0495	-0.0412	0.0540
S1 wave	1.6504	1.8861	1.4717	-0.0033	0	4.7072
S2 wave	1.8452	1.4717	1.6046	0	0.0281	-0.2324

Table 8.4: Kinematic parameters for ORT medium when fractures are introduced after least square upscaling.

Table 8.4 shows the calculation for the kinematic parameters of NMO velocity and anellipticity of a vertically fractured VTI medium of block 3-A. All the calculations steps and fracture weaknesses are the same as those discussed earlier in chapter 6.

8.2 Fractured Reservoir with Overburden Effect

Once all the kinematic parameters on each of the effective medium are gathered, Dix-type equation is performed to observe how the seismic signature behaved for the fractured reservoir given with overburden layers to be accounted for.

As for the calculations of Dix, they are referred to those described in chapter 4. Effective vertical velocity (V_0) and NMO velocity (V_1 and V_2) are obtained by using Equation 4.1. While effective anelliptic parameters (η_1, η_2, and η_{xy}) are obtained by using Equation 4.3. The results of the effective kinematic parameters from the combination of block 1, 2, and 3-A are shown in Table 8.5.

	Effective Medium with Overburden					
	V_0 (km/s)	V_1 (km/s)	V_2 (km/s)	η_1	η_2	η_{xy}
P wave	2.5811	2.5164	2.5854	0.0474	0.0286	0.0876
S1 wave	1.1985	1.3584	1.2987	0.3180	0.3670	2.0042
S2 wave	1.2210	1.2304	1.2474	0.0108	0.0218	-0.0328

Table 8.5: Kinematic parameters for ORT medium with overburden effect.

After the kinematic parameters of this Dix-effective medium are obtained, they are plotted along with the kinematic parameters from the fractured reservoir (ORT medium) only. Plots are done with azimuth dependent in group domain, and the results are provided in Figure 8.1.

The outcome in this figure suggests that the elliptic characteristic that once clearly seen in ORT medium is changing to more circle-wise when the overburden is introduced, particularly in NMO velocities. This situation implies that the effect of overburden layers, which are known to be VTI gives a significant impact on the seismic signature on the first order of curvatures. Elliptic characteristic of a fractured reservoir will be harder to observe due to this overburden effect.

On the contrary, anelliptic parameters also seem to be changing but not close to a circle shape as the NMO velocities have displayed. It implies that the fractured reservoir characteristics remain observable from the second order of curvatures even though overburden layers are accounted for.

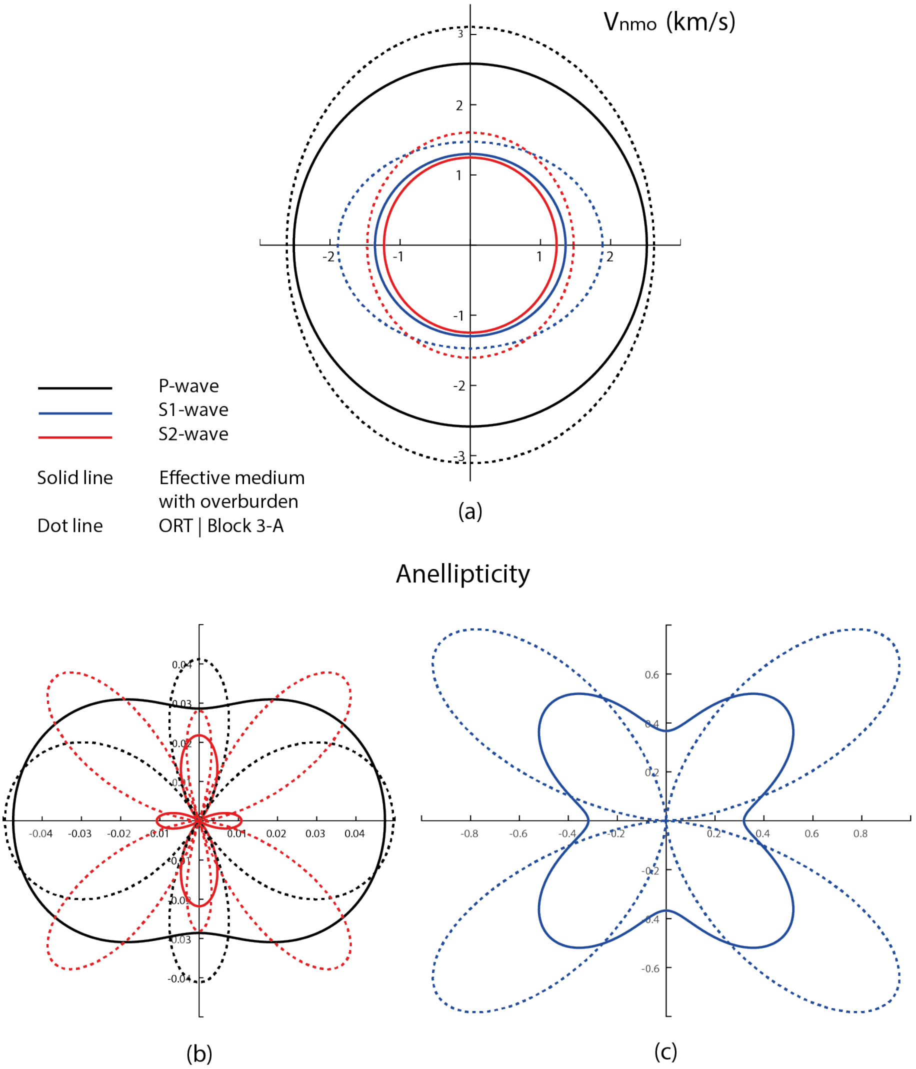

Figure 8.1: Polar plots with azimuth dependent of kinematic parameters of ORT medium with and without overburden effect. a) NMO velocities b) Anelliptic parameters for P and S-2 waves c) Anelliptic parameters for S1-wave. Solid and dot lines represent ORT with and without overburden respectively.

Chapter 9

Conclusion

In this study, the signature of a seismic response on a fractured and non-fractured reservoir from a given well data set at a target interval has been observed. Two methods of upscaling are conducted and compared within that window interval. Two approaches for introducing the fractures at the reservoir are also suggested and put as a comparison. Lastly, the application of Dix-type equations is performed for observing the kinematic parameters of the pure-mode waves when overburden layers are introduced above the fractured reservoir.

In a non-fractured reservoir, the azimuthal dependent of kinematic parameters shows as a circle for both NMO velocities and anellipticities. Such conditions suggest homogeneous materials are present on an axis that is perpendicular to the vertical axis. Furthermore, these responses remain the same when observed in group and phase domain, which implies the characteristic of a VTI medium.

On the contrary, the fractured reservoir observed in the block 3-A of a given well log data shows an elliptic behavior on its kinematic parameters. Both NMO velocities and anellipticities display a different behavior when plotted in phase and group domain with azimuth dependent, which implies the characteristic of an ORT medium. Moreover, the orientation of the vertical fractures can be observed from NMO velocities in either phase or group domain. One can observe the fracture orientation easily by looking in which axis does the P-wave NMO velocity is slower, which correspond to fractures are located vertically perpendicular to that axis.

Two upscaling methods, classic and least square that are tested in the block 3-A show insignificant differences. A possible explanation for this result is due to the data samples that are not drifted too much from each other within the targeted interval. Hence, either of the methods can be safely used to perform upscaling in this particular data. Similar results showing insignificant differences are observed for two approaches of introducing the fractures on before or after upscaling.

Overburden layers that are suggested as a VTI medium give a tremendous effect on the seismic signature of the fractured reservoir. Once the overburden layers are included in the calculations, the response of kinematic parameters is changing towards VTI characteristic. The NMO velocities are more affected by the overburden effect, which leads to difficulties to distinguish it with VTI characteristic. However, the second order of curvatures seems to be more sensitive as the differences are more distinguished when it is compared to those in VTI medium only.

Bibliography

Bakulin, A., Grechka, V., Tsvankin, I., 2000. Estimation of fracture parameters from reflection seismic data-part ii: Fractured models with orthorhombic symmetry. Geophysics 65 (6), p. 1803–1817.

Dix, C. H., 1955. Seismic velocities from surface measurements. Geophysics 20 (1), 68–86.

Grechka, V., Tsvankin, I., 1998. 3-d description of normal moveout in anisotropic inhomogeneous media. Geophysics 63 (3), 1079–1092.

Ivanov, Y., Stovas, A., 2016. Upscaling in orthorhombic media: Behavior of elastic parameters in heterogeneous fractured earthupscaling in orthorhombic media. Geophysics 81 (3), C113–C126.

Kumar, D., 2013. Applying backus averaging for deriving seismic anisotropy of a long-wavelength equivalent medium from well-log data. Journal of Geophysics and Engineering 10 (055001).

Liu, E., Martinez, A., 2012. Seismic Fracture Characterization: Concepts and Practical Applications. EAGE.

Schoenberg, M., Helbig, K., 1997. Orthorhombic media: Modeling elastic wave behavior in a vertically fractured earth. Geophysics 62 (6), p. 1954–1974.

Stovas, A., 2015. Azimuthally dependent kinematic properties of orthorhombic media. Geophysics 80 (6), C107–C122.

Stovas, A., 2016. Kinematic parameters of pure- and converted-mode waves in elastic orthorhombic media. EAGE Geophysical Prospecting.

Thomsen, L., 1986. Weak elastic anisotropy. Geophysics 51 (10), p. 1945–1966.

Tsvankin, I., 1997. Anisotropic parameters and p-wave velocity for orthorhombic media. Geophysics 62 (4), p. 1292–1309.

Wang, Z., 2002. Seismic anisotropy in sedimentary rocks, part 2: Laboratory data. Geophysics 67 (5), 1423–1440.

Appendix A: Matlab Code - Introducing Fracture After Classic Upscaling

```
clc,clear

%% Read Data

% Log Conditioning of bad data is performed on excel

load 'Data5conditioned.txt'

x = readtable('Data5conditioned','headerlines',0);

z        = table2array(x(:,1)); % m
GR       = table2array(x(:,2));
vp0      = table2array(x(:,3)); % m/s
vs0      = table2array(x(:,4)); % m/s
dens     = table2array(x(:,5))*1000; % kg/m^3
eps      = table2array(x(:,6));
del      = table2array(x(:,7));
gam      = table2array(x(:,8));
epsx     = table2array(x(:,6))-table2array(x(:,7)); %e-d

%% Defining Interface

% Interface decision based on GR interpretation of the log data
interface = [1000, 1275, 1430, 1520, 1625, 1770, 2010];

% Finding Location index of the array

for i = 1:length(interface)
    pos(i) = find(abs(z-interface(i)) == min(abs(z-interface(i))));
end

loc1 = [1,pos,length(z)];    % Upper limit for the interface
loc2 = [1,pos-1,length(z)]; % Lower limit for the interface



%% Calculate Cij for every point in VTI medium

```

```
Cij = zeros(6,6,length(z));

% Formulas are following Thomsen Parameter for VTI medium

for i = 1:length(z)
    Cij(3,3,i) = (vp0(i)^2)*dens(i) ;
    Cij(4,4,i) = (vs0(i)^2)*dens(i) ;
    Cij(5,5,i) = Cij(4,4,(i));
    Cij(1,1,i) = (1+2*eps(i))*Cij(3,3,i);
    Cij(6,6,i) = (1+2*gam(i))*Cij(4,4,i);
    Cij(1,3,i) = sqrt(2*del(i)*Cij(3,3,i)*(Cij(3,3,i)-Cij(5,5,i)) + (Cij(3,3,i)-Cij(5,5,i))^2) ...
               - Cij(5,5,i);
    Cij(1,2,i) = Cij(1,1,i) - 2*Cij(6,6,i);

    Cij(2,2,i) = Cij(1,1,i);
    Cij(2,1,i) = Cij(1,2,i);
    Cij(3,1,i) = Cij(1,3,i);
    Cij(3,2,i) = Cij(1,3,i);
    Cij(2,3,i) = Cij(1,3,i);
end

%% Backus Averaging - Classic Upscaling VTI

zone_number = length(interface)+1 ;

% Individual Layers are assumed to be VTI

Cb = zeros(6,6,zone_number);
efdens = zeros(zone_number,1);

for i = 1:length(loc1)-1
  Cb(3,3,i) = mean(Cij(3,3,loc1(i):loc2(i+1)).^(-1)).^(-1);
  Cb(4,4,i) = mean(Cij(4,4,loc1(i):loc2(i+1)).^(-1)).^(-1);
  Cb(6,6,i) = mean(Cij(6,6,loc1(i):loc2(i+1)));

  Cb(1,3,i) = mean(Cij(1,3,loc1(i):loc2(i+1))./Cij(3,3,loc1(i):loc2(i+1)))...
              .* Cb(3,3,i);
  Cb(1,1,i) = mean(Cij(1,1,loc1(i):loc2(i+1))) + ...
              (mean(Cij(1,3,loc1(i):loc2(i+1))./Cij(3,3,loc1(i):loc2(i+1)))).^2 )...
              .* Cb(3,3,i) - ...
              (mean((Cij(1,3,loc1(i):loc2(i+1)).^2)./Cij(3,3,loc1(i):loc2(i+1))));
  Cb(1,2,i) = Cb(1,1,i) - 2.*Cb(6,6,i);

  Cb(2,2,i) = Cb(1,1,i);
  Cb(2,3,i) = Cb(1,3,i);
  Cb(5,5,i) = Cb(4,4,i);
  Cb(2,1,i) = Cb(1,2,i);
  Cb(3,1,i) = Cb(2,3,i);
  Cb(3,2,i) = Cb(2,3,i);

  efdens(i) = mean(dens(loc1(i):loc2(i+1)));

  % Effective parameter of the Anisotropy

  Evp0(i) = sqrt(Cb(3,3,i)/efdens(i));
  Evs0(i) = sqrt(Cb(4,4,i)/efdens(i));

  Ee(i)   = (Cb(1,1,i) - Cb(3,3,i))/(2*Cb(3,3,i));
  Eg(i)   = (Cb(6,6,i) - Cb(4,4,i))/(2*Cb(4,4,i));
  Ed(i)   = ((Cb(1,3,i)+Cb(4,4,i))^2 - (Cb(3,3,i)-Cb(4,4,i))^2) / ...
            (2*Cb(3,3,i)*(Cb(3,3,i) - Cb(4,4,i)));
end

 % Set the effective parameters into every data point (depth)

    Cbef = zeros(6,6,length(z));

    for i = 1:size(z,1)
        if i < loc1(2)
            j = 1;
        elseif i > loc1(2)-1 && i < loc1(3)
            j = 2;
        elseif i > loc1(3)-1 && i < loc1(4)
            j = 3;
        elseif i > loc1(4)-1 && i < loc1(5)
            j = 4;
        elseif i > loc1(5)-1 && i < loc1(6)
            j = 5;
        elseif i > loc1(6)-1 && i < loc1(7)
            j = 6;
        elseif i > loc1(7)-1 && i < loc1(8)
            j = 7;
        else
            j = 8;
        end

      Cbef(3,3,i) = Cb(3,3,j);
      Cbef(4,4,i) = Cb(4,4,j);
      Cbef(5,5,i) = Cb(5,5,j);

      Cbef(1,3,i) = Cb(1,3,j);
      Cbef(2,3,i) = Cb(2,3,j);

      Cbef(6,6,i) = Cb(6,6,j);

      Cbef(1,1,i) = Cb(1,1,j);
      Cbef(2,2,i) = Cb(2,2,j);

      Cbef(1,2,i) = Cb(1,2,j);

      % Effective parameters

      vp0ef(i)  = Evp0(j);
      vs0ef(i)  = Evs0(j);

      densef(i) = efdens(j);

      epsef(i)  = Ee(j);
      gamef(i)  = Eg(j);
      delef(i)  = Ed(j);

    end

%% FRACTURE PARAMETER (ORT)

    C_ort = zeros(6,6,length(z));

for i = 1:size(z,1)
    if i > loc1(3)-1 && i < loc1(4) % BLOCK 3-A
       dn = 0.15;
       dh = 0.2;
       dv = 0.2;
    elseif i > loc1(4)-1 && i < loc1(5) %BLOCK 3-B
       dn = 0.4;
       dh = 0.2;
       dv = 0.2;
    elseif i > loc1(5)-1 && i < loc1(6) %BLOCK 3-C
       dn = 0.2;
       dh = 0.2;
       dv = 0.2;
    elseif i > loc1(6)-1 && i < loc1(7) %BLOCK 3-D
       dn = 0.5;
       dh = 0.2;
       dv = 0.2;
    else
        dn = 0;
        dh = 0;
        dv = 0;
    end

    % ORT Cij

    C_ort(1,1,i) = Cbef(1,1,i)*(1-dn);
    C_ort(2,2,i) = Cbef(1,1,i)-(dn*(Cbef(1,2,i)^2)/Cbef(1,1,i));
    C_ort(2,3,i) = Cbef(1,3,i)*(1-dn*Cbef(1,2,i)/Cbef(1,1,i));
    C_ort(1,2,i) = Cbef(1,2,i)*(1-dn);
    C_ort(1,3,i) = Cbef(1,3,i)*(1-dn);

    C_ort(4,4,i) = Cbef(4,4,i);
    C_ort(3,3,i) = Cbef(3,3,i)-dn*(Cbef(1,3,i)^2)/Cbef(1,1,i);
    C_ort(5,5,i) = Cbef(4,4,i)*(1-dv);
    C_ort(6,6,i) = Cbef(6,6,i)*(1-dh);

    % ORT Anisotropy Parameters

    Vp0_or(i) = sqrt(C_ort(3,3,i)/densef(i));
    Vs0_or(i) = sqrt(C_ort(5,5,i)/densef(i));

              % Plane is Perpendicular to fractures [x1,x3]
    e13(i)    = (C_ort(1,1,i) - C_ort(3,3,i))/(2*C_ort(3,3,i));
    g13(i)    = (C_ort(6,6,i) - C_ort(4,4,i))/(2*C_ort(4,4,i));
    d13(i)    = ((C_ort(1,3,i) + C_ort(5,5,i))^2 - (C_ort(3,3,i) - C_ort(5,5,i))^2) / ...
                (2*C_ort(3,3,i)*(C_ort(3,3,i) - C_ort(5,5,i)));
              % Plane is Paralel to fractures [x2,x3]
    e23(i)    = (C_ort(2,2,i) - C_ort(3,3,i))/(2*C_ort(3,3,i));
    g23(i)    = (C_ort(6,6,i) - C_ort(5,5,i))/(2*C_ort(5,5,i));
    d23(i)    = ((C_ort(2,3,i) + C_ort(4,4,i))^2 - (C_ort(3,3,i) - C_ort(4,4,i))^2) / ...
                (2*C_ort(3,3,i)*(C_ort(3,3,i) - C_ort(4,4,i)));
              % Horizontal Plane
    d12(i)    = ((C_ort(1,2,i) + C_ort(6,6,i))^2 - (C_ort(1,1,i) - C_ort(6,6,i))^2) / ...
                (2*C_ort(1,1,i)*(C_ort(1,1,i) - C_ort(6,6,i)));
end

%% KINEMATIC PARAMETERS OF PURE MODE WAVES

VP  = zeros(length(z),3); %Vertical;NMO[x1,x3];NMO[x2,x3]
VS1 = zeros(length(z),3);
VS2 = zeros(length(z),3);

anelP  = zeros(length(z),3); %eta1[x1,x3];eta2[x2,x3];etaxy[x1,x2]
anelS1 = zeros(length(z),3);
anelS2 = zeros(length(z),3);

for i = 1:size(z,1)

    % Component for anelliptic parameter on Pure mode wave
    r0  = sqrt(C_ort(5,5,i)/C_ort(3,3,i));
    r1  = sqrt((1-(r0^2))*(1+2*d13(i)-(r0^2)));
    r2  = sqrt((1+2*g13(i)-(r0^2)*(1+2*g23(i))) * ...
              ((1+2*d23(i))*(1+2*g13(i))-(r0^2)*(1+2*g23(i))));
    r3  = sqrt((1+2*e13(i)-(r0^2)*(1+2*g23(i))) * ...
              ((1+2*d12(i))*(1+2*e13(i))-(r0^2)*(1+2*g23(i))));

    % Component for anelliptic parameter on P-wave
    b0  = 2*(1+2*d13(i))*(1+2*d23(i))*(1+2*g13(i));
    b2  = -(1+2*d13(i))*(1+2*g23(i))-(1+2*d23(i))*(1+2*g13(i))...
          -2*(1+2*d13(i))*(1+2*d23(i))*(1+g13(i)+g23(i))...
          -2*(1+2*g13(i))*(1+2*g23(i))*(1+d13(i)+d23(i));
    b4  = (1+2*g23(i))*(4+2*d13(i)+2*d23(i)+2*g13(i)+2*g23(i)...
            +(1+2*d13(i))*(1+2*g23(i))+(1+2*d23(i))*(1+2*g13(i)));
    b6  = -2*((1+2*g23(i))^2);

    VP(i,1)    = Vp0_or(i);
    VP(i,2)    = sqrt((Vp0_or(i).^2).*(1+2.*d13(i)));
    VP(i,3)    = sqrt((Vp0_or(i).^2).*(1+2.*d23(i)));
    anelP(i,1) = ((e13(i)-d13(i))*(1+2*d13(i)-(r0^2))) ...
                   /(((1+2*d13(i))^2)*(1-(r0^2)));
    anelP(i,2) = ((e23(i)-d23(i))*((1+2*d23(i))*(1+2*g13(i))-(r0^2)*(1+2*g23(i)))) ...
                   /(((1+2*d23(i))^2)*(1+2*g13(i)-(r0^2)
                      *(1+2*g23(i))));
    anelP(i,3) = (b0+b2*(r0^2)+b4*(r0^4)+b6*(r0^6)-2*r1*r2*r3) ...
                   /(2*(1+2*d13(i))*(1+2*d23(i))*(1+2*g13(i)-(r0^2)*(1+2*g23(i))));


    % Component for anelliptic parameter on S1-wave (C55)
    b0  = ((1+2*g13(i))^2)*( (1+2*d13(i))*(1+2*d23(i)) ...
            +(1+2*d12(i))*((1+2*e13(i))^2));
    b2  = -(1+2*g13(i))*((1+2*d13(i))*(1+2*g23(i))+(1+2*d23(i))*(1+2*g13(i)) ...
            +(1+2*g13(i))*((1+2*d13(i))*(1+2*d23(i))+(1+2*e13(i))*(1+2*g23(i))) ...
            +2*(1+2*e13(i))*(1+2*g23(i))*(1+2*d12(i))*(1+e13(i)+g13(i)));
    b4  = (1+2*g13(i))*(1+2*g23(i))*(3+2*d13(i)+2*d23(i)-2*(1+2*d23(i))*(g23(i)-g13(i)) ...
            +2*(1+2*g23(i))*(1+e13(i)+g13(i))+(1+2*d12(i))
               *(1+2*e13(i))*(1+2*g23(i)));
    b6  = -2*((1+2*g23(i))^2)*(1+2*g13(i)+2*g13(i)*g23(i));

    Vs10(i)     = sqrt(C_ort(5,5,i)/densef(i));
    VS1(i,1)    = Vs10(i);
    VS1(i,2)    = sqrt((Vs10(i).^2).*(1+2.*((e13(i)-d13(i))./(r0^2))));
    VS1(i,3)    = sqrt((Vs10(i).^2).*(1+2.*g23(i)));
    anelS1(i,1) = -  ((e13(i)-d13(i))*(r0^2)*(1+2*d13(i)-(r0^2))) ...
                    /(((1+2*(e13(i)-d13(i))/(r0^2))^2)*(1-(r0^2)));
    anelS1(i,2) = 0;
    anelS1(i,3) = -  (b0+b2*(r0^2)+b4*(r0^4)+b6*(r0^6)-2*r1*r2*r3)...
                    /( 4*(r0^4)*(1-r0^2)*(1+2*(e13(i)-d13(i))/(r0^2))*(g23(i)-g13(i))*(1+2*g23(i)));

    % Component for anelliptic parameter on S2-wave (C44)
    b0  = (1+2*g13(i))*( (1+2*d13(i))*(1+2*d23(i))...
          +(1+2*d12(i))*((1+2*e13(i))^2));
    b2  = -(1+2*d13(i))*(1+2*g23(i))-(1+2*d23(i))*(1+2*g13(i))...
          -(1+2*g23(i))*((1+2*d13(i))*(1+2*d23(i))+(1+2*e13(i))*(1+2*g13(i)))...
          -2*(1+2*e13(i))*(1+2*g13(i))*(1+2*d12(i))*(1+e13(i)+g23(i));
    b4  = (1+2*g23(i))*(3+2*d13(i)+2*d23(i)+2*(1+2*d13(i))*(g23(i)-g13(i))...
          +2*(1+2*g13(i))*(1+e13(i)+g23(i))...
          +(1+2*d12(i))*(1+2*e13(i))*(1+2*g13(i)));
    b6  = -2*(1+2*g23(i))*(1+2*g23(i)+2*g13(i)*g23(i));

    VS20(i)       = sqrt(C_ort(5,5,i)/densef(i));
    VS2(i,1)      = VS20(i)*sqrt((1+2*g23(i))/(1+2*g13(i)));
    VS2(i,2)      = sqrt((VS20(i).^2).*(1+2.*g23(i)));
    VS2(i,3)      = sqrt((VS20(i).^2).*...
                    ( ((1+2.*g23(i))/(1+2*g13(i)))+2*(e23(i)-d23(i))/(r0^2) ) );
    anelS2(i,1) = 0;
    anelS2(i,2) = -((e23(i)-d23(i))*(r0^2)*((1+2*d23(i))-((1+2*g23(i))/(1+2*g13(i)))*(r0^2)))...
                    /(((1+2*g13(i))^2)*((((1+2*g23(i))/(1+2*g13(i)))+2*(e23(i)-d23(i))/(r0^2))^2)...
                    *(1-((1+2*g23(i))/(1+2*g13(i)))*(r0^2)));
    anelS2(i,3) = (b0+b2*(r0^2)+b4*(r0^4)+b6*(r0^6)-2*r1*r2*r3)...
                    /(4*(r0^4)*(1+2*g13(i))*(1+2*g13(i)-(1+2*g23(i))*(r0^2))...
                    *(((1+2*g23(i))/(1+2*g13(i)))+2*(e23(i)-d23(i))/(r0^2))*(g23(i)-g13(i)));

end
```

Appendix B: Matlab Code - Introducing Fracture After Least Square Upscaling

```
clc,clear

%% Read Data

% Log Conditioning of bad data is performed on excel

load 'Data5conditioned.txt'

x = readtable('Data5conditioned','headerlines',0);

h       = table2array(x(:,1)); % m
GR      = table2array(x(:,2));
vp0     = table2array(x(:,3)); % m/s
vs0     = table2array(x(:,4)); % m/s
dens    = table2array(x(:,5))*1000; % kg/m^3
eps     = table2array(x(:,6));
del     = table2array(x(:,7));
gam     = table2array(x(:,8));

%% ---Defining Interface---

% Interface decision based on GR interpretation of the log data
interface = [1000, 1275, 1430, 1520, 1625, 1770, 2010];

% Finding Location index of the array

for i = 1:length(interface)
    pos(i) = find(abs(h-interface(i)) == min(abs(h-interface(i))));
end

loc1 = [1,pos,length(h)];   % Upper limit for the interface
loc2 = [1,pos-1,length(h)]; % Lower limit for the interface


%% ---Calculate Cij for every point in VTI medium---

c33 = zeros(length(h),1);
c44 = zeros(length(h),1);
```

```
c55 = zeros(length(h),1);
c11 = zeros(length(h),1);
c66 = zeros(length(h),1);
c13 = zeros(length(h),1);
c12 = zeros(length(h),1);

% Formulas are following Thomsen Parameter for VTI medium

for i = 1:length(h)
    c33(i,1) = ((vp0(i)^2)*dens(i))/10^9 ;
    c44(i,1) = ((vs0(i)^2)*dens(i))/10^9 ;
    c55(i,1) = c44(i,1);
    c11(i,1) = ((1+2*eps(i))*c33(i,1));
    c66(i,1) = ((1+2*gam(i))*c44(i,1));
    c13(i,1) = sqrt(2*del(i)*c33(i,1)*(c33(i,1)-c55(i,1)) + (c33(i,1)-c55(i,1))^2) ...
               - c55(i,1);
    c12(i,1) = c11(i,1) - 2*c66(i,1);

end

%% ---Defining Block 3---

% Define the designated zone
  n1       = length(loc1(3):loc1(4)-1); % total data Block 3a
  x1       = h(loc1(3):loc1(4)-1); % allocated depth points
  k        = loc1(3);
  l        = loc1(4);

%   n1       = length(loc1(4):loc1(5)-1); % Block 3b
%   x1       = h(loc1(4):loc1(5)-1);
%   k        = loc1(4);
%   l        = loc1(5);
%
%   n1       = length(loc1(5):loc1(6)-1); % Block 3c
%   x1       = h(loc1(5):loc1(6)-1);
%   k        = loc1(5);
%   l        = loc1(6);
%
%   n1       = length(loc1(6):loc1(7)-1); % Block 3d
%   x1       = h(loc1(6):loc1(7)-1);
%   k        = loc1(6);
%   l        = loc1(7);

% Defining the unknown parameter 'a' and 'b' for least square method

  y1(:,1) = 1./c33(k:l-1,1); % 1/c33
  y1(:,2) = 1./c44(k:l-1,1); % 1/c44
  y1(:,3) = c13(k:l-1,1)./c33(k:l-1,1); % c13/c33
  y1(:,4) = c66(k:l-1,1);    % c66
  y1(:,5) = (c13(k:l-1,1).^2)./c33(k:l-1,1); % c13^2/c33
  y1(:,6) = c11(k:l-1,1);    % c11
  y1(:,7) = dens(k:l-1,1);   % density

a1 = zeros(1,7); % 1/c33 | 1/c44 | c13/c33 | c66 | c13^2/c33 | c11 | dens
b1 = zeros(1,7);

for i = 1:7
    a1(1,i) = ((n1*sum(x1.*y1(:,i)))-(sum(x1)*sum(y1(:,i))))/(n1*sum(x1.^2)-(sum(x1)^2));
    b1(1,i) = (sum(y1(:,i))-a1(1,i)*sum(x1))/n1;
end

%% --- VTI BACKGROUND CALCULATION ---

% Least square calculation on VTI medium
% Cij background and density function calculation from least square

C33a  = @(z) 1./(a1(1,1).*z + b1(1,1));
C44a  = @(z) 1./(a1(1,2).*z + b1(1,2));
C13a  = @(z) (a1(1,3).*z + b1(1,3)).*(1./(a1(1,1).*z + b1(1,1)));
C66a  = @(z) a1(1,4).*z + b1(1,4);
C11a  = @(z) (a1(1,6).*z + b1(1,6)) + ((a1(1,3).*z + b1(1,3)).^2).*C33a(z)...
             -(a1(1,5).*z + b1(1,5));
C12a  = @(z) C11a(z)-2.*C66a(z);
Densa = @(z) a1(1,7).*z + b1(1,7);

% Anisotropy Parameter function calculation

Vp0a  = @(z) sqrt(C33a(z).*(10^9)./Densa(z));
Vs0a  = @(z) sqrt(C44a(z).*(10^9)./Densa(z));
epsa  = @(z) (C11a(z)-C33a(z))./(2.*C33a(z));
gama  = @(z) (C66a(z)-C44a(z))./(2.*C44a(z));
```

```
dela   = @(z) ((C13a(z)+C44a(z)).^2-(C33a(z)-C44a(z)).^2)
    ...
             ./(2.*C33a(z).*(C33a(z)-C44a(z)));

%% --- ORT CALCULATION ---

% Cij when fractures are introduced

% Normal Fracture weakness
    dn = 0.15; %3a
%   dn = 0.4;   %3b
%   dn = 0.2;   %3c
%   dn = 0.5;   %3d

% Tangential Fracture weaknesses
    dh = 0.2;
    dv = 0.2;

Co11   = @(z) C11a(z).*(1-dn);
Co22   = @(z) C11a(z)-(dn.*(C12a(z).^2))./C11a(z);
Co23   = @(z) C13a(z).*(1-(dn.*C12a(z)./C11a(z)));
Co12   = @(z) C12a(z).*(1-dn);
Co13   = @(z) C13a(z).*(1-dn);
Co44   = @(z) C44a(z);
Co33   = @(z) C33a(z)-(dn.*(C13a(z).^2))./C11a(z);
Co55   = @(z) C44a(z).*(1-dv);
Co66   = @(z) C66a(z).*(1-dh);

% Anisotropy Parameter Function Calculation

Vp0oa = @(z) sqrt(Co33(z).*(10^9)./Densa(z));
Vs0oa = @(z) sqrt(Co55(z).*(10^9)./Densa(z));

    % Plane is Perpendicular to fractures [x1,x3]

e1    = @(z) (Co11(z)-Co33(z))./(2.*Co33(z));
g1    = @(z) (Co66(z)-Co44(z))./(2.*Co44(z));
d1    = @(z) ((Co13(z)+Co55(z)).^2-(Co33(z)-Co55(z)).^2) ...
             ./(2.*Co33(z).*(Co33(z)-Co55(z)));

    % Plane is Parallel to fractures [x2,x3]

e2    = @(z) (Co22(z)-Co33(z))./(2.*Co33(z));
g2    = @(z) (Co66(z)-Co55(z))./(2.*Co55(z));
d2    = @(z) ((Co23(z)+Co44(z)).^2-(Co33(z)-Co44(z)).^2) ...
```

```
             ./(2.*Co33(z).*(Co33(z)-Co44(z)));

    % Horizontal Plane

d3   = @(z) ((Co12(z)+Co66(z)).^2-(Co11(z)-Co66(z)).^2) ...
             ./(2.*Co11(z).*(Co11(z)-Co66(z)));


%% --- AVERAGE VALUE ANISO PARAMETER USING INTEGRAL ---

VP0_or = integral(Vp0oa,x1(1),x1(end))/(x1(end)-x1(1));
VS0_or = integral(Vs0oa,x1(1),x1(end))/(x1(end)-x1(1));

eps1 = integral(e1,x1(1),x1(end))/(x1(end)-x1(1));
gam1 = integral(g1,x1(1),x1(end))/(x1(end)-x1(1));
del1 = integral(d1,x1(1),x1(end))/(x1(end)-x1(1));

eps2 = integral(e2,x1(1),x1(end))/(x1(end)-x1(1));
gam2 = integral(g2,x1(1),x1(end))/(x1(end)-x1(1));
del2 = integral(d2,x1(1),x1(end))/(x1(end)-x1(1));

del3 = integral(d3,x1(1),x1(end))/(x1(end)-x1(1));

%% --- KINEMATIC PARAMETER ---

% Component for anelliptic parameter on Pure mode wave

r0  =@(z) sqrt(Co55(z)./Co33(z));
r1  =@(z) sqrt((1-(r0(z).^2)).*(1+2.*d1(z)-(r0(z).^2)));
r2  =@(z) sqrt((1+2.*g1(z)-(r0(z).^2).*(1+2.*g2(z))) .* ...
              ((1+2.*d2(z)).*(1+2.*g1(z))-(r0(z).^2)
                 .*(1+2.*g2(z))));
r3  =@(z) sqrt((1+2.*e1(z)-(r0(z).^2).*(1+2.*g2(z))) .* ...
              ((1+2.*d3(z)).*(1+2.*e1(z))-(r0(z).^2)
                 .*(1+2.*g2(z))));

% Component for anelliptic parameter on P-WAVE

b0  =@(z) 2.*(1+2.*d1(z)).*(1+2.*d2(z)).*(1+2.*g1(z));
b2  =@(z) -(1+2.*d1(z)).*(1+2.*g2(z))-(1+2.*d2(z)).*(1+2.*
   g1(z))...
          -2.*(1+2.*d1(z)).*(1+2.*d2(z)).*(1+g1(z)+g2(z))
             ...
          -2.*(1+2.*g1(z)).*(1+2.*g2(z)).*(1+d1(z)+d2(z));
```

```
b4   =@(z)  (1+2.*g2(z)).*(4+2.*d1(z)+2.*d2(z)+2.*g1(z)+2.*g2(z)...
            +(1+2.*d1(z)).*(1+2.*g2(z))+(1+2.*d2(z)).*(1+2.*g1(z)));
b6   =@(z) -2.*((1+2.*g2(z)).^2);

% Kinematic Parameter

VP0     =@(z)  Vp0oa(z);
VP1     =@(z)  sqrt((Vp0oa(z).^2).*(1+2.*d1(z)));
VP2     =@(z)  sqrt((Vp0oa(z).^2).*(1+2.*d2(z)));

anelP1 =@(z)  ((e1(z)-d1(z)).*(1+2.*d1(z)-(r0(z).^2)))...
              ./(((1+2.*d1(z)).^2).*(1-(r0(z).^2)));
anelP2 =@(z)  ((e2(z)-d2(z)).*((1+2.*d2(z)).*(1+2.*g1(z))-(r0(z).^2).*(1+2.*g2(z))))...
              ./(((1+2.*d2(z)).^2).*(1+2.*g1(z)-(r0(z).^2).*(1+2.*g2(z))));
anelP3 =@(z)  (b0(z)+b2(z).*(r0(z).^2)+b4(z).*(r0(z).^4)+b6(z).*(r0(z).^6)-2.*r1(z).*r2(z).*r3(z))...
              ./(2.*(1+2.*d1(z)).*(1+2.*d2(z)).*(1+2.*g1(z)-(r0(z).^2).*(1+2.*g2(z))));

% Component for anelliptic parameter on S1-WAVE (C55)

b0   =@(z)  ((1+2.*g1(z)).^2).*( (1+2.*d1(z)).*(1+2.*d2(z))...
            +(1+2.*d3(z)).*((1+2.*e1(z)).^2));
b2   =@(z) -(1+2.*g1(z)).*((1+2.*d1(z)).*(1+2.*g2(z))+(1+2.*d2(z)).*(1+2.*g1(z))...
            +(1+2.*g1(z)).*((1+2.*d1(z)).*(1+2.*d2(z))+(1+2.*e1(z)).*(1+2.*g2(z)))...
            +2.*(1+2.*e1(z)).*(1+2.*g2(z)).*(1+2.*d3(z)).*(1+e1(z)+g1(z)));
b4   =@(z)  (1+2.*g1(z)).*(1+2.*g2(z)).*(3+2.*d1(z)+2.*d2(z)-2.*(1+2.*d2(z)).*(g2(z)-g1(z))...
            +2.*(1+2.*g2(z)).*(1+e1(z)+g1(z))+(1+2.*d3(z)).*(1+2.*e1(z)).*(1+2.*g2(z)));
b6   =@(z) -2.*((1+2.*g2(z)).^2).*(1+2.*g1(z)+2.*g1(z).*g2(z));

VS10     =@(z)  sqrt(Co55(z).*(10^9)./Densa(z));
VS11     =@(z)  sqrt((VS10(z).^2).*(1+2.*((e1(z)-d1(z))./(r0(z).^2))));
VS12     =@(z)  sqrt((VS10(z).^2).*(1+2.*g2(z)));
```

```
anelS11 =@(z) - ((e1(z)-d1(z)).*(r0(z).^2).*(1+2.*d1(z)-(r0(z).^2)))...
                 ./(((1+2.*(e1(z)-d1(z))/(r0(z).^2)).^2).*(1-(r0(z).^2)));
anelS12 =0;
anelS13 =@(z) - (b0(z)+b2(z).*(r0(z).^2)+b4(z).*(r0(z).^4)+b6(z).*(r0(z).^6)-2.*r1(z).*r2(z).*r3(z))...
                 ./( 4.*(r0(z).^4).*(1-r0(z).^2).*(1+2.*(e1(z)-d1(z))./(r0(z).^2)).*(g2(z)-g1(z)).*(1+2.*g2(z)));

% Component for anelliptic parameter on S2-wave (C44)

b0  =@(z) (1+2.*g1(z)).*( (1+2.*d1(z)).*(1+2.*d2(z))...
          +(1+2.*d3(z)).*((1+2.*e1(z)).^2));
b2  =@(z) -(1+2.*d1(z)).*(1+2.*g2(z))-(1+2.*d2(z)).*(1+2.*g1(z))...
          -(1+2.*g2(z)).*((1+2.*d1(z)).*(1+2.*d2(z))+(1+2.*e1(z)).*(1+2.*g1(z)))...
          -2.*(1+2.*e1(z)).*(1+2.*g1(z)).*(1+2.*d3(z)).*(1+e1(z)+g2(z));
b4  =@(z) (1+2.*g2(z)).*(3+2.*d1(z)+2.*d2(z)+2.*(1+2.*d1(z)).*(g2(z)-g1(z))...
          +2.*(1+2.*g1(z)).*(1+e1(z)+g2(z))...
          +(1+2.*d3(z)).*(1+2.*e1(z)).*(1+2.*g1(z)));
b6  =@(z) -2.*(1+2.*g2(z)).*(1+2.*g2(z)+2.*g1(z).*g2(z));

Vs20    =@(z) sqrt(Co55(z).*(10^9)./Densa(z));
VS20    =@(z) Vs20(z).*sqrt((1+2.*g2(z))./(1+2.*g1(z)));
VS21    =@(z) sqrt((Vs20(z).^2).*(1+2.*g2(z)));
VS22    =@(z) sqrt((Vs20(z).^2).*...
              ( ((1+2.*g2(z))./(1+2.*g1(z)))+2.*(e2(z)-d2(z))./(r0(z).^2) ) );
anelS21 = 0;
anelS22 =@(z) -((e2(z)-d2(z)).*(r0(z).^2).*((1+2.*d2(z))-((1+2.*g2(z))./(1+2.*g1(z))).*(r0(z).^2)))...
              ./(((1+2.*g1(z)).^2).*((((1+2.*g2(z))./(1+2.*g1(z)))+2.*(e2(z)-d2(z))./(r0(z).^2)).^2)...
              .*(1-((1+2.*g2(z))./(1+2.*g1(z))).*(r0(z).^2)));
anelS23 =@(z) (b0(z)+b2(z).*(r0(z).^2)+b4(z).*(r0(z).^4)+b6(z).*(r0(z).^6)-2.*r1(z).*r2(z).*r3(z))...
              ./(4.*(r0(z).^4).*(1+2.*g1(z)).*(1+2.*g1(z)-(1+2.*g2(z)).*(r0(z).^2))...
               .*(((1+2.*g2(z))./(1+2.*g1(z)))+2.*(e2(z)-d2(z))./(r0(z).^2)).*(g2(z)-g1(z)));

%% --- AVERAGE VALUE KINEMATIC PARAMETERS USING INTEGRAL ---

% P-WAVE

VP0     = integral(VP0,x1(1),x1(end))/(x1(end)-x1(1));
VP1     = integral(VP1,x1(1),x1(end))/(x1(end)-x1(1));
VP2     = integral(VP2,x1(1),x1(end))/(x1(end)-x1(1));

anelP1 = integral(anelP1,x1(1),x1(end))/(x1(end)-x1(1));
anelP2 = integral(anelP2,x1(1),x1(end))/(x1(end)-x1(1));
anelP3 = integral(anelP3,x1(1),x1(end))/(x1(end)-x1(1));

% S1-WAVE

VS10     = integral(VS10,x1(1),x1(end))/(x1(end)-x1(1));
VS11     = integral(VS11,x1(1),x1(end))/(x1(end)-x1(1));
VS12     = integral(VS12,x1(1),x1(end))/(x1(end)-x1(1));

anelS11 = integral(anelS11,x1(1),x1(end))/(x1(end)-x1(1));
anelS12 = anelS12;
anelS13 = integral(anelS13,x1(1),x1(end))/(x1(end)-x1(1));

% S2-WAVE

VS20     = integral(VS20,x1(1),x1(end))/(x1(end)-x1(1));
VS21     = integral(VS21,x1(1),x1(end))/(x1(end)-x1(1));
VS22     = integral(VS22,x1(1),x1(end))/(x1(end)-x1(1));

anelS21 = anelS21;
anelS22 = integral(anelS22,x1(1),x1(end))/(x1(end)-x1(1));
anelS23 = integral(anelS23,x1(1),x1(end))/(x1(end)-x1(1));
```

Appendix C: Matlab Code - Introducing Fracture Before Classic Upscaling

```
clc,clear

%% Read Data

% Log Conditioning of bad data is performed on excel

load 'Data5conditioned.txt'

x = readtable('Data5conditioned','headerlines',0);

z        = table2array(x(:,1)); % m
GR       = table2array(x(:,2));
vp0      = table2array(x(:,3)); % m/s
vs0      = table2array(x(:,4)); % m/s
dens     = table2array(x(:,5))*1000; % kg/m^3
eps      = table2array(x(:,6));
del      = table2array(x(:,7));
gam      = table2array(x(:,8));

%% Defining Interface

% Interface decision based on GR interpretation of the log data
interface = [1000, 1275, 1430, 1520, 1625, 1770, 2010];

% Finding Location index of the array

for i = 1:length(interface)
    pos(i) = find(abs(z-interface(i)) == min(abs(z-interface(i))));
end

loc1 = [1,pos,length(z)];   % Upper limit for the interface
loc2 = [1,pos-1,length(z)]; % Lower limit for the interface

%% Calculate Cij for every point in VTI medium

Cij = zeros(6,6,length(z));

% Formulas are following Thomsen Parameter for VTI medium
```

```

for i = 1:length(z)
    Cij(3,3,i) = (vp0(i)^2)*dens(i) ;
    Cij(4,4,i) = (vs0(i)^2)*dens(i) ;
    Cij(5,5,i) = Cij(4,4,(i));
    Cij(1,1,i) = (1+2*eps(i))*Cij(3,3,i);
    Cij(6,6,i) = (1+2*gam(i))*Cij(4,4,i);
    Cij(1,3,i) = sqrt(2*del(i)*Cij(3,3,i)*(Cij(3,3,i)-Cij(5,5,i)) + (Cij(3,3,i)-Cij(5,5,i))^2) ...
               - Cij(5,5,i);
    Cij(1,2,i) = Cij(1,1,i) - 2*Cij(6,6,i);

    Cij(2,2,i) = Cij(1,1,i);
    Cij(2,1,i) = Cij(1,2,i);
    Cij(3,1,i) = Cij(1,3,i);
    Cij(3,2,i) = Cij(1,3,i);
    Cij(2,3,i) = Cij(1,3,i);

end

%% FRACTURE PARAMETER (ORT)

    C_ort = zeros(6,6,length(z));
%     x1 = z(loc1(3):loc1(4)-1);
%      k = loc1(3);
%      l = loc1(4);
for i = 1:size(z,1)
    if i > loc1(3)-1 && i < loc1(4) %BLOCK 3-A
       dn = 0.15;
       dh = 0.2;
       dv = 0.2;
    elseif i > loc1(4)-1 && i < loc1(5) %BLOCK 3-B
       dn = 0.4;
       dh = 0.2;
       dv = 0.2;
    elseif i > loc1(5)-1 && i < loc1(6) %BLOCK 3-C
       dn = 0.2;
       dh = 0.2;
       dv = 0.2;
    elseif i > loc1(6)-1 && i < loc1(7) %BLOCK 3-D
       dn = 0.5;
       dh = 0.2;
       dv = 0.2;
    else
        dn = 0;
        dh = 0;
        dv = 0;
    end

    % ORT Cij

    C_ort(1,1,i) = Cij(1,1,i)*(1-dn);
    C_ort(2,2,i) = Cij(1,1,i)-(dn*(Cij(1,2,i)^2)/Cij(1,1,i)
       );
    C_ort(2,3,i) = Cij(1,3,i)*(1-dn*Cij(1,2,i)/Cij(1,1,i));
    C_ort(1,2,i) = Cij(1,2,i)*(1-dn);
    C_ort(1,3,i) = Cij(1,3,i)*(1-dn);

    C_ort(4,4,i) = Cij(4,4,i);
    C_ort(3,3,i) = Cij(3,3,i)-dn*(Cij(1,3,i)^2)/Cij(1,1,i);
    C_ort(5,5,i) = Cij(4,4,i)*(1-dv);
    C_ort(6,6,i) = Cij(6,6,i)*(1-dh);

end

%% Backus Averaging (ORT)

zone_number = length(interface)+1 ;

% Individual Layers are assumed to be ORT

Cb = zeros(6,6,zone_number);
efdens = zeros(zone_number,1);

for i = 1:length(loc1)-1
  Cb(3,3,i) = mean(C_ort(3,3,loc1(i):loc2(i+1)).^(-1))
     .^(-1);
  Cb(4,4,i) = mean(C_ort(4,4,loc1(i):loc2(i+1)).^(-1))
     .^(-1);
  Cb(5,5,i) = mean(C_ort(5,5,loc1(i):loc2(i+1)).^(-1))
     .^(-1);
  Cb(6,6,i) = mean(C_ort(6,6,loc1(i):loc2(i+1)));

  Cb(1,3,i) = mean(C_ort(1,3,loc1(i):loc2(i+1))./C_ort(3,3,
     loc1(i):loc2(i+1)))...
              .* Cb(3,3,i);
  Cb(2,3,i) = mean(C_ort(2,3,loc1(i):loc2(i+1))./C_ort(3,3,
     loc1(i):loc2(i+1)))...
              .* Cb(3,3,i);

```

```
Cb(1,1,i) = mean(C_ort(1,1,loc1(i):loc2(i+1))) + ...
            (mean(C_ort(1,3,loc1(i):loc2(i+1))./C_ort
               (3,3,loc1(i):loc2(i+1))).^2 )...
            .* Cb(3,3,i) - ...
            (mean((C_ort(1,3,loc1(i):loc2(i+1)).^2)./
               C_ort(3,3,loc1(i):loc2(i+1))));
Cb(2,2,i) = mean(C_ort(2,2,loc1(i):loc2(i+1))) + ...
            (mean(C_ort(2,3,loc1(i):loc2(i+1))./C_ort
               (3,3,loc1(i):loc2(i+1))).^2 )...
            .* Cb(3,3,i) - ...
            (mean((C_ort(2,3,loc1(i):loc2(i+1)).^2)./
               C_ort(3,3,loc1(i):loc2(i+1))));

Cb(1,2,i) = mean(C_ort(1,2,loc1(i):loc2(i+1))) + ...
            mean(C_ort(1,3,loc1(i):loc2(i+1))./C_ort(3,3,
               loc1(i):loc2(i+1)))...
            .* mean(C_ort(2,3,loc1(i):loc2(i+1))./C_ort
               (3,3,loc1(i):loc2(i+1)))...
            .* Cb(3,3,i) - ...
            mean((C_ort(1,3,loc1(i):loc2(i+1)).*C_ort
               (2,3,loc1(i):loc2(i+1)))...
            ./C_ort(3,3,loc1(i):loc2(i+1)));


efdens(i) = mean(dens(loc1(i):loc2(i+1)));

% Effective parameter of the Anisotropy

  Evp0(i) = sqrt(Cb(3,3,i)/efdens(i));
  Evs0(i) = sqrt(Cb(5,5,i)/efdens(i));

            % Plane is Perpendicular to fractures
  eps13(i)    = (Cb(1,1,i) - Cb(3,3,i))/(2*Cb(3,3,i));
  gam13(i)    = (Cb(6,6,i) - Cb(4,4,i))/(2*Cb(4,4,i));
  del13(i)    = ((Cb(1,3,i) + Cb(5,5,i))^2 - (Cb(3,3,i) -
      Cb(5,5,i))^2) / ...
              (2*Cb(3,3,i)*(Cb(3,3,i) - Cb(5,5,i)));
            % Plane is Paralel to fractures
  eps23(i)    = (Cb(2,2,i) - Cb(3,3,i))/(2*Cb(3,3,i));
  gam23(i)    = (Cb(6,6,i) - Cb(5,5,i))/(2*Cb(5,5,i));
  del23(i)    = ((Cb(2,3,i) + Cb(4,4,i))^2 - (Cb(3,3,i) -
      Cb(4,4,i))^2) / ...
              (2*Cb(3,3,i)*(Cb(3,3,i) - Cb(4,4,i)));
            % Horizontal Plane
```

```
    del12(i)     = ((Cb(1,2,i) + Cb(6,6,i))^2 - (Cb(1,1,i) - Cb(6,6,i))^2) / ...
                (2*Cb(1,1,i)*(Cb(1,1,i) - Cb(6,6,i)));

end

 % Set the effective parameters into every data point (depth)

    Cef = zeros(6,6,length(z));

for i = 1:size(z,1)
        if i < loc1(2)
            j = 1;
        elseif i > loc1(2)-1 && i < loc1(3)
            j = 2;
        elseif i > loc1(3)-1 && i < loc1(4)
            j = 3;
        elseif i > loc1(4)-1 && i < loc1(5)
            j = 4;
        elseif i > loc1(5)-1 && i < loc1(6)
            j = 5;
        elseif i > loc1(6)-1 && i < loc1(7)
            j = 6;
        elseif i > loc1(7)-1 && i < loc1(8)
            j = 7;
        else
            j = 8;
        end

      Cef(3,3,i) = Cb(3,3,j);
      Cef(4,4,i) = Cb(4,4,j);
      Cef(5,5,i) = Cb(5,5,j);

      Cef(1,3,i) = Cb(1,3,j);
      Cef(2,3,i) = Cb(2,3,j);

      Cef(6,6,i) = Cb(6,6,j);

      Cef(1,1,i) = Cb(1,1,j);
      Cef(2,2,i) = Cb(2,2,j);

      Cef(1,2,i) = Cb(1,2,j);

      % Effective parameters
```

```
        vp0ef(i)   = Evp0(j);
        vs0ef(i)   = Evs0(j);

        densef(i)  = efdens(j);

        e13(i)     = eps13(j);
        g13(i)     = gam13(j);
        d13(i)     = del13(j);

        e23(i)     = eps23(j);
        g23(i)     = gam23(j);
        d23(i)     = del23(j);

        d12(i)     = del12(j);

end

%% Kinematic Parameter

VP   = zeros(length(z),3);% Vertical NMO[x1,x3] NMO[x2,x3]
VS1  = zeros(length(z),3);
VS2  = zeros(length(z),3);

anelP   = zeros(length(z),3);% eta1[x1,x3] eta2[x2,x3] etaxy [x1,x2]
anelS1  = zeros(length(z),3);
anelS2  = zeros(length(z),3);

n = size(z,1);

[VP,VS1,VS2,anelP,anelS1,anelS2] = ...
    kinematic3(vp0ef,Cef,e13,g13,d13,e23,g23,d23,d12,densef,n);
```

Kinematic3 Function:

```
function [VP,VS1,VS2,anelP,anelS1,anelS2] = ...
    kinematic3(Vp0_or,C_ort,e13,g13,d13,e23,g23,d23,d12,densef,n)



for i = 1:n

    % Component for anelliptic parameter on Pure mode wave
    r0   = sqrt(C_ort(5,5,i)/C_ort(3,3,i));
    r1  = sqrt((1-(r0^2))*(1+2*d13(i)-(r0^2)));
    r2  = sqrt((1+2*g13(i)-(r0^2)*(1+2*g23(i)))* ...
        ((1+2*d23(i))*(1+2*g13(i))-(r0^2)*(1+2*g23(i))));
    r3  = sqrt((1+2*e13(i)-(r0^2)*(1+2*g23(i))) * ...
              ((1+2*d12(i))*(1+2*e13(i))-(r0^2)*(1+2*g23(i))));

    % Component for anelliptic parameter on P-wave
    b0  = 2*(1+2*d13(i))*(1+2*d23(i))*(1+2*g13(i));
    b2  = -(1+2*d13(i))*(1+2*g23(i))-(1+2*d23(i))*(1+2*g13(i))...
          -2*(1+2*d13(i))*(1+2*d23(i))*(1+g13(i)+g23(i))...
          -2*(1+2*g13(i))*(1+2*g23(i))*(1+d13(i)+d23(i));
    b4  = (1+2*g23(i))*(4+2*d13(i)+2*d23(i)+2*g13(i)+2*g23(i)...
          +(1+2*d13(i))*(1+2*g23(i))+(1+2*d23(i))*(1+2*g13(i)));
    b6  = -2*((1+2*g23(i))^2);

    VP(i,1)    = Vp0_or(i);
    VP(i,2)    = sqrt((Vp0_or(i).^2).*(1+2.*d13(i)));
    VP(i,3)    = sqrt((Vp0_or(i).^2).*(1+2.*d23(i)));
    anelP(i,1) = ((e13(i)-d13(i))*(1+2*d13(i)-(r0^2)))...
                   /(((1+2*d13(i))^2)*(1-(r0^2)));
    anelP(i,2) = ((e23(i)-d23(i))*((1+2*d23(i))*(1+2*g13(i))-(r0^2)*(1+2*g23(i)))))...
                   /(((1+2*d23(i))^2)*(1+2*g13(i)-(r0^2)*(1+2*g23(i))));
    anelP(i,3) = (b0+b2*(r0^2)+b4*(r0^4)+b6*(r0^6)-2*r1*r2*r3)...
                   /(2*(1+2*d13(i))*(1+2*d23(i))*(1+2*g13(i)-(r0^2)*(1+2*g23(i))));

    % Component for anelliptic parameter on S1-wave (C55)
    b0  = ((1+2*g13(i))^2)*( (1+2*d13(i))*(1+2*d23(i))...
          +(1+2*d12(i))*((1+2*e13(i))^2));
    b2  = -(1+2*g13(i))*((1+2*d13(i))*(1+2*g23(i))+(1+2*d23(i))*(1+2*g13(i))...
          +(1+2*g13(i))*((1+2*d13(i))*(1+2*d23(i))+(1+2*e13(i))*(1+2*g23(i)))...
          +2*(1+2*e13(i))*(1+2*g23(i))*(1+2*d12(i))*(1+e13(i)+g13(i)));
    b4  = (1+2*g13(i))*(1+2*g23(i))*(3+2*d13(i)+2*d23(i)-2*(1+2*d23(i))*(g23(i)-g13(i))...
          +2*(1+2*g23(i))*(1+e13(i)+g13(i))+(1+2*d12(i))
```

```
             *(1+2*e13(i))*(1+2*g23(i)));
    b6  = -2*((1+2*g23(i))^2)*(1+2*g13(i)+2*g13(i)*g23(i));

    Vs10(i)      = sqrt(C_ort(5,5,i)/densef(i));
    VS1(i,1)     = Vs10(i);
    VS1(i,2)     = sqrt((Vs10(i).^2).*(1+2.*((e13(i)-d13(i))
       ./(r0^2))));
    VS1(i,3)     = sqrt((Vs10(i).^2).*(1+2.*g23(i)));
    anelS1(i,1)  = - ((e13(i)-d13(i))*(r0^2)*(1+2*d13(i)-(r0
       ^2)))...
                    /(((1+2*(e13(i)-d13(i))/(r0^2))^2)*(1-(
                       r0^2)));
    anelS1(i,2)  = 0;
    anelS1(i,3)  = - (b0+b2*(r0^2)+b4*(r0^4)+b6*(r0^6)-2*r1*
       r2*r3)...
                    /( 4*(r0^4)*(1-r0^2)*(1+2*(e13(i)-d13(i
                       ))/(r0^2))*(g23(i)-g13(i))*(1+2*g23(
                       i)));

    % Component for anelliptic parameter on S2-wave (C44)
    b0  = (1+2*g13(i))*( (1+2*d13(i))*(1+2*d23(i))...
          +(1+2*d12(i))*((1+2*e13(i))^2));
    b2  = -(1+2*d13(i))*(1+2*g23(i))-(1+2*d23(i))*(1+2*g13(
       i))...
          -(1+2*g23(i))*((1+2*d13(i))*(1+2*d23(i))+(1+2*e13
             (i))*(1+2*g13(i)))...
          -2*(1+2*e13(i))*(1+2*g13(i))*(1+2*d12(i))*(1+e13(
             i)+g23(i));
    b4  = (1+2*g23(i))*(3+2*d13(i)+2*d23(i)+2*(1+2*d13(i))
       *(g23(i)-g13(i))...
          +2*(1+2*g13(i))*(1+e13(i)+g23(i))...
          +(1+2*d12(i))*(1+2*e13(i))*(1+2*g13(i)));
    b6  = -2*(1+2*g23(i))*(1+2*g23(i)+2*g13(i)*g23(i));

    VS20(i)      = sqrt(C_ort(5,5,i)/densef(i));
    VS2(i,1)     = VS20(i)*sqrt((1+2*g23(i))/(1+2*g13(i)));
    VS2(i,2)     = sqrt((VS20(i).^2).*(1+2.*g23(i)));
    VS2(i,3)     = sqrt((VS20(i).^2).*...
                    ( ((1+2.*g23(i))/(1+2*g13(i)))+2*(e23(i
                       )-d23(i))/(r0^2) ) );
    anelS2(i,1)  = 0;
    anelS2(i,2)  = -((e23(i)-d23(i))*(r0^2)*((1+2*d23(i))
       -((1+2*g23(i))/(1+2*g13(i)))*(r0^2)))...
                    /(((1+2*g13(i))^2)*((((1+2*g23(i))
                       /(1+2*g13(i)))+2*(e23(i)-d23(i))/(r0
```

```
                        ^2))^2)...
                    *(1-((1+2*g23(i))/(1+2*g13(i)))*(r0^2))
                        );
    anelS2(i,3) = (b0+b2*(r0^2)+b4*(r0^4)+b6*(r0^6)-2*r1*r2
       *r3)...
                    /(4*(r0^4)*(1+2*g13(i))*(1+2*g13(i)
                        -(1+2*g23(i))*(r0^2))...
                    *(((1+2*g23(i))/(1+2*g13(i)))+2*(e23(i)
                        -d23(i))/(r0^2))*(g23(i)-g13(i)));
end
```

Appendix D: Matlab Code - Introducing Fracture Before Least Square Upscaling

```
clc,clear

%% Read Data

% Log Conditioning of bad data is performed on excel

load 'Data5conditioned.txt'

x = readtable('Data5conditioned','headerlines',0);

h       = table2array(x(:,1)); % m
GR      = table2array(x(:,2));
vp0     = table2array(x(:,3)); % m/s
vs0     = table2array(x(:,4)); % m/s
dens    = table2array(x(:,5))*1000; % kg/m^3
eps     = table2array(x(:,6));
del     = table2array(x(:,7));
gam     = table2array(x(:,8));

%% Defining Interface

% Interface decision based on GR interpretation of the log data
interface = [1000, 1275, 1430, 1520, 1625, 1770, 2010];

% Finding Location index of the array

for i = 1:length(interface)
    pos(i) = find(abs(h-interface(i)) == min(abs(h-interface(i))));
end

loc1 = [1,pos,length(h)];    % Upper limit for the interface
loc2 = [1,pos-1,length(h)]; % Lower limit for the interface


%% Calculate Cij for every point in VTI medium

c33 = zeros(length(h),1);
c44 = zeros(length(h),1);
```

```
c55 = zeros(length(h),1);
c11 = zeros(length(h),1);
c66 = zeros(length(h),1);
c13 = zeros(length(h),1);
c12 = zeros(length(h),1);

% Formulas are following Thomsen Parameter for VTI medium

for i = 1:length(h)
    c33(i,1) = ((vp0(i)^2)*dens(i))/(10^9) ;
    c44(i,1) = ((vs0(i)^2)*dens(i))/(10^9) ;
    c55(i,1) = c44(i,1);
    c11(i,1) = ((1+2*eps(i))*c33(i,1));
    c66(i,1) = ((1+2*gam(i))*c44(i,1));
    c13(i,1) = sqrt(2*del(i)*c33(i,1)*(c33(i,1)-c55(i,1)) + (c33(i,1)-c55(i,1))^2) ...
               - c55(i,1);
    c12(i,1) = c11(i,1) - 2*c66(i,1);
end

%% FRACTURE PARAMETER (ORT)

co33 = zeros(length(h),1);
co44 = zeros(length(h),1);
co55 = zeros(length(h),1);
co11 = zeros(length(h),1);
co66 = zeros(length(h),1);
co13 = zeros(length(h),1);
co12 = zeros(length(h),1);
co22 = zeros(length(h),1);
co23 = zeros(length(h),1);


for i = 1:size(h,1)
    if i > loc1(3)-1 && i < loc1(4)
       dn = 0.15;
       dh = 0.2;
       dv = 0.2;
    elseif i > loc1(4)-1 && i < loc1(5)
       dn = 0.4;
       dh = 0.2;
       dv = 0.2;
    elseif i > loc1(5)-1 && i < loc1(6)
       dn = 0.2;
       dh = 0.2;
       dv = 0.2;
    elseif i > loc1(6)-1 && i < loc1(7)
       dn = 0.5;
       dh = 0.2;
       dv = 0.2;
    else
        dn = 0;
        dh = 0;
        dv = 0;
    end

    % ORT Cij

    co11(i,1) = c11(i,1)*(1-dn);
    co22(i,1) = c11(i,1)-(dn*(c12(i,1)^2)/c11(i,1));
    co23(i,1) = c13(i,1)*(1-dn*c12(i,1)/c11(i,1));
    co12(i,1) = c12(i,1)*(1-dn);
    co13(i,1) = c13(i,1)*(1-dn);

    co44(i,1) = c44(i,1);
    co33(i,1) = c33(i,1)-dn*(c13(i,1)^2)/c11(i,1);
    co55(i,1) = c44(i,1)*(1-dv);
    co66(i,1) = c66(i,1)*(1-dh);

end
%% --- Defining Block 3 ---

  n1      = length(loc1(3):loc1(4)-1); % total data Block 3a
  x1      = h(loc1(3):loc1(4)-1); % allocated depth points
  k       = loc1(3);
  l       = loc1(4);

%   n1      = length(loc1(4):loc1(5)-1); % Block 3b
%   x1      = h(loc1(4):loc1(5)-1);
%   k       = loc1(4);
%   l       = loc1(5);
%
%   n1      = length(loc1(5):loc1(6)-1); % Block 3c
%   x1      = h(loc1(5):loc1(6)-1);
%   k       = loc1(5);
%   l       = loc1(6);
%
%   n1      = length(loc1(6):loc1(7)-1); % Block 3d
%   x1      = h(loc1(6):loc1(7)-1);
%   k       = loc1(6);
%   l       = loc1(7);

% Calculating the unknown 'a' and 'b' for least square

  y1(:,1) = 1./co33(k:l-1,1); % 1/c33
  y1(:,2) = 1./co44(k:l-1,1); % 1/c44
  y1(:,3) = 1./co55(k:l-1,1); % 1/c55
  y1(:,4) = co13(k:l-1,1)./co33(k:l-1,1); % c13/c33
  y1(:,5) = co23(k:l-1,1)./co33(k:l-1,1); % c23/c33
  y1(:,6) = co66(k:l-1,1);   % c66
  y1(:,7) = co11(k:l-1,1);   % c11
  y1(:,8) = (co13(k:l-1,1).^2)./co33(k:l-1,1); % c13^2/c33
  y1(:,9) = co22(k:l-1,1);   % c22
  y1(:,10)= (co23(k:l-1,1).^2)./co33(k:l-1,1); % c23^2/c33
  y1(:,11)= co12(k:l-1,1);   % c12
  y1(:,12)= co13(k:l-1,1).*co23(k:l-1,1)./co33(k:l-1,1); % c13*c23/c33
  y1(:,13) = dens(k:l-1,1);  % density

a1 = zeros(1,13); % 1/c33 | 1/c44 | 1/c55 | c13/c33 | c23/c33 | c66 | c11 |
                  % c13^2/c33 | c22 | c23^2/c33 | c12 | c13*c23/c33 | dens
b1 = zeros(1,13);

for i = 1:13
    a1(1,i) = ((n1*sum(x1.*y1(:,i)))-(sum(x1)*sum(y1(:,i))))/(n1*sum(x1.^2)-(sum(x1)^2));
    b1(1,i) = (sum(y1(:,i))-a1(1,i)*sum(x1))/n1;
end

%--- LEAST SQUARE CALCULATION on ORT Medium ---

% Cij and density function calculation

C33a  = @(z) 1./(a1(1,1).*z + b1(1,1));
C44a  = @(z) 1./(a1(1,2).*z + b1(1,2));
C55a  = @(z) 1./(a1(1,3).*z + b1(1,3));
C13a  = @(z) (a1(1,4).*z + b1(1,4)).*C33a(z);
C23a  = @(z) (a1(1,5).*z + b1(1,5)).*C33a(z);
C66a  = @(z) a1(1,6).*z + b1(1,6);
C11a  = @(z) (a1(1,7).*z + b1(1,7)) + ((a1(1,4).*z + b1(1,4)).^2).*C33a(z)...
             -(a1(1,8).*z + b1(1,8));
```

```
C22a  = @(z) (a1(1,9).*z + b1(1,9)) + ((a1(1,5).*z + b1(1,5)).^2).*C33a(z)...
             -(a1(1,10).*z + b1(1,10));
C12a  = @(z) (a1(1,11).*z + b1(1,11)) + (((a1(1,4).*z + b1(1,4)).*(a1(1,5).*z + b1(1,5))).*C33a(z))...
             -(a1(1,12).*z + b1(1,12));
Densa = @(z) a1(1,13).*z + b1(1,13);

% Anisotropy Parameter Function Calculation

Vp0oa = @(z) sqrt(C33a(z).*(10^9)./Densa(z));
Vs0oa = @(z) sqrt(C55a(z).*(10^9)./Densa(z));

    % Plane is Perpendicular to fractures [x1,x3]

e1   = @(z) (C11a(z)-C33a(z))./(2.*C33a(z));
g1   = @(z) (C66a(z)-C44a(z))./(2.*C44a(z));
d1   = @(z) ((C13a(z)+C55a(z)).^2-(C33a(z)-C55a(z)).^2) ...
             ./(2.*C33a(z).*(C33a(z)-C55a(z)));

    % Plane is Parallel to fractures [x2,x3]

e2   = @(z) (C22a(z)-C33a(z))./(2.*C33a(z));
g2   = @(z) (C66a(z)-C55a(z))./(2.*C55a(z));
d2   = @(z) ((C23a(z)+C44a(z)).^2-(C33a(z)-C44a(z)).^2) ...
             ./(2.*C33a(z).*(C33a(z)-C44a(z)));

    % Horizontal Plane

d3   = @(z) ((C12a(z)+C66a(z)).^2-(C11a(z)-C66a(z)).^2) ...
             ./(2.*C11a(z).*(C11a(z)-C66a(z)));


%% ----- AVERAGE VALUE ANISO PARAMETER USING INTEGRAL ------

VP0_or = integral(Vp0oa,x1(1),x1(end))/(x1(end)-x1(1));
VS0_or = integral(Vs0oa,x1(1),x1(end))/(x1(end)-x1(1));

eps1 = integral(e1,x1(1),x1(end))/(x1(end)-x1(1));
gam1 = integral(g1,x1(1),x1(end))/(x1(end)-x1(1));
del1 = integral(d1,x1(1),x1(end))/(x1(end)-x1(1));

eps2 = integral(e2,x1(1),x1(end))/(x1(end)-x1(1));
gam2 = integral(g2,x1(1),x1(end))/(x1(end)-x1(1));
```

```
del2 = integral(d2,x1(1),x1(end))/(x1(end)-x1(1));

del3 = integral(d3,x1(1),x1(end))/(x1(end)-x1(1));

%% --- KINEMATIC PARAMETER ---

% Component for anelliptic parameter on Pure mode wave

r0  =@(z) sqrt(C55a(z)./C33a(z));
r1  =@(z) sqrt((1-(r0(z).^2)).*(1+2.*d1(z)-(r0(z).^2)));
r2  =@(z) sqrt((1+2.*g1(z)-(r0(z).^2).*(1+2.*g2(z))) .* ...
              ((1+2.*d2(z)).*(1+2.*g1(z))-(r0(z).^2)
                 .*(1+2.*g2(z))));
r3  =@(z) sqrt((1+2.*e1(z)-(r0(z).^2).*(1+2.*g2(z))) .* ...
              ((1+2.*d3(z)).*(1+2.*e1(z))-(r0(z).^2)
                 .*(1+2.*g2(z))));


% Component for anelliptic parameter on P-WAVE

b0  =@(z) 2.*(1+2.*d1(z)).*(1+2.*d2(z)).*(1+2.*g1(z));
b2  =@(z) -(1+2.*d1(z)).*(1+2.*g2(z))-(1+2.*d2(z)).*(1+2.*
   g1(z))...
          -2.*(1+2.*d1(z)).*(1+2.*d2(z)).*(1+g1(z)+g2(z))
             ...
          -2.*(1+2.*g1(z)).*(1+2.*g2(z)).*(1+d1(z)+d2(z));
b4  =@(z) (1+2.*g2(z)).*(4+2.*d1(z)+2.*d2(z)+2.*g1(z)+2.*g2
   (z)...
          +(1+2.*d1(z)).*(1+2.*g2(z))+(1+2.*d2(z)).*(1+2.*
             g1(z)));
b6  =@(z) -2.*((1+2.*g2(z)).^2);

% Kinematic Parameter

VP0     =@(z) Vp0oa(z);
VP1     =@(z) sqrt((Vp0oa(z).^2).*(1+2.*d1(z)));
VP2     =@(z) sqrt((Vp0oa(z).^2).*(1+2.*d2(z)));

anelP1 =@(z) ((e1(z)-d1(z)).*(1+2.*d1(z)-(r0(z).^2)))...
             ./(((1+2.*d1(z)).^2).*(1-(r0(z).^2)));
anelP2 =@(z) ((e2(z)-d2(z)).*((1+2.*d2(z)).*(1+2.*g1(z))-(
   r0(z).^2).*(1+2.*g2(z))))...
             ./(((1+2.*d2(z)).^2).*(1+2.*g1(z)-(r0(z).^2)
                .*(1+2.*g2(z))));
```

```
anelP3 =@(z)  (b0(z)+b2(z).*(r0(z).^2)+b4(z).*(r0(z).^4)+b6(z).*(r0(z).^6)-2.*r1(z).*r2(z).*r3(z))...
                ./(2.*(1+2.*d1(z)).*(1+2.*d2(z)).*(1+2.*g1(z)-(r0(z).^2).*(1+2.*g2(z))));

% Component for anelliptic parameter on S1-WAVE

b0  =@(z)  ((1+2.*g1(z)).^2).*( (1+2.*d1(z)).*(1+2.*d2(z)) ...
          +(1+2.*d3(z)).*((1+2.*e1(z)).^2));
b2  =@(z)  -(1+2.*g1(z)).*((1+2.*d1(z)).*(1+2.*g2(z))+(1+2.*d2(z)).*(1+2.*g1(z))...
          +(1+2.*g1(z)).*((1+2.*d1(z)).*(1+2.*d2(z))+(1+2.*e1(z)).*(1+2.*g2(z)))...
          +2.*(1+2.*e1(z)).*(1+2.*g2(z)).*(1+2.*d3(z)).*(1+e1(z)+g1(z)));
b4  =@(z)  (1+2.*g1(z)).*(1+2.*g2(z)).*(3+2.*d1(z)+2.*d2(z)-2.*(1+2.*d2(z)).*(g2(z)-g1(z))...
          +2.*(1+2.*g2(z)).*(1+e1(z)+g1(z))+(1+2.*d3(z)).*(1+2.*e1(z)).*(1+2.*g2(z)));
b6  =@(z)  -2.*((1+2.*g2(z)).^2).*(1+2.*g1(z)+2.*g1(z).*g2(z));

VS10    =@(z)  sqrt(C55a(z).*(10^9)./Densa(z));
VS11    =@(z)  sqrt((VS10(z).^2).*(1+2.*((e1(z)-d1(z))./(r0(z).^2))));
VS12    =@(z)  sqrt((VS10(z).^2).*(1+2.*g2(z)));
anelS11 =@(z)  - ((e1(z)-d1(z)).*(r0(z).^2).*(1+2.*d1(z)-(r0(z).^2)))...
                ./(((1+2.*(e1(z)-d1(z))/(r0(z).^2)).^2).*(1-(r0(z).^2)));
anelS12 =0;
anelS13 =@(z)  - (b0(z)+b2(z).*(r0(z).^2)+b4(z).*(r0(z).^4)+b6(z).*(r0(z).^6)-2.*r1(z).*r2(z).*r3(z))...
                ./( 4.*(r0(z).^4).*(1-r0(z).^2).*(1+2.*(e1(z)-d1(z))./(r0(z).^2)).*(g2(z)-g1(z)).*(1+2.*g2(z)));

% Component for anelliptic parameter on S2-wave

b0  =@(z)  (1+2.*g1(z)).*( (1+2.*d1(z)).*(1+2.*d2(z))...
          +(1+2.*d3(z)).*((1+2.*e1(z)).^2));
b2  =@(z)  -(1+2.*d1(z)).*(1+2.*g2(z))-(1+2.*d2(z)).*(1+2.*g1(z))...
```

```
          -(1+2.*g2(z)).*((1+2.*d1(z)).*(1+2.*d2(z))+(1+2.*e1(z)).*(1+2.*g1(z)))...
          -2.*(1+2.*e1(z)).*(1+2.*g1(z)).*(1+2.*d3(z)).*(1+e1(z)+g2(z));
b4  =@(z) (1+2.*g2(z)).*(3+2.*d1(z)+2.*d2(z)+2.*(1+2.*d1(z)).*(g2(z)-g1(z))...
          +2.*(1+2.*g1(z)).*(1+e1(z)+g2(z))...
          +(1+2.*d3(z)).*(1+2.*e1(z)).*(1+2.*g1(z)));
b6  =@(z) -2.*(1+2.*g2(z)).*(1+2.*g2(z)+2.*g1(z).*g2(z));

Vs20    =@(z) sqrt(C55a(z).*(10^9)./Densa(z));
VS20    =@(z) Vs20(z).*sqrt((1+2.*g2(z))./(1+2.*g1(z)));
VS21    =@(z) sqrt((Vs20(z).^2).*(1+2.*g2(z)));
VS22    =@(z) sqrt((Vs20(z).^2).*...
              ( ((1+2.*g2(z))./(1+2.*g1(z)))+2.*(e2(z)-d2(z))./(r0(z).^2) ) );
anelS21 = 0;
anelS22 =@(z) -((e2(z)-d2(z)).*(r0(z).^2).*((1+2.*d2(z))-((1+2.*g2(z))./(1+2.*g1(z))).*(r0(z).^2)))...
              ./(((1+2.*g1(z)).^2).*((((1+2.*g2(z))./(1+2.*g1(z)))+2.*(e2(z)-d2(z))./(r0(z).^2)).^2)...
              .*(1-((1+2.*g2(z))./(1+2.*g1(z))).*(r0(z).^2)));
anelS23 =@(z) (b0(z)+b2(z).*(r0(z).^2)+b4(z).*(r0(z).^4)+b6(z).*(r0(z).^6)-2.*r1(z).*r2(z).*r3(z))...
              ./(4.*(r0(z).^4).*(1+2.*g1(z)).*(1+2.*g1(z)-(1+2.*g2(z)).*(r0(z).^2))...
              .*(((1+2.*g2(z))./(1+2.*g1(z)))+2.*(e2(z)-d2(z))./(r0(z).^2)).*(g2(z)-g1(z)));

%% ------ AVERAGE VALUE KINEMATIC PARAMETERS USING INTEGRAL ---------

% P-WAVE

VP0    = integral(VP0,x1(1),x1(end))/(x1(end)-x1(1));
VP1    = integral(VP1,x1(1),x1(end))/(x1(end)-x1(1));
VP2    = integral(VP2,x1(1),x1(end))/(x1(end)-x1(1));

anelP1 = integral(anelP1,x1(1),x1(end))/(x1(end)-x1(1));
anelP2 = integral(anelP2,x1(1),x1(end))/(x1(end)-x1(1));
anelP3 = integral(anelP3,x1(1),x1(end))/(x1(end)-x1(1));

% S1-WAVE
```

```

VS10    = integral(VS10,x1(1),x1(end))/(x1(end)-x1(1));
VS11    = integral(VS11,x1(1),x1(end))/(x1(end)-x1(1));
VS12    = integral(VS12,x1(1),x1(end))/(x1(end)-x1(1));

anelS11 = integral(anelS11,x1(1),x1(end))/(x1(end)-x1(1));
anelS12 = anelS12;
anelS13 = integral(anelS13,x1(1),x1(end))/(x1(end)-x1(1));

% S2-WAVE

VS20    = integral(VS20,x1(1),x1(end))/(x1(end)-x1(1));
VS21    = integral(VS21,x1(1),x1(end))/(x1(end)-x1(1));
VS22    = integral(VS22,x1(1),x1(end))/(x1(end)-x1(1));

anelS21 = anelS21;
anelS22 = integral(anelS22,x1(1),x1(end))/(x1(end)-x1(1));
anelS23 = integral(anelS23,x1(1),x1(end))/(x1(end)-x1(1));
```

Appendix D: Matlab Code - Overburden Effect

Calculation for obtaining the effective VTI background parameter for block 1 and 2:

```matlab
clc,clear

%% Read Data

% Log Conditioning of bad data is performed on excel

load 'Data5conditioned.txt'

x = readtable('Data5conditioned','headerlines',0);

h       = table2array(x(:,1)); % m
GR      = table2array(x(:,2));
vp0     = table2array(x(:,3)); % m/s
vs0     = table2array(x(:,4)); % m/s
dens    = table2array(x(:,5))*1000; % kg/m^3
eps     = table2array(x(:,6));
del     = table2array(x(:,7));
gam     = table2array(x(:,8));

%% Defining Interface

% Interface decision based on GR interpretation of the log data
interface = [1000, 1275, 1430, 1520, 1625, 1770, 2010];

% Finding Location index of the array

for i = 1:length(interface)
    pos(i) = find(abs(h-interface(i)) == min(abs(h-interface(i))));
end

loc1 = [1,pos,length(h)];    % Upper limit for the interface
loc2 = [1,pos-1,length(h)]; % Lower limit for the interface


%% Calculate Cij for every point in VTI medium

c33 = zeros(length(h),1);
c44 = zeros(length(h),1);
```

```
c55 = zeros(length(h),1);
c11 = zeros(length(h),1);
c66 = zeros(length(h),1);
c13 = zeros(length(h),1);
c12 = zeros(length(h),1);

% Formulas are following Thomsen Parameter for VTI medium

for i = 1:length(h)
    c33(i,1) = ((vp0(i)^2)*dens(i))/10^9 ;
    c44(i,1) = ((vs0(i)^2)*dens(i))/10^9 ;
    c55(i,1) = c44(i,1);
    c11(i,1) = ((1+2*eps(i))*c33(i,1));
    c66(i,1) = ((1+2*gam(i))*c44(i,1));
    c13(i,1) = sqrt(2*del(i)*c33(i,1)*(c33(i,1)-c55(i,1)) + (c33(i,1)-c55(i,1))^2) ...
               - c55(i,1);
    c12(i,1) = c11(i,1) - 2*c66(i,1);

end

%% --- Defining the Block ---

%   n1      = length(loc1(1):loc1(2)-1); % total data Block 1
%   x1      = h(loc1(1):loc1(2)-1); % allocated depth points
%   k       = loc1(1);
%   l       = loc1(2);


%   n1      = length(loc1(2):loc1(3)-1); % total data Block 2
%   x1      = h(loc1(2):loc1(3)-1); % allocated depth points
%   k       = loc1(2);
%   l       = loc1(3);
%
  n1      = length(loc1(3):loc1(4)-1); % total data Block 3a
  x1      = h(loc1(3):loc1(4)-1); % allocated depth points
  k       = loc1(3);
  l       = loc1(4);


  y1(:,1) = 1./c33(k:l-1,1); % 1/c33
  y1(:,2) = 1./c44(k:l-1,1); % 1/c44
  y1(:,3) = c13(k:l-1,1)./c33(k:l-1,1); % c13/c33
  y1(:,4) = c66(k:l-1,1);   % c66
  y1(:,5) = (c13(k:l-1,1).^2)./c33(k:l-1,1); % c13^2/c33
  y1(:,6) = c11(k:l-1,1);   % c11
  y1(:,7) = dens(k:l-1,1);  % density

a1 = zeros(1,7); % 1/c33 | 1/c44 | c13/c33 | c66 | c13^2/c33 | c11 | dens
b1 = zeros(1,7);

for i = 1:7
    a1(1,i) = ((n1*sum(x1.*y1(:,i)))-(sum(x1)*sum(y1(:,i))))/(n1*sum(x1.^2)-(sum(x1)^2));
    b1(1,i) = (sum(y1(:,i))-a1(1,i)*sum(x1))/n1;
end

%---------VTI BACKGROUND CALCULATION-------------

% Cij background and density function calculation

C33a  = @(z) 1./(a1(1,1).*z + b1(1,1));
C44a  = @(z) 1./(a1(1,2).*z + b1(1,2));
C13a  = @(z) (a1(1,3).*z + b1(1,3)).*(1./(a1(1,1).*z + b1(1,1)));
C66a  = @(z) a1(1,4).*z + b1(1,4);
C11a  = @(z) (a1(1,6).*z + b1(1,6)) + ((a1(1,3).*z + b1(1,3)).^2).*C33a(z)...
             -(a1(1,5).*z + b1(1,5));
C12a  = @(z) C11a(z)-2.*C66a(z);
Densa = @(z) a1(1,7).*z + b1(1,7);
C55a  = @(z) C44a(z);

% Anisotropy Parameter function calculation

Vp0a  = @(z) sqrt(C33a(z).*(10^9)./Densa(z));
Vs0a  = @(z) sqrt(C44a(z).*(10^9)./Densa(z));
epsa  = @(z) (C11a(z)-C33a(z))./(2.*C33a(z));
gama  = @(z) (C66a(z)-C44a(z))./(2.*C44a(z));
dela  = @(z) ((C13a(z)+C44a(z)).^2-(C33a(z)-C44a(z)).^2) ...
             ./(2.*C33a(z).*(C33a(z)-C44a(z)));

e1    = @(z) epsa(z);
```

```
e2     = @(z) epsa(z);
g1     = @(z) gama(z);
g2     = @(z) gama(z);
d1     = @(z) dela(z);
d2     = @(z) dela(z);
d3     = @(z) 0;

%% ------ AVERAGE VALUE ANISOTROPY PARAMETERS USING INTEGRAL ----------

% P-WAVE

vp0ef    = integral(Vp0a,x1(1),x1(end))/(x1(end)-x1(1));
vs0ef    = integral(Vs0a,x1(1),x1(end))/(x1(end)-x1(1));
epsef    = integral(epsa,x1(1),x1(end))/(x1(end)-x1(1));
gamef    = integral(gama,x1(1),x1(end))/(x1(end)-x1(1));
delef    = integral(dela,x1(1),x1(end))/(x1(end)-x1(1));
densef   = integral(Densa,x1(1),x1(end))/(x1(end)-x1(1));

%% KINEMATIC PARAMETERS OF PURE MODE WAVES in VTI Medium

% Component for anelliptic parameter on Pure mode wave

r0  =@(z) sqrt(C55a(z)./C33a(z));
r1  =@(z) sqrt((1-(r0(z).^2)).*(1+2.*d1(z)-(r0(z).^2)));
r2  =@(z) sqrt((1+2.*g1(z)-(r0(z).^2).*(1+2.*g2(z))) .* ...
              ((1+2.*d2(z)).*(1+2.*g1(z))-(r0(z).^2).*(1+2.*g2(z))));
r3  =@(z) sqrt((1+2.*e1(z)-(r0(z).^2).*(1+2.*g2(z))) .* ...
              ((1+2.*d3(z)).*(1+2.*e1(z))-(r0(z).^2).*(1+2.*g2(z))));

% Component for anelliptic parameter on P-WAVE

b0  =@(z) 2.*(1+2.*d1(z)).*(1+2.*d2(z)).*(1+2.*g1(z));
b2  =@(z) -(1+2.*d1(z)).*(1+2.*g2(z))-(1+2.*d2(z)).*(1+2.*g1(z))...
          -2.*(1+2.*d1(z)).*(1+2.*d2(z)).*(1+g1(z)+g2(z))...
          -2.*(1+2.*g1(z)).*(1+2.*g2(z)).*(1+d1(z)+d2(z));
b4  =@(z) (1+2.*g2(z)).*(4+2.*d1(z)+2.*d2(z)+2.*g1(z)+2.*g2(z)...
          +(1+2.*d1(z)).*(1+2.*g2(z))+(1+2.*d2(z)).*(1+2.*g1(z)));
b6  =@(z) -2.*((1+2.*g2(z)).^2);
```

```

% Kinematic Parameter
% P wave vertical and nmo velocity

VP0    =@(z) Vp0a(z);
VP1    =@(z) sqrt((Vp0a(z).^2).*(1+2.*d1(z)));
VP2    =@(z) sqrt((Vp0a(z).^2).*(1+2.*d2(z)));

anelP1 =@(z) ((e1(z)-d1(z)).*(1+2.*d1(z)-(r0(z).^2)))...
             ./(((1+2.*d1(z)).^2).*(1-(r0(z).^2)));
anelP2 =@(z) ((e2(z)-d2(z)).*((1+2.*d2(z)).*(1+2.*g1(z))-(r0(z).^2).*(1+2.*g2(z))))...
             ./(((1+2.*d2(z)).^2).*(1+2.*g1(z)-(r0(z).^2).*(1+2.*g2(z))));
anelP3 =@(z) 2.*anelP1(z);


% S1 wave (SV) vertical and nmo velocity

VS10    =@(z) sqrt(C55a(z).*(10^9)./Densa(z));
VS11    =@(z) sqrt((VS10(z).^2).*(1+2.*((e1(z)-d1(z))./(r0(z).^2))));
VS12    =@(z) sqrt((VS10(z).^2).*(1+2.*((e1(z)-d1(z))./(r0(z).^2))));
anelS11 =@(z) (e1(z)-d1(z)).*(VP0(z).^2)./(VS10(z).^2);
anelS12 =@(z) (e1(z)-d1(z)).*(VP0(z).^2)./(VS10(z).^2);
anelS13 =@(z) 2.*anelS11(z);

% S2 wave (SH) vertical and nmo velocity

Vs20    =@(z) sqrt(C44a(z).*(10^9)./Densa(z));
VS20    =@(z) Vs20(z).*sqrt((1+2.*g2(z))./(1+2.*g1(z)));
VS21    =@(z) sqrt((Vs20(z).^2).*(1+2.*g2(z)));
VS22    =@(z) sqrt((Vs20(z).^2).*(1+2.*g2(z)));
anelS21 =0;
anelS22 =0;
anelS23 =0;

%% ------ AVERAGE VALUE KINEMATIC PARAMETERS USING INTEGRAL ---------

% P-WAVE

VP0    = integral(VP0,x1(1),x1(end))/(x1(end)-x1(1));
VP1    = integral(VP1,x1(1),x1(end))/(x1(end)-x1(1));
```

```
VP2     = integral(VP2,x1(1),x1(end))/(x1(end)-x1(1));

anelP1 = integral(anelP1,x1(1),x1(end))/(x1(end)-x1(1));
anelP2 = integral(anelP2,x1(1),x1(end))/(x1(end)-x1(1));
anelP3 = integral(anelP3,x1(1),x1(end))/(x1(end)-x1(1));

% S1-WAVE

VS10     = integral(VS10,x1(1),x1(end))/(x1(end)-x1(1));
VS11     = integral(VS11,x1(1),x1(end))/(x1(end)-x1(1));
VS12     = integral(VS12,x1(1),x1(end))/(x1(end)-x1(1));

anelS11 = integral(anelS11,x1(1),x1(end))/(x1(end)-x1(1));
anelS12 = integral(anelS12,x1(1),x1(end))/(x1(end)-x1(1));
anelS13 = integral(anelS13,x1(1),x1(end))/(x1(end)-x1(1));

% S2-WAVE

VS20     = integral(VS20,x1(1),x1(end))/(x1(end)-x1(1));
VS21     = integral(VS21,x1(1),x1(end))/(x1(end)-x1(1));
VS22     = integral(VS22,x1(1),x1(end))/(x1(end)-x1(1));

% anelS21 = integral(anelS22,x1(1),x1(end))/(x1(end)-x1(1));
% anelS22 = integral(anelS22,x1(1),x1(end))/(x1(end)-x1(1));
% anelS23 = integral(anelS23,x1(1),x1(end))/(x1(end)-x1(1));
```

Calculation for Dix-type equations:

```
clc,clear

%% Read Data

% Log Conditioning of bad data is performed on excel

load 'Data5conditioned.txt'

x = readtable('Data5conditioned','headerlines',0);

h       = table2array(x(:,1)); % m
GR      = table2array(x(:,2));
vp0     = table2array(x(:,3)); % m/s
vs0     = table2array(x(:,4)); % m/s
dens    = table2array(x(:,5))*1000; % kg/m^3
```

```
eps     = table2array(x(:,6));
del     = table2array(x(:,7));
gam     = table2array(x(:,8));

%% Defining Interface

% Interface decision based on GR interpretation of the log data
interface = [1000, 1275, 1430, 1520, 1625, 1770, 2010];

% Finding Location index of the array

for i = 1:length(interface)
    pos(i) = find(abs(h-interface(i)) == min(abs(h-interface(i))));
end

loc1 = [1,pos,length(h)];   % Upper limit for the interface
loc2 = [1,pos-1,length(h)]; % Lower limit for the interface

%% ----- NMO VELOCITY ------
% vertical velocity
          %Block1  Block2  Block3A
v0(1,:) = [2361.9; 2708.7; 3236.7]; % P  wave
v0(2,:) = [1088.6; 1208.6; 1650.4]; % S1 wave
v0(3,:) = [1088.6; 1208.6; 1845.2]; % S2 wave

for i = 1:3
        for j = 1:3
            z(j) = h(loc2(j+1)) - h(loc1(j));
            t0(i,j) = 2*z(j)/v0(i,j);
        end
    T0(i,1) = sum(t0(i,:));
end

for i = 1:3
    a(i,1)  = (sum((v0(i,:).^2).*t0(i,:)));

    V0(i,1) = sqrt(a(i,1)/T0(i,1));
end
% vnmo1
          %Block1  Block2  Block3A
v1(1,:) = [2347.8  2821.2  2618.1]; % P  wave
v1(2,:) = [1051.4  1665.5  1886.1]; % S1 wave
v1(3,:) = [1079.3  1430.0  1471.7]; % S2 wave
```

```

for i = 1:3
   b(i,1)=(sum((v1(i,:).^2).*t0(i,:)));

   V1(i,1) = sqrt(b(i,1)/T0(i,1));
end

% vnmo2
          %Block1  Block2  Block3A
v2(1,:) = [2347.8  2821.2  3107.5];
v2(2,:) = [1051.4  1665.5  1471.7];
v2(3,:) = [1079.3  1430.0  1604.6];

for i = 1:3
   c(i,1)=(sum((v2(i,:).^2).*t0(i,:)));

   V2(i,1) = sqrt(c(i,1)/T0(i,1));
end

%% ----- ANELLIPTICITY -----
             %Block1  Block2  Block3A
eta1(1,:) =  [0.0025  0.0840  0.0495]; %  P -wave
eta1(2,:) =  [0.0266  0.4494  -0.0033]; % S1-wave
eta1(3,:) =  [0        0       0     ];

for i = 1:3
    d(i,1) = (sum((1+8.*eta1(i,:)).*(v1(i,:).^4).*t0(i,:)))
       ./...
             ((V1(i,1).^4).*T0(i,1)) ;

    E1(i,1) = (d(i,1) - 1) / 8;
end

eta2(1,:) = [0.0025  0.0840  -0.0412]; % P -wave
eta2(2,:) = [0.0266  0.4494  0];       % S1-wave
eta2(3,:) = [0       0       0.0281];  % S2-wave

for i = 1:3
    e(i,1) = (sum((1+8.*eta2(i,:)).*(v2(i,:).^4).*t0(i,:)))
       ./...
             ((V2(i,1).^4).*T0(i,1)) ;

    E2(i,1) = (e(i,1) - 1) / 8;
end

```

```
eta3(1,:) = [0.0049  0.1681  0.0540]; % P -wave
eta3(2,:) = [0.0532  0.8988  4.7072]; % S1-wave
eta3(3,:) = [0       0       -0.2324];% S2-wave

for i = 1:3
    f(i,1) = (sum((1+4.*eta3(i,:)).*(v1(i,:).^2).*(v2(i,:)
       .^2).*t0(i,:)))./...
             ((V1(i,1).^2).*(V2(i,1).^2).*T0(i,1)) ;

    E3(i,1) = (f(i,1) - 1) / 4;
end
```